Spring 5-6-2012

Synthesis, Characterization, and Photocatalytic Testing of Titania-Based Aerogels for the Degradation of Volatile Organic Compounds

Dayton Thomas Horvath
University of Connecticut - Storrs, d@hyphos.com

Synthesis, Characterization, and Photocatalytic Testing of Titania-Based Aerogels for the Degradation of Volatile Organic Compounds

Dayton Thomas Horvath

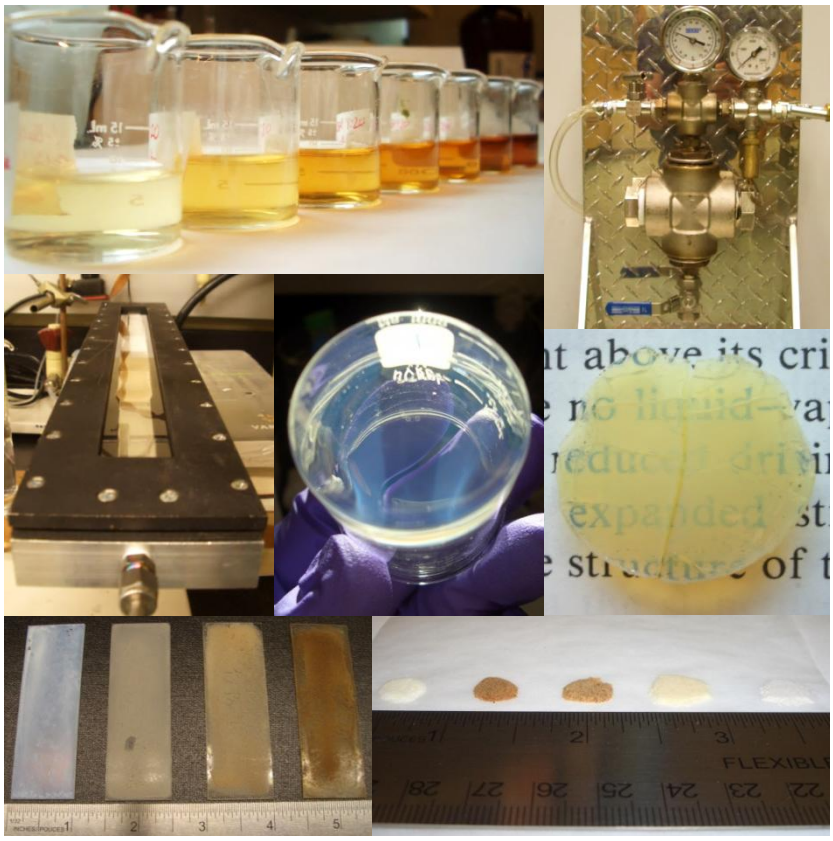

A Thesis

Submitted in Partial Fulfillment of the

Requirements for Graduation as

University Scholar and Honors Scholar

At the University of Connecticut

Storrs

2012

APPROVAL PAGE

University Scholar Thesis

Synthesis, Characterization, and Photocatalytic Testing of Titania-Based Aerogels for the Degradation of Volatile Organic Compounds

Presented by
Dayton Thomas Horvath

Research Advisor: _____
Steven L. Suib

Associate Advisor: _____
Mark Aindow

Associate Advisor: _____
C. Vijaya Kumar

Honors Advisor: _____
Thomas A. P. Seery

University of Connecticut
2012

Acknowledgements

I would like to express my immense gratitude to Dr. Steven L. Suib, who has supported and guided my research and academic studies these last four years. His enabling nature has given me countless opportunities to follow my interests and grow as a scientist and as a student. I am grateful to Dr. Mark Aindow, who has served as an incredibly positive influence in supporting the interdisciplinary nature of my studies. His passion for materials science has passed on to me throughout the last three years and has supplemented my academic and research studies. Furthermore, I'd like to thank Dr. Kumar for serving as my associate advisor, supporting me at multiple key points throughout this endeavor. Lastly, my honors academic advisor, Dr. Thomas Seery, has kept my best interests at heart and has always been a phone call away.

I would like to express my appreciation and thanks to Dr. Stephen Hay; his enthusiasm, time commitment, and incredible knowledge in the field of photocatalysis was vital to the completion of this study. The helpful and productive environment provided by members of Dr. Suib's research group made discussions productive and positive. I'd like to mention Homer Genuino, Justin Reutenauer, Altug Poyraz, David Kriz, Fabian Garces, Chung-Hao Kuo, Tim Coons, Gavin Richards, Eric Njagi, and others in Dr. Suib's research group for helping me in various aspects of this work. The skills and time of Dr. James Stuart, Dr. Lichun Zhang, Bruce Goodwin, and Dr. William Willis have also aided greatly in the technical aspects of the study. Daniel Daleb and Brian Cardinal deserve mention for putting up with my requests and helping assemble the supercritical drying apparatus.

My friends and family have been sympathetic, understanding, and forever supportive of my endeavors in chemistry. Particular thanks go to Alex Capecelatro for introducing me to aerogels, and to my father for the skills and the particularly large wrench needed to perform the

mechanical tasks required in building and maintaining the synthesis and catalysis systems. Lastly, and most importantly, I thank my mother for her endless love and care for my well-being.

This study was made possible by the Office of Undergraduate Research (OUR), the University Scholar Program, the Department of Chemistry's Summer Fund Program, the Honors Program, the Bruce Tomkins Undergraduate Travel Scholarship, an OUR undergraduate research travel grant, the Rizza Scholarship, and the United States Department of Energy.

Table of Contents

List of Figures

List of Tables

Chapter 1:

Chapter 3:

Abstract

The need to degrade volatile organic compounds (VOC's) has grown with recent economic and environmental concerns. Advanced oxidation processes governing breakdown of VOC's have received significant attention due to environmentally conscious practices and objectives. Photocatalysis is a logical approach for VOC removal in air because of minimal energy requirements and ease of implementation. Titania with high pore volume and surface area are synthesized using a modified sol-gel method in conjunction with carbon dioxide supercritical drying. Vanadium doping increases the visible absorption of titania aerogels. Solvent removal is achieved using a custom-built high pressure chamber designed for carbon dioxide supercritical drying. This method preserves pore structure of the sol-gels and results in low density monoliths. Characterization of the materials suggests photoactivity based on high surface area, nanoscale morphology, absorption spectra, and crystallinity. The aerogels were characterized by X-ray powder diffraction (XRD), UV-Visible diffuse reflectance spectroscopy (UV-Vis DRS), scanning electron microscopy with energy dispersive X-ray spectroscopy (SEM/EDXS), transmission electron microscopy (TEM), thermal gravimetric analysis (TGA), and Brunauer-Emmet-Teller (BET) physisorption surface analysis. Materials were tested for activity in degrading propionaldehyde, a model VOC, under ultraviolet light using a flow-through type quartz plate reactor and gas chromatograph. Titania and vanadium-doped titania aerogels exhibited propionaldehyde degradation at a rate of 1.04 μ-mol$cm^{-2}h^{-1}$ confirming the materials as active gas-phase photocatalysts.

Chapter 1: Introduction

1.1 Overview

The intersection of inorganic chemistry and materials science is an area defined by the synthesis, characterization, and application of novel materials. Heterogeneous catalysis is a chemical process in which the catalyst facilitating a reaction exists in a different state of matter from the reactants and products. This branch of catalysis is a vital part of inorganic chemistry research due to the ever increasing demand for chemicals and cleaner processes throughout industry. Being a key part in the industrial revolution, heterogeneous catalysis continues to be an essential field of study to modern-day life.[1]

Metal oxides are widely used as heterogeneous catalysts during and after many industrial processes. The goal of this study was to synthesize photocatalytically active aerogels tailored to the degradation of volatile organic compounds (VOCs) in air. Commercial applicability of photocatalysis directs the focus of this project to titanium oxide (titania), a versatile and inexpensive material. To create porous materials with high surface area, sol-gel synthesis is employed. Sol-gels are inorganic polymeric networks formed through hydrolysis and condensation of metal organic precursors. Two significant advantages were evident in using sol-gel synthesis and supercritical drying to produce titania:

1. high surface area allows for more active sites on the surface, while
2. high pore volume enables faster diffusion of gaseous products.

Once synthesized, characterization of the catalysts suggested photocatalytic activity and potential effectiveness in degrading VOCs. Catalytic goals involved degradation of propionaldehyde under simulated atmospheric conditions.

1.2 Degradation of Volatile Organic Compounds

Within the realm of gas-phase heterogeneous catalysis, two general categories of interest are product synthesis by selective oxidation and reduction[2], and advanced oxidation processes (AOP) for degradation of hazardous chemicals.[3] The latter category receives significant attention as a result of health and environmentally conscious practices and objectives. Volatile organic compounds and their resulting degradation products may be significant in cancer epidemiology and respiratory conditions, as well as ozone depletion. Demeestere et al. report three standard abatement technologies for harmful VOCs in air.[3] Absorption and adsorption technologies are primarily a method of capture rather than degradation, creating contaminated compounds in the process. Thermal and catalytic incineration involves high energy input and may produce harmful byproducts. Thirdly, biotechnological degradation, which is limited to biodegradable compounds and excludes an array of harmful chlorinated VOC's. A fourth possibility lies in photocatalysis, a promising technology for VOC degradation in aqueous and gas-phase environments.[4-7] Current problems regarding the implementation of photocatalysis include catalyst activity and deactivation.[8-10]

1.3 Photocatalysis

The definition of photocatalysis is stated as "a catalytic process during which one or more reaction steps occur by means of electron–hole pairs photogenerated on the surface of semiconducting materials illuminated by light of suitable energy".[3] The benefit of photocatalytic degradation of pollutants is the room temperature oxidation process that uses sunlight or artificial light as an energy source. The ease of implementation in commercial settings in addition to minimal energy requirements makes photocatalysis a logical choice for VOC removal in air.[4]

1.3.1 Gas-phase Photocatalysis

The steps necessary in completing a heterogeneous catalytic cycle include: adsorption of reactants and other species to the surface, activation of the semiconductor surface by ultraviolet radiation producing electron-hole pairs, reaction of adsorbed species on the surface with free radicals produced by trapped electron-hole pairs, and propagation of degradation steps until desorption of products occurs.[11] Photogenerated conduction band electrons and valence band holes are consumed by charge scavengers to form an excited reductant and active oxygen species, namely a redox couple on the catalyst surface mineralizing adsorbed species.[12] The interaction of the molecule with the surface is dependent on the compounds involved, and can be optimized for a given material. The ideal case occurs when sufficient time is given for degradation to occur while desorbing soon after the reaction liberating the active site to repeat the cycle. Because humidity is a significant and variable component in gas-phase applications, studies have been devoted to understanding the role of water at various concentrations on the surface of standard photocatalysts. In the case of titania, competitive adsorption of water at high concentrations causes a decrease in the removal reaction rate, yet is a vital component in photodegradation of ethylene at lower concentrations.[13] Water on titania's surface traps electron-hole pairs and must be regenerated to continue photodegradation. Propionaldehyde is a low molecular weight VOC that has a high dipole moment of 2.52 Debye, resulting in a stronger adsorption to the polar hydroxyl groups populating the TiO_2 surface. The oxidation rate for propionaldehyde can be calculated following the steady state assumptions and a 10% degradation relative to standard uncatalyzed conditions as suggested by Obee and Hay.[13]

1.3.2 Titanium Oxide as a Model Photocatalyst

The most common semiconductor used for environmental catalysis and photocatalysis is Titanium Dioxide (TiO_2), also known as titania. The high photocatalytic activity, favorable band gap energy, low cost, chemical stability, non-toxic nature, and versatility of titania as a catalytic support make titania highly popular for research in this area.[4,12,14] Titania exhibits polymorphism, displaying anatase, rutile, or brookite forms of which the anatase and rutile polymorphs have been the subject of extensive study with respect to photocatalysis.[14, 15] Synthesis of titania, and to a lesser extent, interstitially mixed vanadia-titania is possible through wet impregnation, co-precipitation, adsorption/ion exchange, solid state reactions, and sol gel-based reactions.[16] A standard titania used as a photocatalyst benchmark is Degussa's Aeroxide P25 TiO_2. Synthesized via aerosol flame synthesis[17], P25 consists of a 3:1 mixture of anatase to rutile particles ranging in diameter from 25 to 85 nm in 0.1 μm aggregates.[12, 15] The nonporous 55 m^2g^{-1} photocatalyst's activity resides in its high crystallinity and mixture of phases, which may inhibit electron-hole recombination to some extent.[15]

1.3.3 Vanadium Doping in Titania

The value of interstitial and surface dopants to widen the bandgap of titania and to increase the photoactivity into the visible portion of the solar spectrum has been explored extensively.[12,18,19-23] Vanadium in particular has been a subject of debate in its role to inhibit or enhance the photoactivity of titania. The unique aspect of vanadium is the minimal electrochemical difference between the V^{4+} and V^{5+} oxidation states and similar effective ionic radii to Ti^{4+}. Both metals are available as metal organic isopropoxide precursors and the potential effects of oxidation state control of Ti^{3+}/Ti^{4+} and the corresponding $V^{3+}/V^{4+}/V^{5+}$ states in an

oxide material suggest a controllable synthesis tailoring oxidation state towards optimal photoactivity.

1.4 The Sol-gel Process

A Sol-gel method consists of two subsequent reactions in which alcohol molecules are produced followed by the formation of a ceramic gel similar to glass. The sol-gel process can be modified by varying the precursor concentration, reaction temperature, and different proportions of acid, water, and precursors. Titanium tetraisopropoxide (TTIP) (Alfa Aesar, 97+% pure), is an inexpensive, commonly used titania precursor because the isopropoxide functional groups provide medium activity within the spectrum of titanium organic precursors. Larger functional groups such as n-butoxide are sterically hindered and less active compared to ethoxides or methoxides in hydrolysis and condensation reactions. With this in mind, the concentration of the precursor determines the rate of hydrolysis and condensation to obtain a sol-gel.

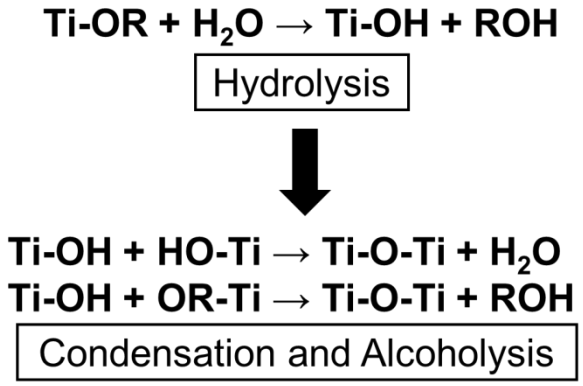

Figure 1: Sol-gel formation process.

The acidic conditions catalyze the above hydrolysis in figure 1 by protonating the negatively charged alkoxide functional groups on the precursor, making them excellent leaving groups. A 3:1 water to metal precursor ratio is commonly used for hydrolysis[24-26], whereas acid concentration varies significantly among sol-gel protocols.[25]

A unique property of sol-gels is their 'bounce', which is a qualitative indicator of shear modulus.[25] A beaker containing the gel is tapped on a hard surface creating movement of the gel which is felt as a vibrating resonance.[25] A gel with a long and pronounced 'bounce' possesses a small shear modulus, and suggests a uniform, continuous polymer network.[25] Aging of sol-gels, also known as syneresis, is a process that occurs after gelation in which the sol-gel shrinks as titanium-oxygen bonds continue to form *via* the condensation step. This process is slow and does not significantly impact the synthesis of aerogels significantly due to the solvent exchange process carried out after gelation has occurred.

1.5 Supercritical Drying of Sol-gels

A sol-gel is mostly solvent held in a metal oxide network making solvent removal necessary before the metal oxide can be utilized. Sol-gels that are thermally treated result in a low surface area xerogel (dried sol-gel with collapsed pore network). If a sufficiently low vapor pressure solvent is present in the sol-gel, an ambigel with higher surface areas between 100 m^2g^{-1} and 300 m^2g^{-1} as well as a more expanded metal oxide network results.[27, 28] Lastly, exchanging the solvent (acetone, 2-propanol, or ethanol) with liquid carbon dioxide makes supercritical drying possible. The low critical point temperature and pressure of carbon dioxide (31.1°C and 72.9 atm) make it safer to achieve supercritical conditions than using alcohols which require high temperature and similarly high pressure.

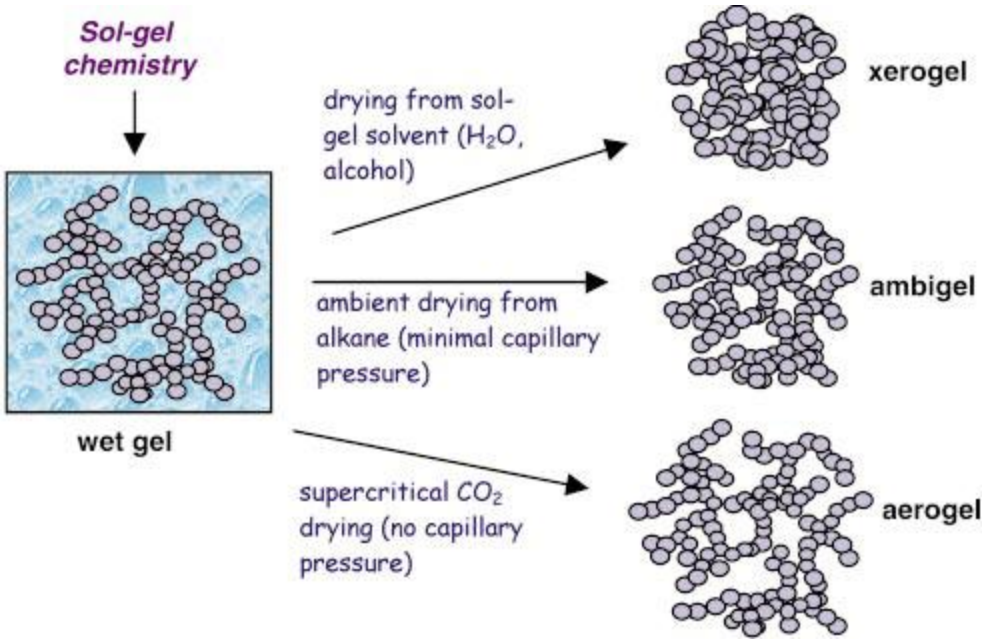

Figure 2: Methods of solvent removal from a wet sol-gel[28]

The primary advantage of supercritical drying is the fundamental elimination of capillary forces which cause pore collapse under atmospheric conditions (as shown in figure 2). The nature of supercritical fluids prevents pore collapse, leaving the gel network intact and providing a high surface area, high pore volume, thermally insulating material.[29] Supercritical drying is advantageous due to the extreme morphology and high surface area catalysts produced, particularly for gas phase photocatalytic VOC degradation.[30]

1.6 Aerogels for Catalysis

A testament to the applicability of aerogels is given by D.R. Rolison in a review on catalytic nanoarchitectures, in which it is stated that "The large surface area and high porosity of aerogels and related mesoporous nanoarchitectures, combined with the molecular-level control of surface character inherent to ligand-stabilized colloid syntheses, should considerably improve the performance of metal-oxide composites as small-molecule oxidation catalysts specifically, and should allow the design of well-controlled architectures of multifunctional 3-D nanocomposites generally".[31] The combination of nano-scale structure, high surface area, and

versatility as supports and bifunctional catalysts make these materials a logical choice for gas-phase catalysis, and photocatalysis given wide band gap semiconductors synthesized using supercritical drying of sol-gels.

Chapter 2: Experimental

2.1 Sol-gel Synthesis and Solvent Exchange

Titanium (IV) tetraisopropoxide (TTIP, 97+% purity), vanadium (V) oxytriisopropoxide (VTIP, 95%-99%), vanadium (III) 2,4-pentanedionate (V(acac), 97%), ammonium vanadate, nitric acid (70%), and 1-butanol were obtained from Alfa Aesar and used as received. Solvents including 2-propanol, 1-propanol, 2-butanol, ethanol and HPLC grade acetone were used as received from Sigma Aldrich. Titania sol-gels were prepared by mixing TTIP:1-BuOH:H_2O:HNO_3 in a 1:20:3:0.08 ratio. For example, 12.33 mL of 1-butanol was split into two beakers of equal volume: A and B.[25, 26, 28, 30, 32-34] Beaker A contained 7.00 mL of 1-butanol to which 2.00 mL TTIP was added. Beaker B contained 5.33 mL of the solvent in addition to 0.034 mL concentrated HNO_3 and 0.363 mL distilled deionized H_2O. The solution in beaker B was added dropwise to the solution in beaker A while stirring. Ideal mixing of solutions prior to gelation was important due to the viscosity of the solutions. For ease of transfer to the supercritical drier, a 20 mL beaker was used to contain the solution. Covering with parafilm prevented premature solvent evaporation and aging for 40h resulted in a clear sol-gel with bounce.[25] A number of different precursor concentrations were tested ranging from a ratio of 1:5 for TTIP to 1-BuOH increasing up to 1:20.

Titania Sol-gel Preparation Varying TTIP:1-BuOH Concentration

TTIP:1-BuOH	1:5	1:10	1:15	1:20
TTIP (mL)	2.000	2.000	2.000	2.000
1-BuOH (mL)	3.075	6.149	9.224	12.329
H_2O (mL)	0.363	0.363	0.363	0.363
HNO_3 (mL)	0.034	0.034	0.034	0.034

Vanadium doping was carried out by creating similar solutions A and B, where A contained both metal organic precursors and approximately half of the solvent volume given. Solution B contained the remainder of the solvent volume and the acidic water. Sonication of

solution A for five minutes in addition to constant stirring yielded a moisture sensitive precursor solution. Sonication and extensive mixing was necessary to ensure homogeneity when using multiple metal organic precursors. Dropwise addition of solution B to solution A in a 20 mL beaker gave a sol-gel with increasing color intensity correlating to higher vanadium concentrations.

Vanadium-doped Titania Sol-gel Preparation Varying VTIP Concentration

VTIP:TTIP Ratio	1:1000	5:1000	10:1000	15:1000	2:100	5:100	10:100
% V Doping	0.1%	0.5%	1.0%	1.5%	2.0%	4.8%	9.1%
TTIP (mL)	2.000	2.000	2.000	2.000	2.000	2.000	2.000
VTIP (mL)	0.002	0.008	0.016	0.024	0.032	0.079	0.159
1-BuOH (mL)	12.329	12.329	12.329	12.329	12.329	12.329	12.329
H_2O (mL)	0.364	0.365	0.367	0.369	0.370	0.381	0.400
HNO_3 (mL)	0.034	0.034	0.035	0.035	0.035	0.036	0.038

When ammonium vanadate was used as a vanadium precursor, 0.5:100 and 1:100 mole ratios of V:Ti sol-gels were prepared. The solid precursor was dissolved in an acidic aqueous solution composed of the same volume of water and nitric acid (0.363 mL H_2O: 0.034 mL HNO_3) and added to a standard 1:20 TTIP:1-BuOH titania sol-gel formulation.

Vanadium acetylacetonate (2,4-pentanedionate) was doped into titania aerogels using the scheme below, following the two solution method to prevent premature sol formation. The solutions gel over time and vary based on conditions, sometimes requiring slight exposure to ambient conditions to complete gelation (typically high dopant concentration sol-gels).

Vanadium-doped Titania Sol-gel Preparation Varying V(acac) Concentration

V(acac):TTIP Ratio	1:1000	5:1000	10:1000	15:1000	2:100	5:100	10:100
% V Doping	0.1%	0.5%	1.0%	1.5%	2.0%	4.8%	9.1%
TTIP (mL)	2.000	2.000	2.000	2.000	2.000	2.000	2.000
VTIP (mL)	0.002	0.012	0.023	0.035	0.047	0.117	0.234
1-BuOH (mL)	12.329	12.329	12.329	12.329	12.329	12.329	12.329
H_2O (mL)	0.364	0.365	0.367	0.369	0.370	0.381	0.400
HNO_3 (mL)	0.034	0.034	0.035	0.035	0.035	0.036	0.038

Solvent washing of sol-gels was carried out in multiple steps, requiring a beaker sufficiently large to allow for inversion of a 20 mL beaker containing a sol-gel. The gel in the beaker was washed three times every 12 to 18 h with 100 to 150 mL of fresh acetone (depending on gel volume of 5 to 8 mL). The beaker containing the sol-gel was inverted in the larger beaker which aided in the diffusion of denser 1-butanol from the sol-gel and less dense acetone into the sol-gel. The sol-gel should be kept sealed in an excess of acetone at all times to prevent solvent evaporation and surface cracking.

2.2 Characterization

2.2.1 X-ray Diffraction (XRD)

Powder XRD patterns were recorded on a Rigaku Ultima IV X-ray diffractometer operated at 40 kV and 44 mA using Cu K_α radiation (1.5418 Å). Crystallite size was estimated using the Halder-Wagner method in the Rigaku PDXL software (v.1.4.0.0) for peaks over 40° 2θ compared to a LaB_6 standard pattern (ICDD Card #00-059-0332). All patterns were taken as continuous scans at 2.00° min^{-1}.

2.2.2 Field Emission Scanning Electron Microscopy (FE-SEM)

Aerogel morphology was imaged using a Zeiss DSM 982 Gemini FE-SEM with a Schottky emitter operating at 2.0 kV with a beam current of 1.0 mA as well as a FEI nanoSEM 450. Gold palladium sputter-coated silicon chips were mounted on aluminum stubs with ample silver paint. After drying, catalyst-ethanol suspensions were pipetted onto silicon chips and placed under vacuum for 24 h prior to analysis.

2.2.3 Transmission Electron Microscopy (TEM)

TEM studies were conducted on a JEOL JEM-2010 FasTEM operating at 200 kV. Aerogel samples were loaded onto carbon coated copper grids from catalyst-ethanol suspensions and dried at room temperature and then placed under vacuum for 24 h prior to analysis.

Subsequent image analysis and d-spacing calculations were conducted using Gatan DigitalMicrograph software (v.3.9.0).

2.2.4 Thermal Gravimetric Analysis / Differential Scanning Calorimetry (TGA/DSC)

Thermal studies were carried out using a TA Instruments SDT Q600 TGA/DSC and analyzed using TA Instruments Universal Analysis 2000 software (v.4.7A). All samples were characterized under air atmosphere at a flow rate of 100 $mLmin^{-1}$.

2.2.5 Brunauer-Emmet-Teller Nitrogen Physisorption (BET)

BET porosity and surface area measurements were performed using a Quantachrome Autosorb iQ_2 automated gas sorption analyzer. Samples were degassed at 150°C for 5 h prior to analysis. Surface area was determined by multi-point Brunauer-Emmett-Teller (BET) method while pore volume was calculated from the adsorption branch of the isotherm using the Barrett-Joyner-Halenda (BJH) method. Both methods were employed using the Quantachrome ASiQwin software (v.1.11).

2.2.6 Energy Dispersive X-ray Spectroscopy (EDX)

Elemental analyses of aerogels were carried out using an Amray model 1810D scanning electron microscope operated at 20.0 kV equipped with an Amray model PV 9800 EDX system. Each catalyst was mounted on aluminum stubs using carbon tape and put under vacuum for 24 h prior to analysis.

2.2.7 UV-Vis Diffuse Reflectance Spectroscopy (UV-Vis DRS)

Diffuse reflectance spectroscopy analysis was conducted using a Shimadzu UV-2450 UV-Vis spectrophotometer with ISR-2200 integrating sphere attachment. Samples were prepared by adding 0.030 g catalyst to 3.00 g barium sulfate, grinding in a mortar and pestle for 5 min, compressing in a dye, and taking a spectrum against pure barium sulfate (Wako Chemical Co.)

2.3 Manuclave Construction and Operation

To take advantage of carbon dioxide's low supercritical point and medium polarity, an autoclave-like apparatus was constructed based on readily available schematics found online.[35] The materials engineer who designed, assembled, and tested the design affirmed the system's feasibility for the purposes of this study. A comprehensive parts list is available with basic instructions for assembly and welding required. Modifications made to the original design[35] include a needle valve at the outlet for controlled depressurization, a window to observe liquid carbon dioxide within the system, the custom manufacture of an aluminum stand, and an outlet line to a fume hood.

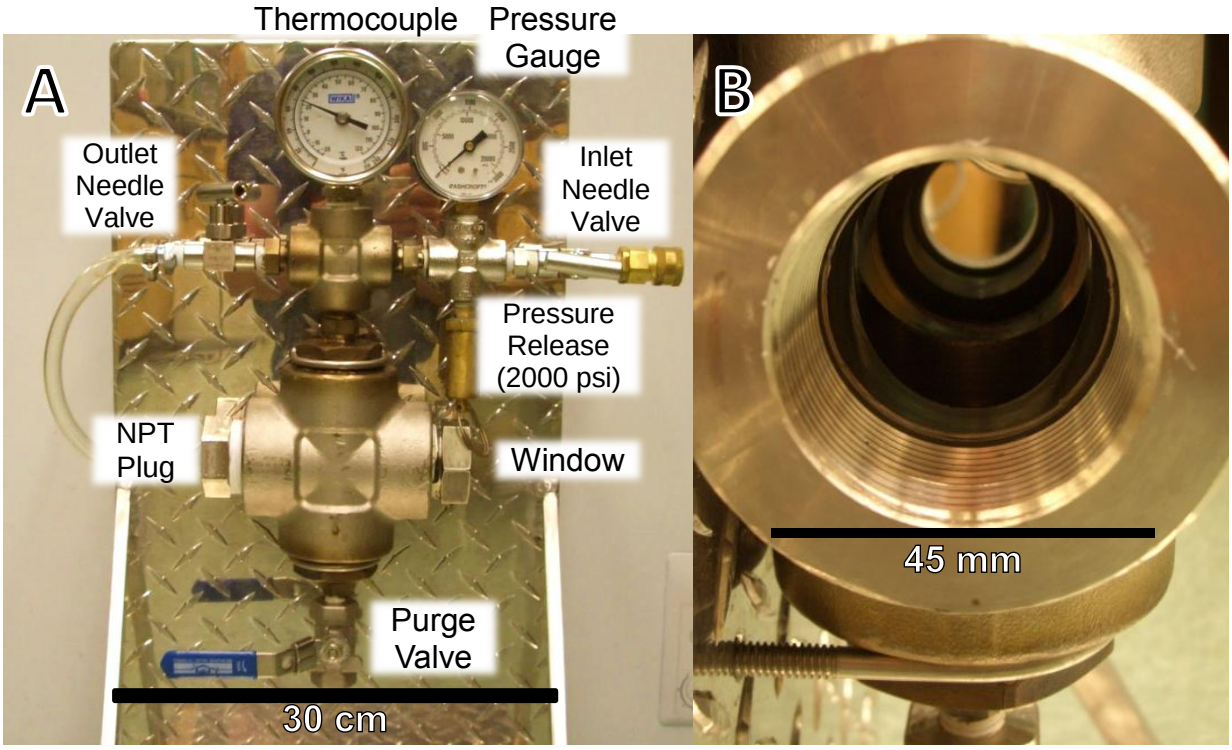

Figure 3: Supercritical drier components (A) and interior (B)

The NPT threaded 1¾ inch (44.5 mm) opening allowed for a 20 mL beaker to be loaded horizontally and stood up in the center of the cross. Approximately 7 ml of acetone was added to keep the sol-gel from drying out during the loading process. A pipe plug was tightened with three layers of Teflon tape with a 1¾ inch box end wrench. The manuclave was slowly filled

with liquid carbon dioxide through the inlet needle valve, building pressure in the system until the gas was sufficiently pressurized to become a liquid. The liquid continued to flow in from the top of the manuclave, washing the beaker containing the sol-gel and excess acetone. The system was purged repeatedly through the bottom and the solid white carbon dioxide-acetone mixture was collected in a beaker for measurement. Appropriate lab attire including thermally insulated gloves was necessary to prevent the carbon dioxide-acetone mixture from causing freeze burns while operating the purge valve and handling the collection beaker. After the appropriate wash cycles were performed and the system taken through supercritical conditions, the outlet needle valve allowed for slow depressurization of the system to a fume hood via plastic tubing over 3 to 6 h. Containment of the manuclave in a standard deep freezer during purge cycles and the supercritical steps adds an additional level of protection and enables consistent syphoning of liquid carbon dioxide from the tank pictured in figure 4B.

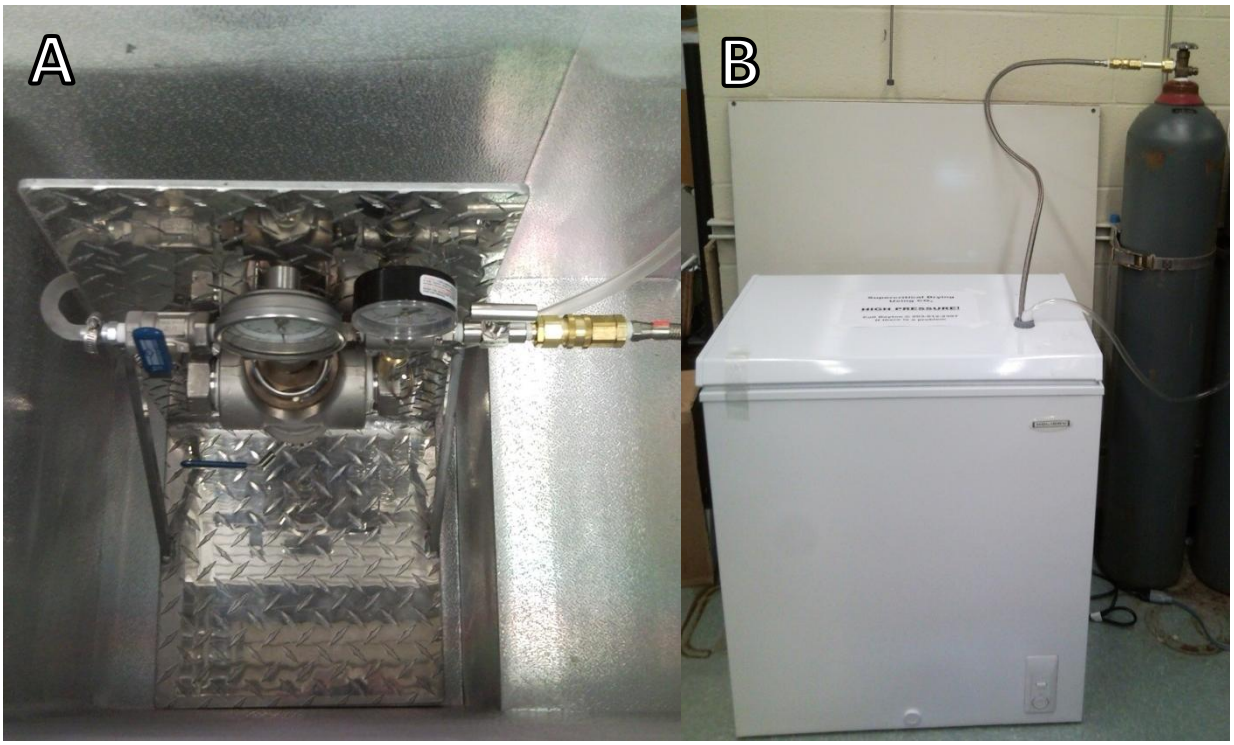

Figure 4: Supercritical drier within freezer (A) and liquid carbon dioxide source near freezer (B)

The carbon dioxide cylinder contains a syphon tube providing liquid carbon dioxide through the high pressure line to continue the solvent extraction process. The system is meant for low temperature use (below 100°C) and rated up to 2000 psi, with the standard solvent extraction procedure remaining under 1400 psi at 60°C.

2.4 Supercritical Drying and Processing of Sol-gels

The three purge cycles were performed every 12 or 24 h depending on sol-gel volume (5 to 8 mL). Approximately 1500 mL of loosely packed solid carbon dioxide was purged from the system each cycle. The volume of acetone remaining after carbon dioxide evaporation was recorded and compared to initial solvent volume. To minimize thermal strain on the sol-gel network, the temperature of the system was kept below 5°C during each cycle. Additional purges were necessary if acetone was not completely washed from the manuclave.

To attain supercritical conditions of 1071 psi at 31°C or higher, interplay between a heat gun and the needle outlet valve provided the temperature and pressure control necessary to reach the following conditions.

- The manuclave body was heated to 42°C and 1300 psi in small steps from -20°C to 42°C. Carbon dioxide was slowly released as the manuclave was heated to keep pressure from changing drastically. Pressure fluctuation was kept within ±100 psi from the steady pressure value.
    - -20°C to -10°C: 800 psi base point
    - -10°C to 0°C: 900 psi
    - 0°C to 10°C: 1000 psi
    - 10°C to 20°C: 1050 psi
    - 20°C to 30°C: 1100 psi
    - 30°C to 42°C: 1200 psi

- Finish at 42°C and 1300 psi

- Temperature and pressure were held for thirty minutes followed by additional heating to the 55°C-60°C range with a pressure of 1400 psi.
- Temperature and pressure were held for twenty minutes, after which the system was reheated to 55°C-60°C and pressure gently released as needed to attain 1300 psi.
- The manuclave was heated to 60°C at a pressure of 1300 psi.
- Slow depressurization of the manuclave over 3 to 6 h completes the process.

Slowly open all valves once the manuclave is depressurized, remove the NPT plug and gently pull beaker out of manuclave containing the supercritically dried sol-gel. The aerogel monolith was lightly ground using an agate mortar and pestle in an environment with minimal air movement. Subsequent heat treatments to convert the amorphous aerogels to anatase were carried out for six hours under flowing air, being cautious not to disperse the low density powders.

2.5 Quartz Plate Photocatalytic Reactor Design and Method

A flow-through type glass-plate photocatalytic reactor was used in conjunction with a gas chromatograph equipped with a flame ionization detector to study oxidation of propionaldehyde by titania. A Spectroline XX-15A lamp with two black-light bulbs was used to illuminate glass slides (1" x 3" Fisher Scientific) spray coated with photocatalyst. The lamp intensity was adjusted by varying the distance from the reactor surface to the lamp, giving an intensity of 2.7 $mWcm^{-2}$ three inches above the slides and 1.3 $mWcm^{-2}$ at six inches above the slides. A UV intensity meter (Oriel UVA Goldilux) was used to check lamp intensity as well as check coated slides for sufficient catalyst loading to prevent UV bleed through. A 5% w/w water solution of Degussa P25 or titania aerogel catalyst was deposited on glass slides and dried at 110°C for two

hours. Multiple coatings were performed until a catalyst loading of 15 to 20 mg per slide was achieved, equating to a coating of 0.97 $mgcm^{-2}$ reported to be optically dense to UVA[13] and checked with a UVA meter. Airgas provided a certified specialty gas containing 1% (10,000 ppm) propionaldehyde in nitrogen. All other gases were ultra-high purity, with air flowing through a bubbler containing distilled deionized water for the humidity component of the system. The overall flow rate of 25 $mLmin^{-1}$ was composed of 5 $mLmin^{-1}$ propionaldehyde in nitrogen and 25 $mLmin^{-1}$ air, creating approximately 1700 ppm pollutant level in the reactor. EPDM rubber gaskets between the quartz plate and the aluminum reactor block sealed the reactor.

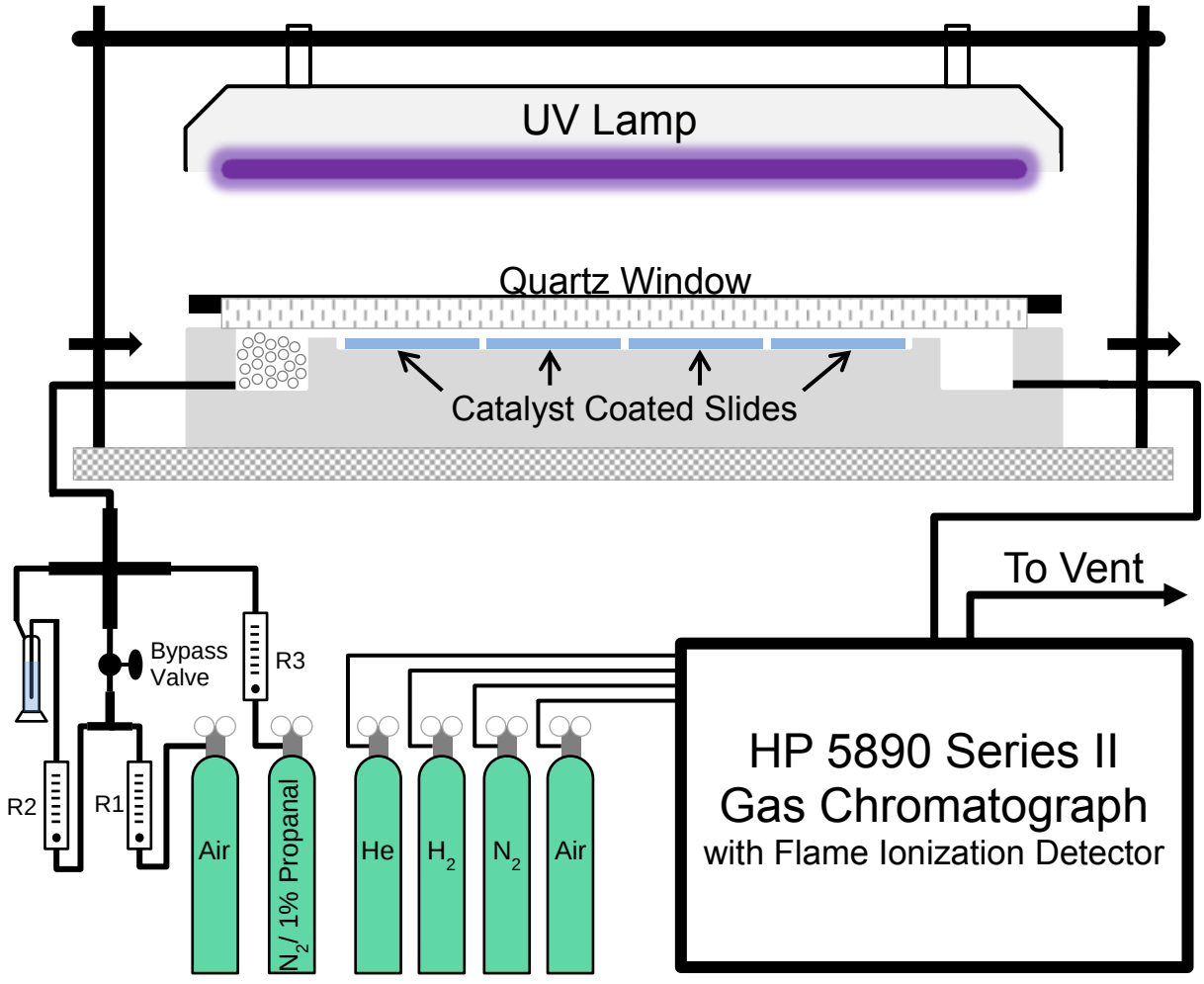

Figure 5: Quartz plate photoreactor and gas flow diagram.

A nitrogen actuated on-line injector with a 1mL loop was utilized in the HP 5890 Series 2 Gas Chromatograph with accompanying HP 3396 Series 3 Integrator. A 50% cyanopropyl, 50% phenylmethyl fused silica capillary column (30 m x 0.53 mm ID x 0.5 µm film thickness) from Quadrex was employed for this study. Column temperature was set at 110°C with 5°C min^{-1} ramp rate to 150°C. Injector temperature was set to 120°C while the detector inlet temperature was set to 130°C. Column flow was set with a 10:1 split ratio giving 3 mL/min prior to oven preheating.

Chapter 3: Results and Discussion

3.1 Synthesis of Aerogels

The preparation of aerogels requires high quality sol-gels based on clarity, bounce, and time to gelation.[25] Following the successful preparation of ethanol-based titania sol-gels[26], a comparison of solvents was carried out with varying TTIP to solvent mole ratios. The use of straight-chain alcohols gave clear gels with more noticeable bounce as carbon chain length of

Qualitative Analysis of Titania Sol-gels using Different Solvents

Solvent	Gel Quality	Gelation Time*
ethanol	Clear, brittle gel	1-5 min
2-propanol	Cloudy gel, white precipitate	5-60 sec
1-propanol	Clear gel	12 min-36 h
2-butanol	Cloudy gel, white precipitate	30 min
1-butanol	Clear gel	1 min-40 h
*Refers to all Ti:1-BuOH ratios for which a gel was obtained.		

solvent increased. Gelation time was determined as the time required for the sol-gel to retain its form when inverted. Using 1-butanol as the solvent provided the greatest flexibility in synthesis conditions compared to other straight chain and branched alcohols tested. The use of branched alcohols did not produce homogenous sol-gels, a white precipitate was observed in the otherwise clear sol-gel. This precipitate is commonly observed and is produced exclusively using different Ti:solvent:H_2O mol ratios for the synthesis of sols and nanoparticles.[36, 37] Within the Ti:1-BuOH

Gelation Time as a Function of Precursor Concentration

Gel Ratio (Ti:1-BuOH)	Gelation Time	Clarity
1:5	<1 sec	Precipitate
1:10	1 min	Clear
1:15	45 min	Clear
1:20	36 hrs	Clear

sol-gels, a non-linear increase in gelation time was observed in addition to an increase in bounce with Ti:1-BuOH ratio. The 1:20:3:0.08 Ti:1-BuOH:H_2O:HNO_3 was selected as the optimal sol-gel for aerogel synthesis based on consistency of gel-time during repeated syntheses, clarity and prominent bounce compared to other sol-gels in the series. The 1:20 titania aerogel had a surface

area of 384 m^2g^{-1} and pore volume of 1.231 cm^3g^{-1} compared to the 1:10 titania aerogel's 440 m^2g^{-1} surface area and 1.422 cm^3g^{-1} pore volume. Similar surface areas and pore volumes between the two materials along with higher absorption in the 1:20 titania's diffuse reflectance spectra further support its selection as the optimal sol-gel (see appendix). All aerogels are referred to as titania for ease of distinction from Degussa P25 TiO_2 except in figures and tables for the sake of brevity. All titania aerogels referred to from hereon were synthesized using the 1:20 Ti:1-BuOH ratio. Heat treatment temperatures in tables refer to the 1:20 titania aerogel.

Doping vanadium into the titania aerogel was accomplished using three vanadium precursors included at different points of sol-gel synthesis. The availability of vanadium (V) oxytriisopropoxide (VTIP), a vanadium metal organic precursor with matching isopropoxide ligands to TTIP, was ideal for preparing TTIP/VTIP mixtures in 1-butanol prior to hydrolysis. The synthesis accounted for total moles of metal in the sol-gel and kept water and acid ratios constant. Sol-gels of seven dopant levels were prepared: 0.1%, 0.5%, 1.0%, 1.5%, 2.0%, 4.8% and 9.1% vanadium. All but 1.5% and 2.0% V-Ti samples were supercritically dried and characterized. Ammonium vanadate was used as a comparison precursor by being dissolved in

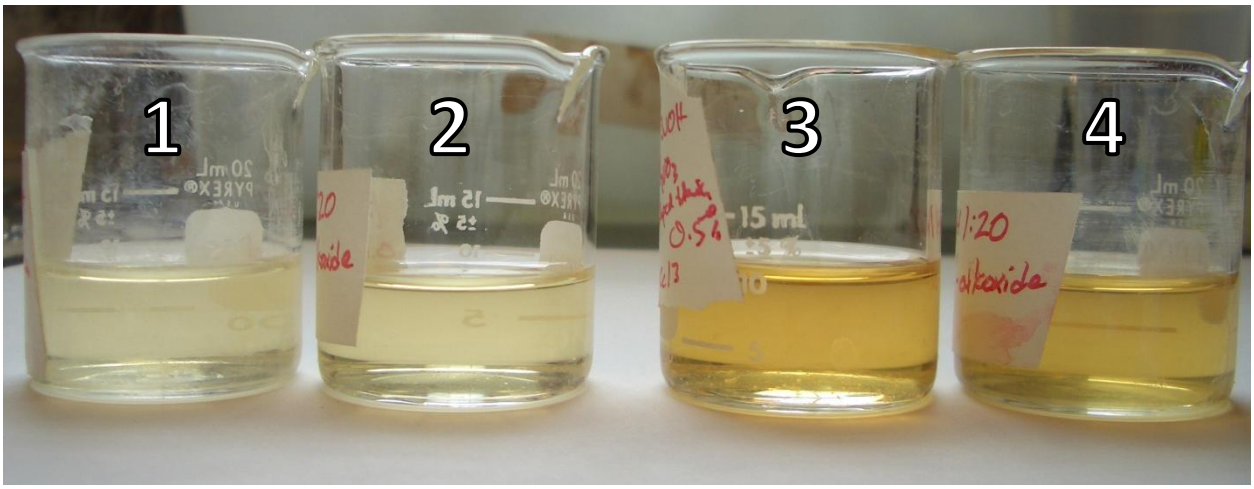

Figure 6: Comparison of 0.1% and 0.5% vanadium doping using ammonium vanadate in beaker one and three, and VTIP in beakers two and four.

the aqueous components of the sol-gel synthesis prior to mixing and gelation. The doping concentration was limited to 0.1% and 0.5% due to the solubility limit of NH_4VO_3 in 1:0.08 H_2O:HNO_3. Figure 6 shows the consistent color between VTIP and NH_4VO_3 doped titania sol-gels confirming the irrelevance of vanadium (V) doping from an aqueous VO_3^- ion or a metal organic $VO(OPr^i)_3$ compound. A comparison of UV-Vis diffuse reflectance spectra of the supercritically dried aerogel analogs to sol-gels three and four in figure 6 confirms the synthesis method as flexible when considering liquid or solid precursors (see appendix).

To determine the effect of vanadium precursor oxidation state on the titania aerogel, Vanadium (III) acetylacetonate was used to prepare the same concentrations of V-Ti sol-gels as VTIP. The resulting sol-gels in figure 7 showed increasing color intensity corresponding to

Figure 7: Increasing mole ratio of V:Ti in titania sol-gel using
VTIP (A) and V(acac) (B). Left to right: 0%, 0.1%, 0.5%, 1%, 1.5%, 2%, 4.8%, 9.1%

increasing vanadium concentration. The color resembles the orange oxide of vanadium, V_2O_5, which is typically attributed to d-d transitions of V^{4+} in distorted octahedral symmetry as well as V^{5+} in an octahedral environment.[38] The 4.8% and 9.1% V-Ti sol-gel exhibited significantly darker color and longer gelation times with the V(acac) precursor compared to VTIP. The reflection of red visible light qualitatively indicates the absorption of shorter wavelength blue light, a preliminary indication of titania's absorption band expanding towards the visible part of the electromagnetic spectrum. The darker color sol-gels from V(acac) can be attributed to the complexation of acetylacetone to titania in observable amounts. Acetylacetone binds to four-coordinated titanium preferentially over isopropoxide ligands, forming an orange five-coordinate species, $Ti(OPr^i)_3acac$, in which acetylacetone acts as a bidentate ligand. This color from the five-coordinate titanium species remains due to the strong binding of acetylacetone to the TTIP molecules[39] and contributes to the sol-gel's color in addition to the color present from vanadium doping. Supercritical drying of the sol-gels (5 to 8 mL volume) produced small translucent monoliths as shown in figure 8. Weighing 0.5 g on average, the monoliths were fragile and in some cases had mild cracks due to swelling during solvent exchange from 1-butanol to acetone.

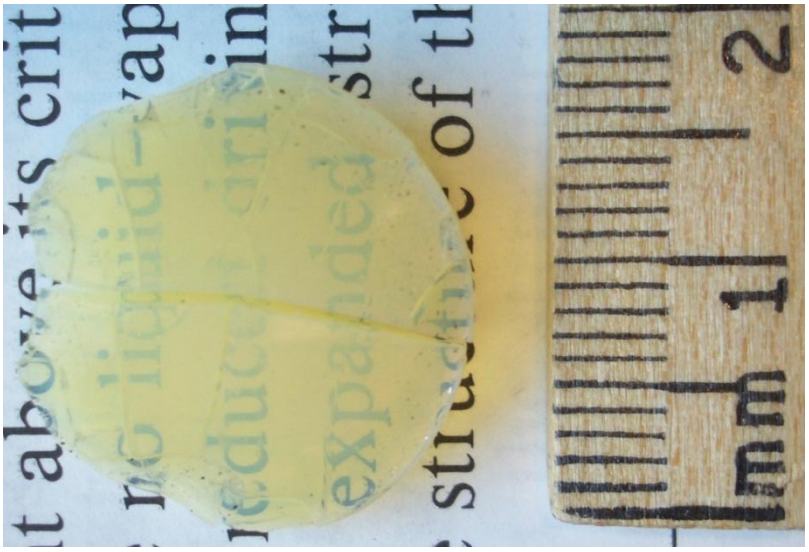

Figure 8: Standard titania aerogel monolith

3.2 Aerogel Characterization

3.2.1 Structure and Crystallinity: XRD, TEM, TGA/DSC

Aerogels processed using supercritical carbon dioxide were exposed to maximum temperatures of 50°C during synthesis and resulted in materials amorphous to X-ray diffraction. Heat treatment of aerogel powders is a critical step in producing anatase titania, the more active polymorph compared to rutile for VOC degradation. Consecutive heat treatments at 50°C intervals showed the evolution of the (101) miller plane at 25° 2θ in figure 9. Starting at 300°C, standard titania aerogel began significant crystal growth until 450°C. All V-Ti doped aerogels had similar structural changes to anatase at a slightly higher temperature of 350°C with the exception of the 9.1% V-Ti aerogel. The inclusion of a high vanadium loading inhibited the formation of anatase until 400°C (see appendix). Anatase formed clearly at 400°C in all aerogel materials without additional crystallinity observed at 450°C; this is a relatively high temperature given the minimal heat treatment desired to preserve pore volume and surface area.

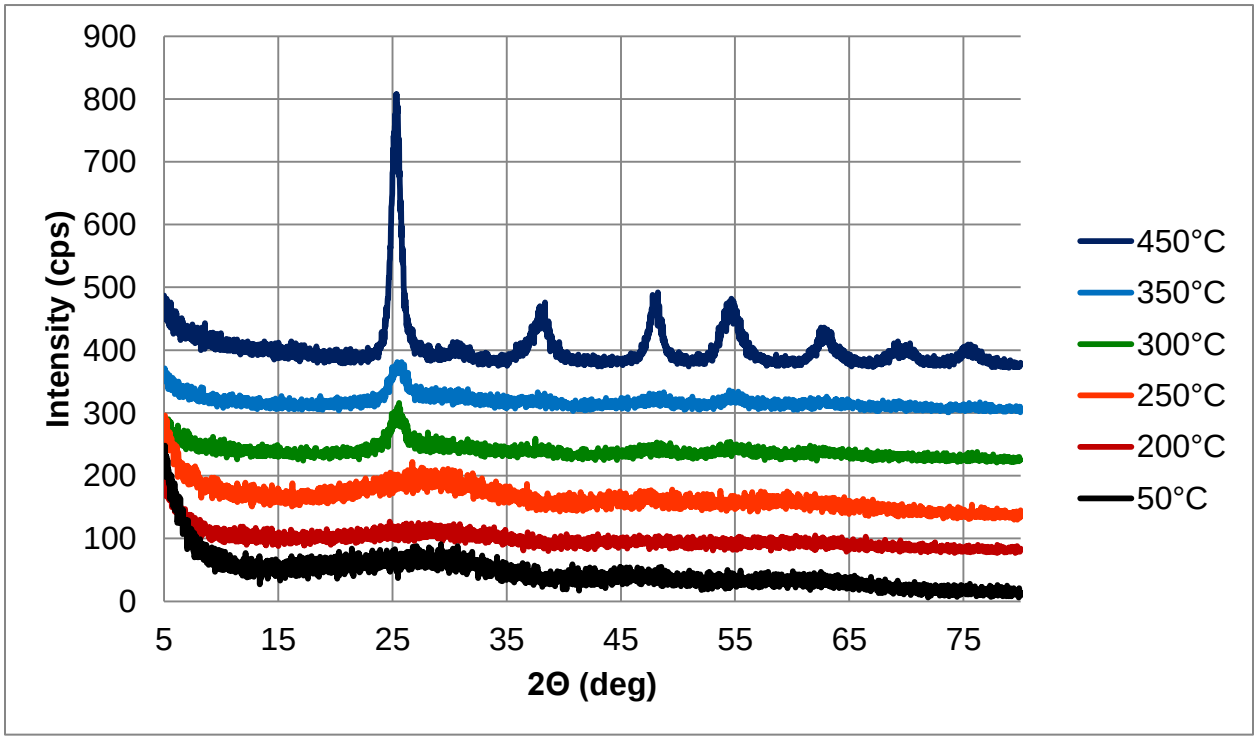

Figure 9: Diffraction patterns of heat treated titania aerogel

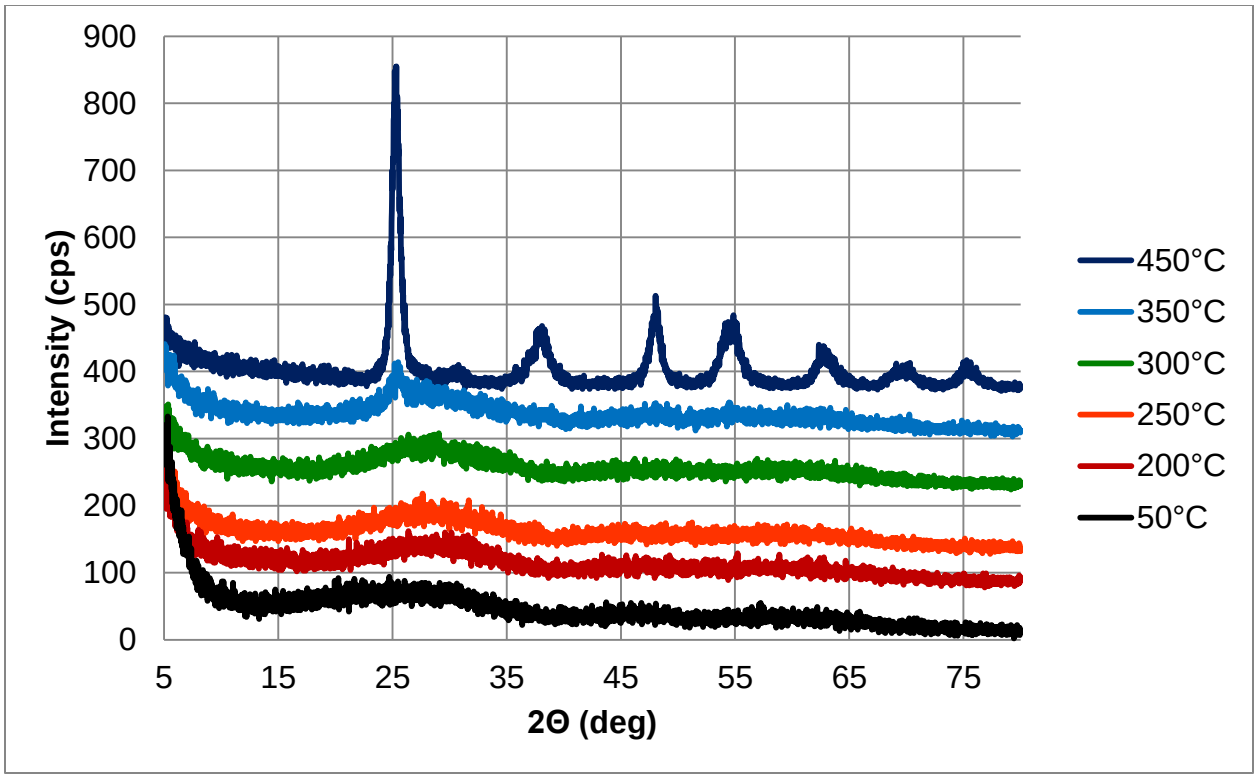

Figure 10: Diffraction patterns of heat treated 0.1% V-Ti aerogel

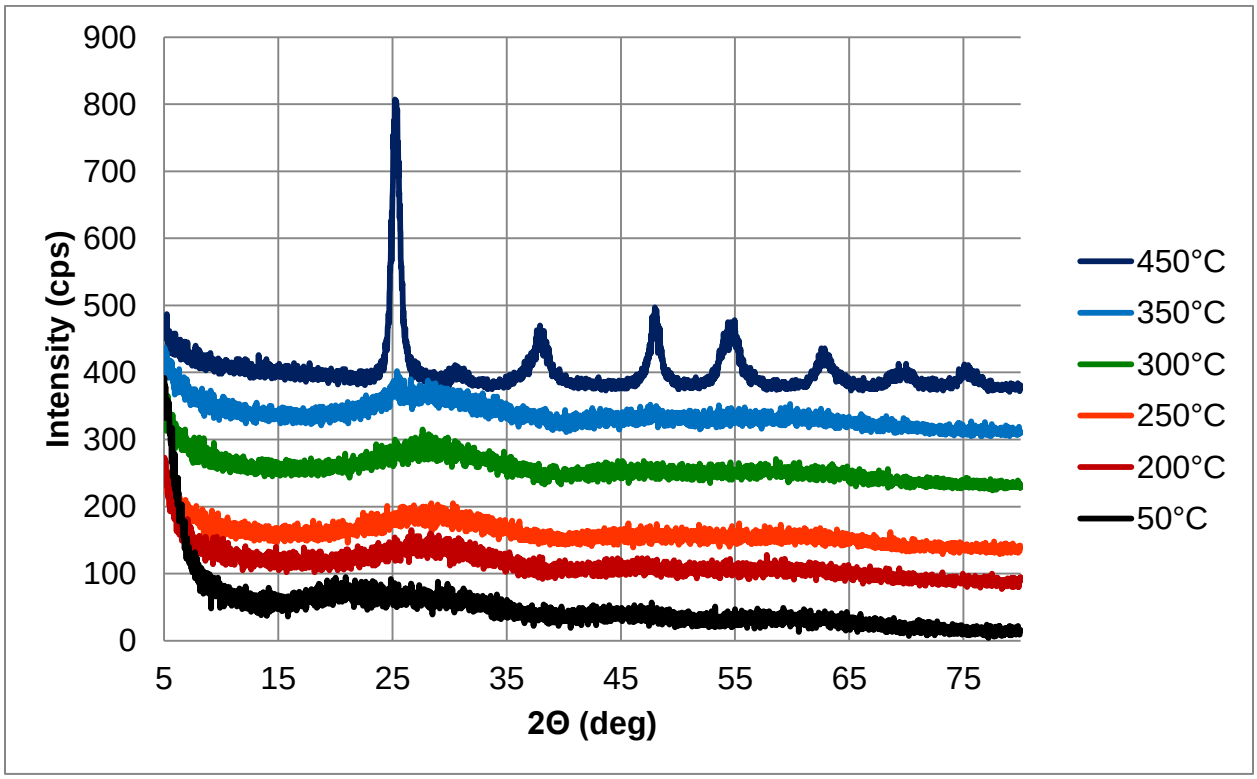

Figure 11: Diffraction patterns of heat treated 0.5% V-Ti aerogel

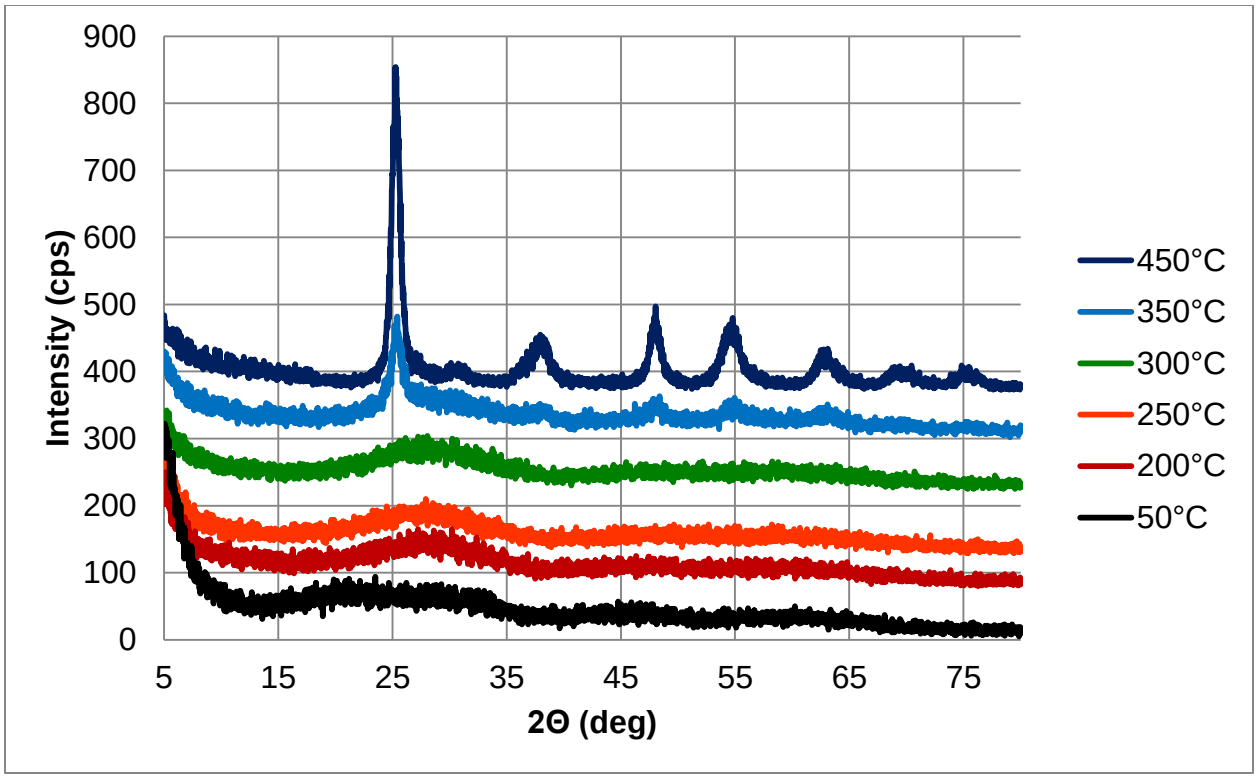

Figure 12: Diffraction patterns of heat treated 1.0% V-Ti aerogel

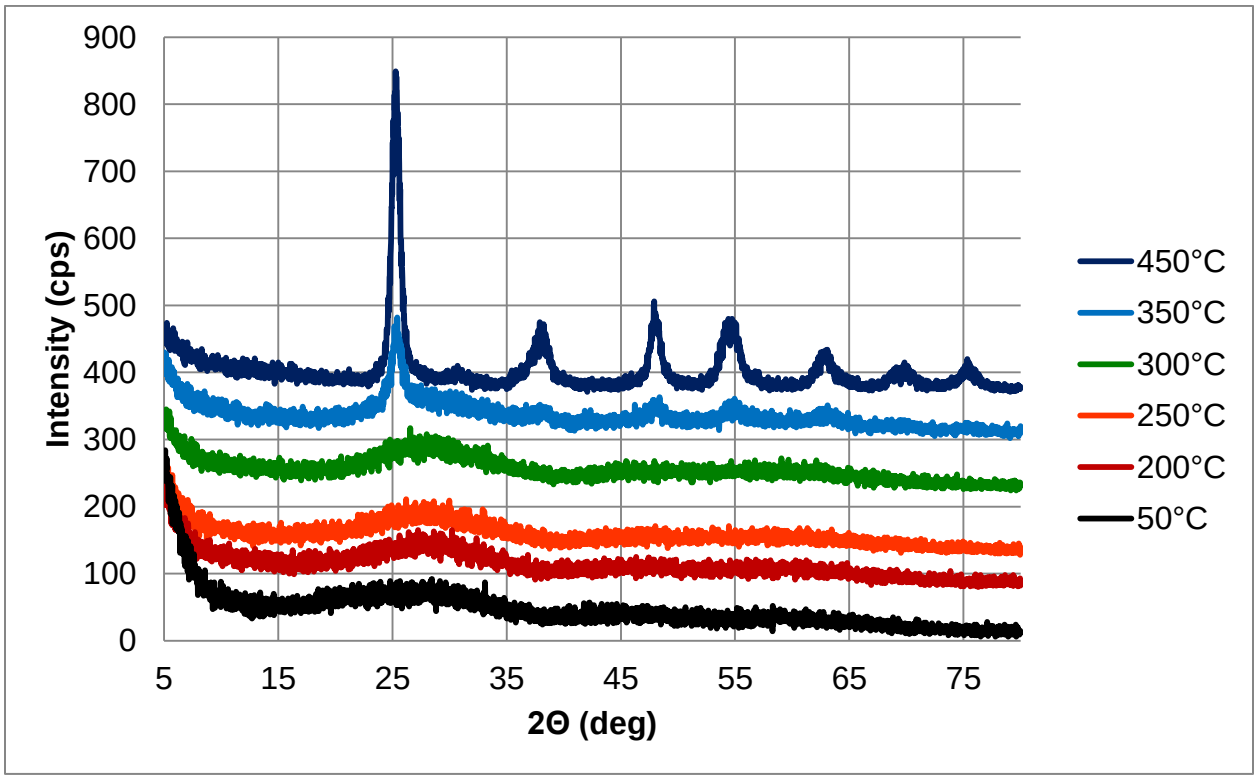

Figure 13: Diffraction patterns of heat treated 4.8% V-Ti aerogel

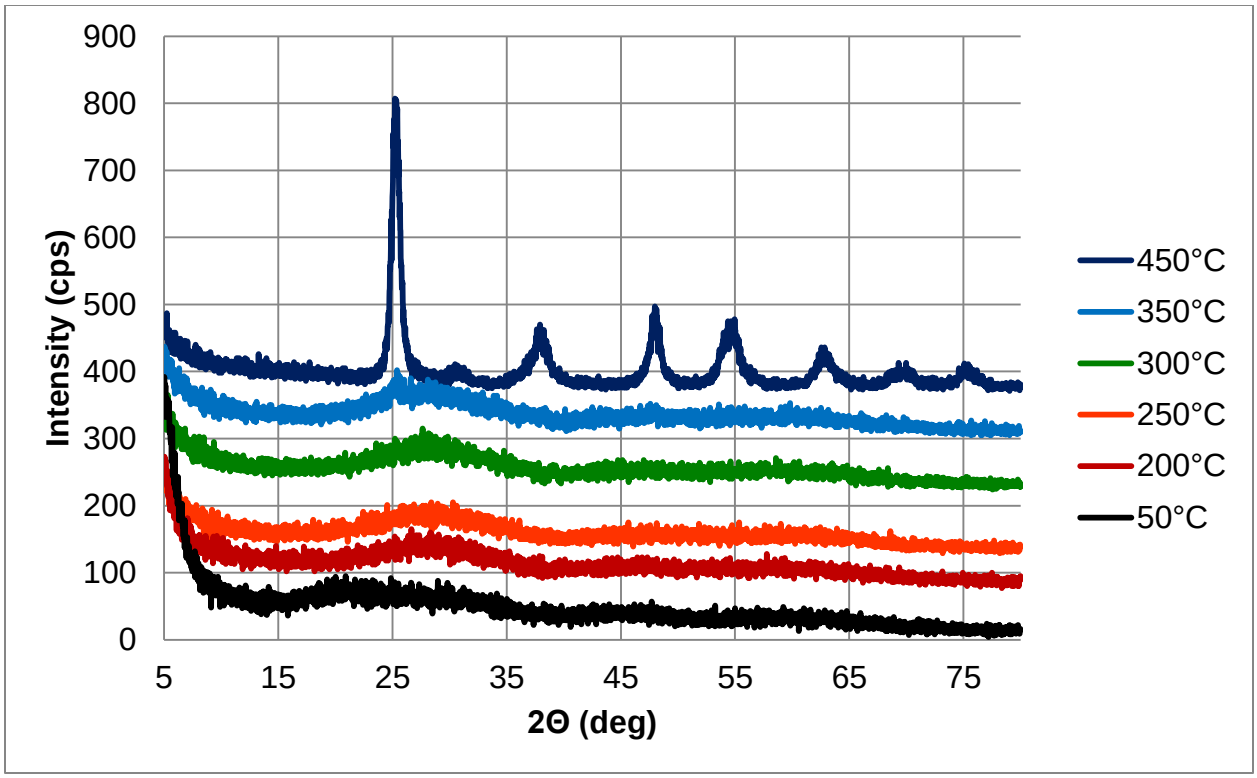

Figure 14: Diffraction patterns of heat treated 9.1% V-Ti aerogel

Crystallite size estimates were derived from figures 9-14 using Halder-Wagner plots of the anatase peaks above 40° 2θ (see appendix). A comparison to Degussa P25 was included to verify aerogel crystallite sizes in relation to accepted P25 crystallite sizes as well as to an external LaB_6 standard for peak width normalization. The anatase peaks for Degussa P25 gave

Halder-Wagner Crystallite Size Determination

Material:	XRD Crystallite Size (nm)
Anatase Peaks Degussa P25 TiO_2	18.3
Rutile Peaks Degussa P25 TiO_2	45.2
Standard Titania Aerogel 450°C	4.8
0.1% V-Ti Aerogel 450°C	5.3
0.5% V-Ti Aerogel 450°C	5.1
1.0% V-Ti Aerogel 450°C	4.2
4.8% V-Ti Aerogel 450°C	5.5
9.1% V-Ti Aerogel 450°C	8.4

an average crystallite size of 18.3 nm while rutile gave an average of 45.2 nm (see appendix for P25 diffraction pattern). Compared to literature values stating 30 nm crystallites[12], or more

specifically 25 nm anatase and 85 nm rutile crystallites[15], the method for ascertaining crystallite sizes is effective. The average crystallite size among aerogels excluding 9.1% V-Ti is 5.0±0.5 nm, with the high vanadium concentration increasing the minimum stable crystallite size to 8.4 nm. Although sufficient amounts of vanadium are present to slightly increase crystallite size in the 9.1% V-Ti aerogel, a V_2O_5 phase was not recorded in figure 14. Furthermore, the consistent sizes between the titania aerogel and V-Ti aerogels suggests that vanadium was successfully incorporated into the titania aerogel in concentrations from 0.1% to 9.1%. Possessing a much smaller anatase crystallite size compared to P25, titania aerogels potentially exhibit quantum mechanical properties[12] as well as increased surface area for surface-limited VOC degradation.

Both standard and high resolution transmission electron microscopy show the porous nanoparticle-like network characteristic of titania aerogels. Size determination of particles supports the crystallite size analysis performed on diffraction patterns. Verification of the particle shape uniformity as well as minimal deviation in particle size is seen in figure 15A and 15B. This nanoscale framework possesses partial crystallinity when heat treated at 275°C as seen in figure 15C and 15D, suggesting that X-ray diffraction's ability to discern crystallinity in a material at the onset is limited as a bulk measurement. Although the particles 16A are more densely packed as expected by heat treatment at a 450°C, the particle diameter remains in the 5 nm to 10 nm with no significant change in shape compared to 15B. Crystallinity at 450° is observed throughout the images as lattice fringes are clearly visible in figure 16B compared to a lesser extent in 15D. The addition of vanadium into the titania framework did not affect particle shape or crystallinity, confirming nearly identical X-ray diffraction patterns for titania and V-Ti aerogels at 450°C. Slightly larger crystallites are visible in figure 17B compared to 16B, supporting the crystallite sizes previously determined.

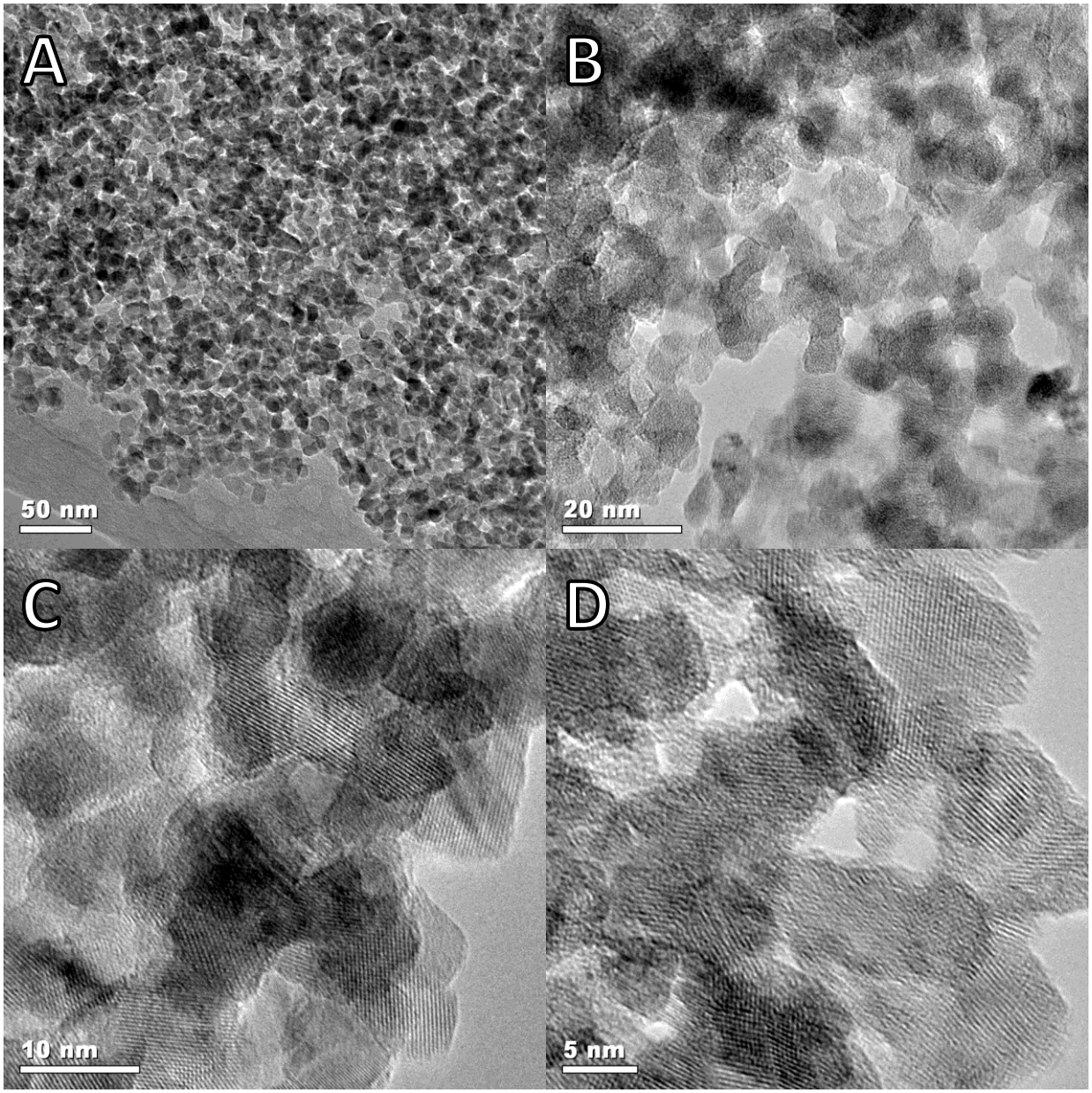

Figure 15: TEM images of standard titania aerogel 275°C

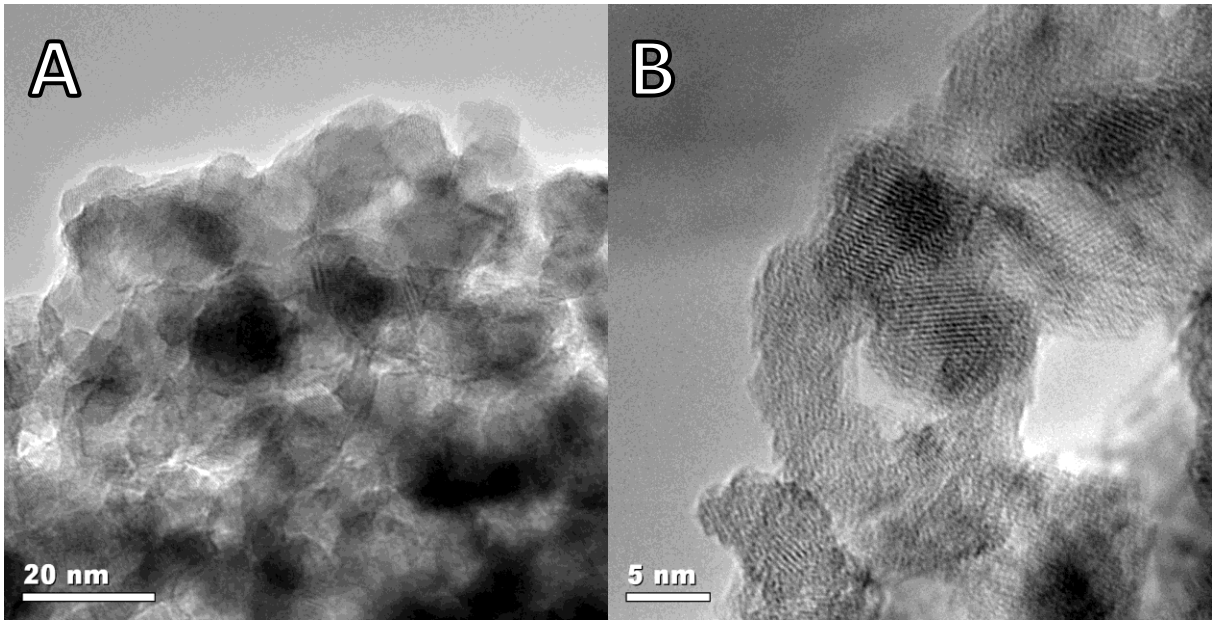

Figure 16: TEM images of standard titania aerogel 450°C

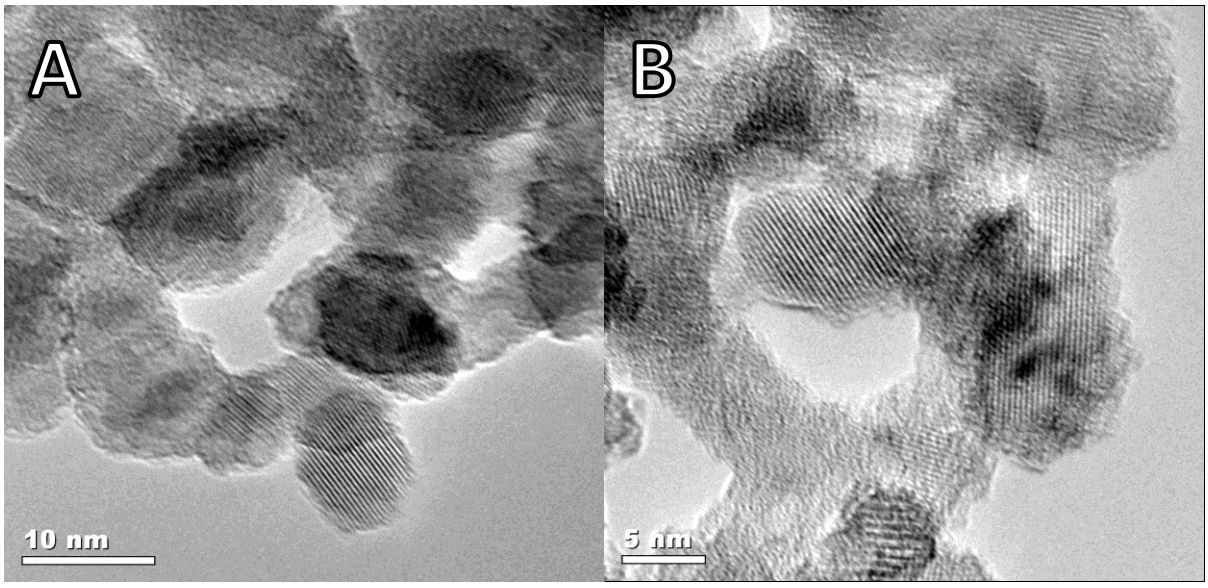

Figure 17: TEM images of 9.1% V-Ti aerogel 450°C

Lattice measurements were carried out on a number of TEM images and averaged to detect changes in the d-spacing of the (101) plane of titania and 9.1% doped V-Ti aerogels heat treated at 450°C. Given the accepted value of the most visible lattice spacing in each specimen, 3.517 Å, average d-spacings for all three aerogels were found to be within two standard deviations. The experimental value of 3.469 Å for the 9.1% V-Ti aerogel lies between the two

titania aerogel values, indicating that no lattice strain or distortion is apparent even at 9.1% vanadium doping. An examination of effective ionic radii reveals that four coordinate Ti^{4+}

Lattice Spacing of Standard and Doped Titania Aerogels

	275°C	450°C	9.1% V-Ti 450°C
Average d-spacing (Å)	3.4855	3.437	3.469
Standard Deviation (Å)	0.0304	0.046	0.050

See appendix for image sections analyzed

measures 0.42 Å compared to 0.355 Å for four coordinate V^{5+}, indicating that substitution of V^{5+} into titania would not put a strain on the material, even if five coordinate V^{5+} or Ti^{4+} were present given that both possess radii similar to four coordinate Ti^{4+}.[40] The combination of thermal gravimetric analysis with differential scanning calorimetry elucidated the behavior of standard titania aerogel at a 2° min^{-1} heating rate. The initial jump in heat flow shown in figure 18 in the dotted box and expanded at the right indicates a change in the material. Both diffraction pattern

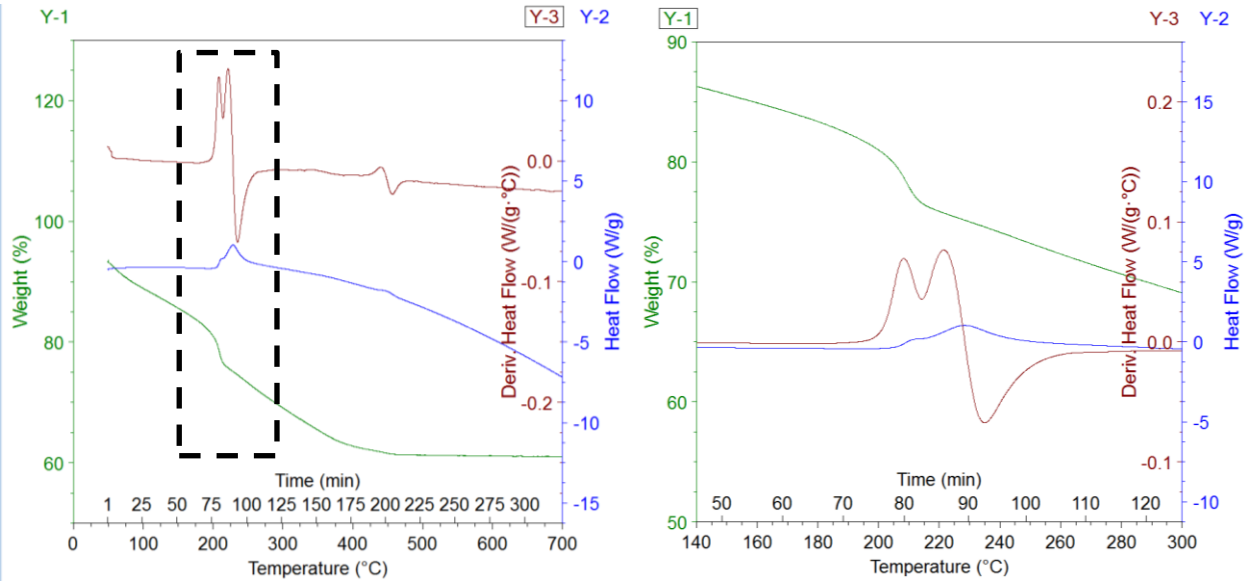

Figure 18: TGA/DSC of standard titania aerogel with heat loss and derivative heat loss curves. Amorphous to anatase transition shown expanded at right.

data and TEM images suggest that titania begins to crystallize prior to the 300°C and 275°C temperatures verified with each technique. A local maximum and minimum of the derivative heat flow between 200°C and 240°C is indicative of a structural change beginning at 210°C and

proceeding gradually until a second maximum and minimum occurs at 450°C. The second set of peaks is much less prominent and can be attributed to the expulsion of any remaining organics and the completion of anatase formation in the aerogel.

3.2.2 Morphology, Porosity, Composition: FE-SEM, BET, EDXS

Morphological studies carried out by field emission scanning electron microscopy provide a useful picture of titania aerogel's macroporosity. The comparison between figure 19A and 19B with 19C and 19D shows the aggregation and sintering expected from heat treatment. As a size comparison, approximately 10 nm gold palladium nanoparticles coating the silicon surface are visible in figure 19B and 19D measure individual aerogel particles as small as 30 nm.

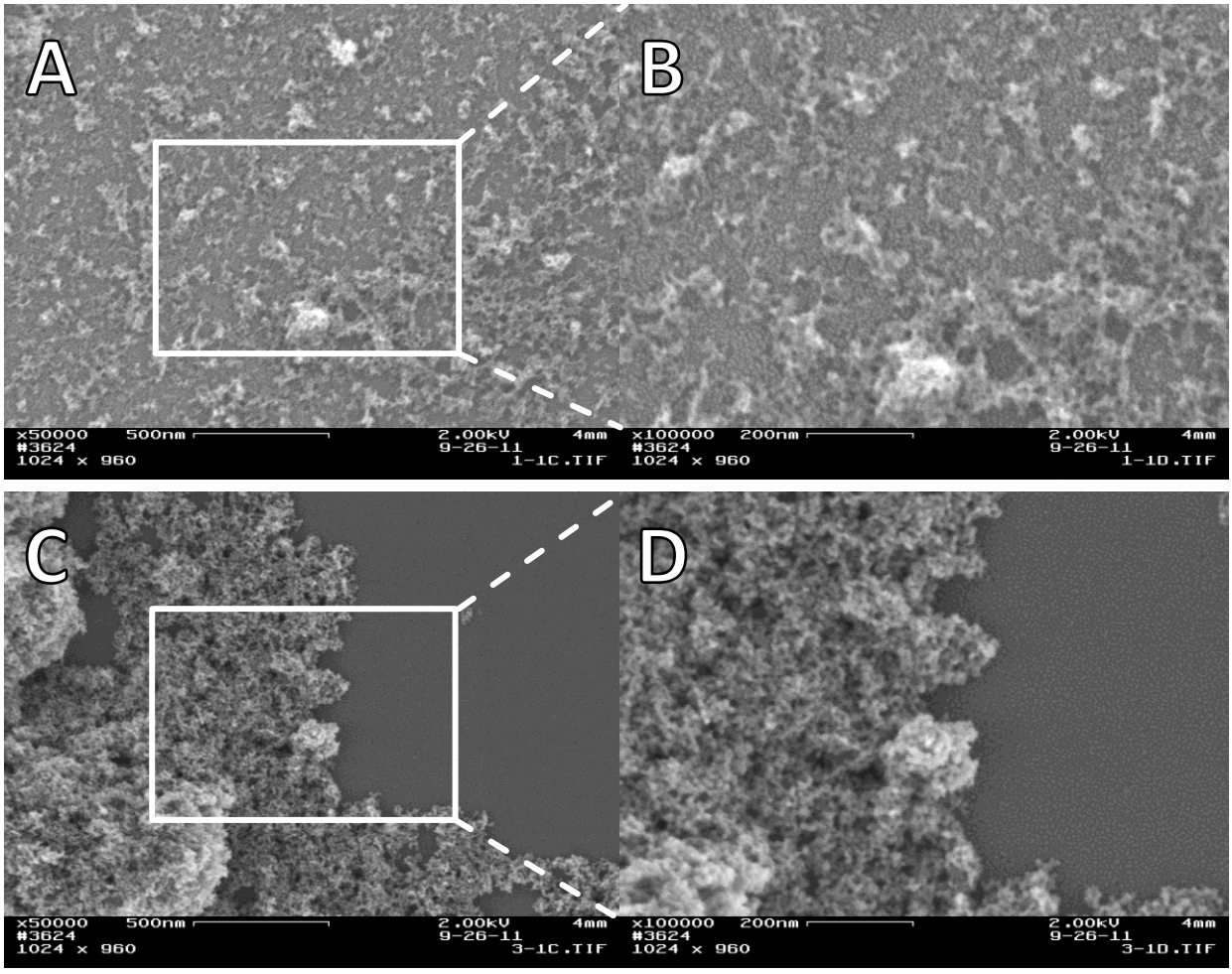

Figure 19: FE-SEM images of standard titania aerogel without heat treatment (A) and (B) and heat treated at 450°C (C) and (D).

The neat aerogel's 20 to 50 nm macropores are noticeable in figure 19B and more extensively in figure 20A and 20B, where a broad pore size distribution is evident in the web-like porous network.

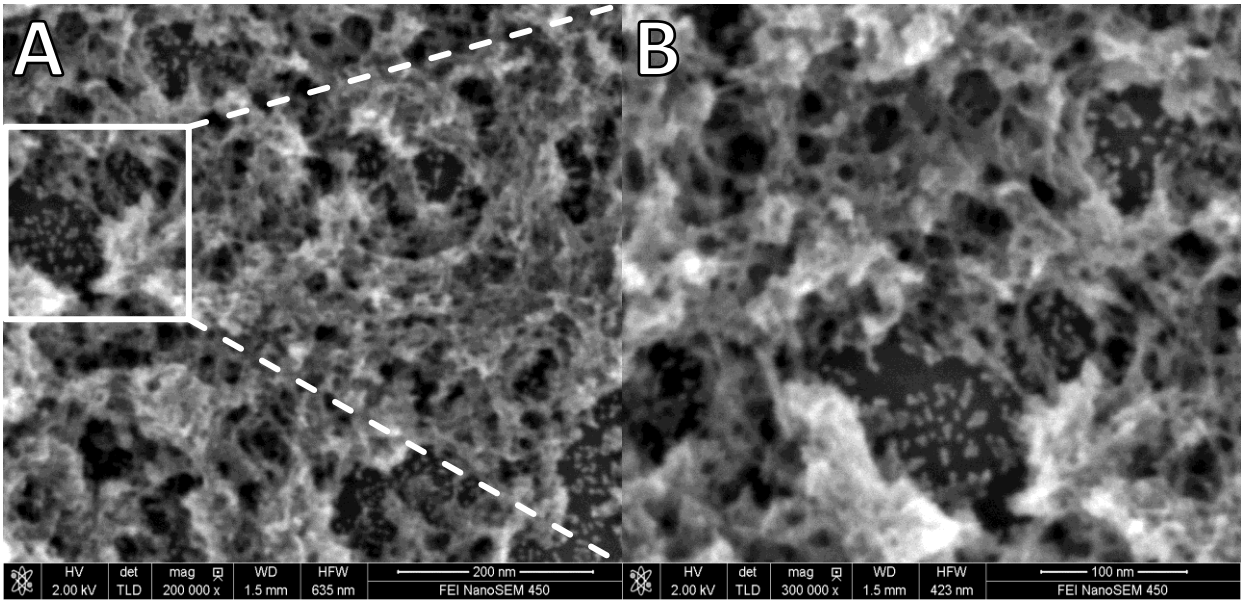

Figure 20: Higher resolution FE-SEM images of standard titania aerogel without heat treatment at 200,000x (A) and 300,000x (B)

Studying the effect of temperature on the BET surface area and pore volume of titania aerogel gave an optimal heat treatment temperature for use as photocatalysts. The standard titania aerogel's surface area and pore volume increased significantly with heat treatment at 200°C. This phenomenon is uncommon due to sintering and network collapse associated with heat treatment, but prior to experiencing these factors there exist residual organic compounds present in the aerogel. The brown color of titania aerogel at 200°C indicates the oxidation of organic compounds remaining from sol-gel synthesis. Removal of these compounds increases the surface area by nearly 20% and the pore volume by a factor of 2.6. Although heat treatment at 200°C has been previously recommended for titania aerogels[25], the drastic increase in pore volume to 3.223 cm^3g^{-1} has not been reported in standard ethanol-based titania aerogel syntheses.[25, 26] Heat treatment above 200°C decreases surface area and pore volume at the benefit

Standard Titania Aerogel BET Results After Calcination

Calcination Temp	None	200°C	250°C	350°C	450°C
Surface Area (m^2g^{-1})	384	460	347	238	124
Pore Volume (cm^3g^{-1})	1.231	3.223	2.443	1.809	0.885

of crystallinity, suggesting that an optimal heat treatment temperature exists at which pore volume, surface area, and crystallinity are maximized for use in gas-phase photocatalysis. The

Doped V-Ti Aerogel BET Results

Doping Percentage	0.1% V-Ti	0.5% V-Ti	1.0% V-Ti	4.8% V-Ti	9.1% V-Ti
Surface Area (m^2 g^{-1})	461	405	415	354	444
Pore Volume (cm^3g^{-1})	2.726	1.479	2.166	1.782	2.879

impact of vanadium on the surface area and pore volume shows no increasing or decreasing trend given a margin of error up to 50 m^2g^{-1} for surface areas above 400 m^2g^{-1}. Variation in pore volume may be the result of inconsistent volumes of carbon dioxide collected during solvent exchanges, having removed more organics in some cases. Also, up to three days variation in time between sol-gel synthesis and supercritical drying may have resulted in preliminary aging of gels[29]. Despite these variations in the V-Ti aerogels, high pore volumes and surface areas similar to standard titania aerogels confirm the minimal impact of vanadium doping on the morphology and structural properties of titania aerogel.

Elemental analysis was carried out to confirm the incorporation of vanadium into titania aerogels. EDXS shows good agreement in percentage vanadium present at high concentrations

Energy Dispersive X-ray Spectroscopy (EDXS) of V-Ti Aerogels

EDX	0.1% V-Ti	0.5% V-Ti	1.0% V-Ti	4.8% V-Ti	9.1% V-Ti
V%	Below limit	0.35%	0.47%	4.71%	8.26%

while the high margin of error at percentages below 1% limited the accuracy of 0.5% and 1.0% V-Ti aerogel analysis.

3.2.3 UV-Vis Diffuse Reflectance Spectroscopy (UV-Vis DRS)

Absorption of ultraviolet light in titania remains one of the primary indicators of photoactivity as shown by the spectra in figure 21. Increasing heat treatment temperature decreases the absorption of ultraviolet light in titania aerogels above 200°C. An initial 200°C treatment removes most residual organics in the aerogel and exposes the amorphous titania. As crystallinity and surface area decrease, so does the UV absorption of the materials.

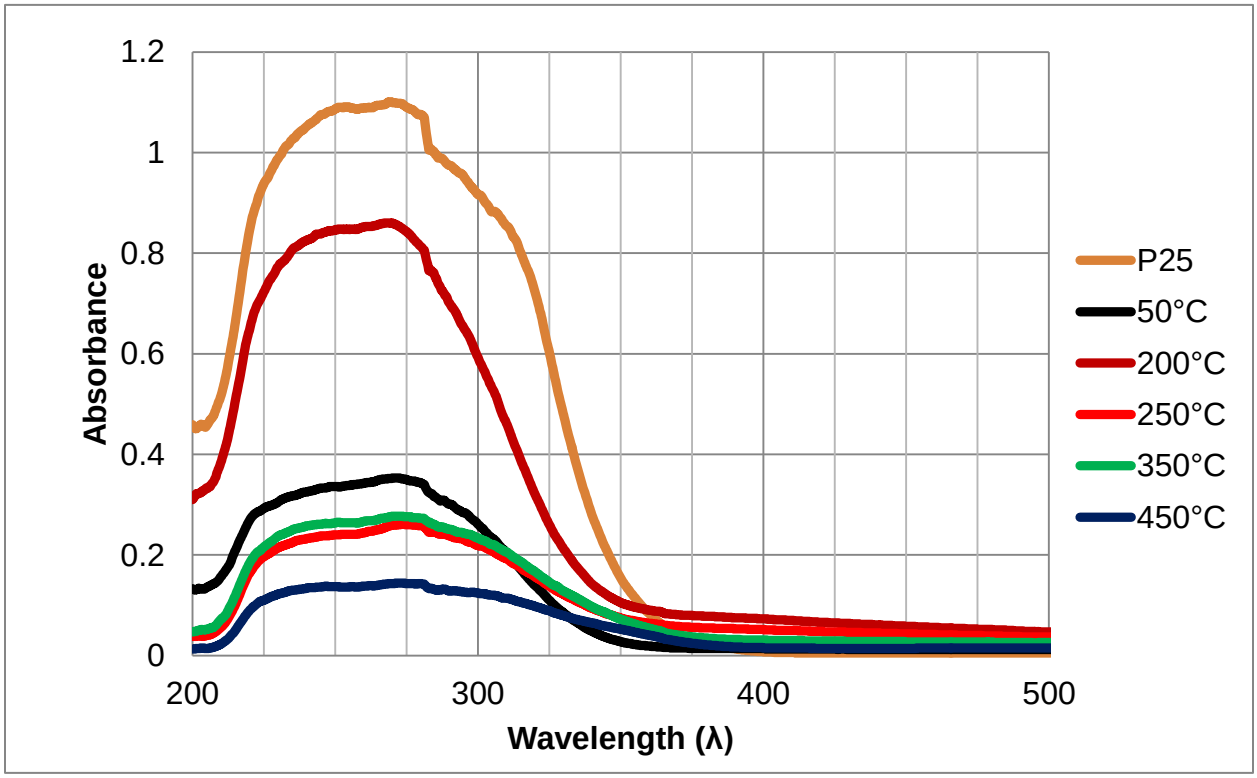

Figure 21: UV-Vis Diffuse Reflectance Spectra of titania aerogel

No increase in absorption is observed at 200°C in V-Ti aerogels, with the untreated V-Ti aerogel displaying the greatest absorption regardless of dopant concentration (fig 22-26). Interestingly enough, absorption from 350 nm to 450 nm in all the materials was noticeably higher for the 200°C heat treatment, except in the 9.1% V-Ti aerogel where the 450°C heat treatment matched the 200°C material (fig 26), suggesting a small expansion of anatase's bandgap into the visible region. The absorption of the 450°C and 200°C 9.1% V-Ti is significantly higher than P25 above

350 nm, however the large ultraviolet absorption of Degussa P25 was not matched by amorphous or anatase-only titania. Part of Degussa's expected advantage comes from the presence of rutile as well as anatase which increases activity of titania due to an interplay between the two phases.[15]

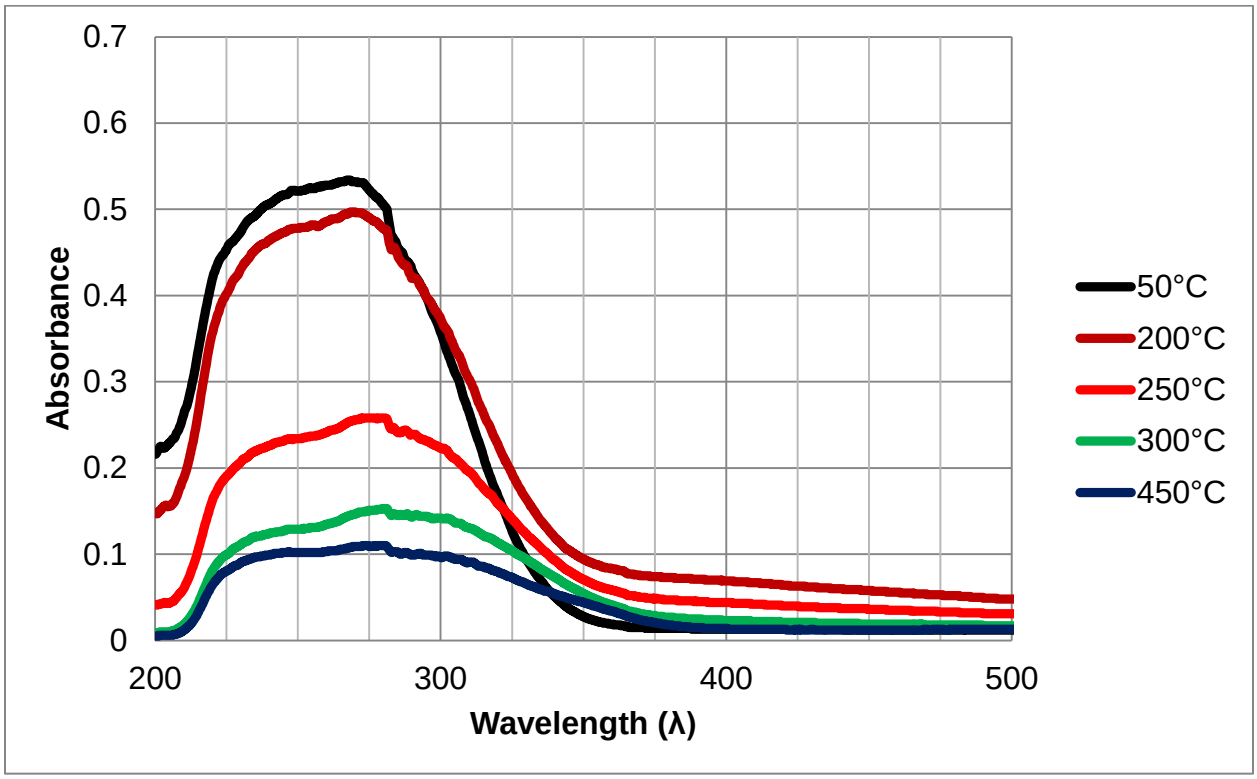

Figure 22: UV-Vis Diffuse Reflectance Spectra of 0.1%V-Ti aerogel

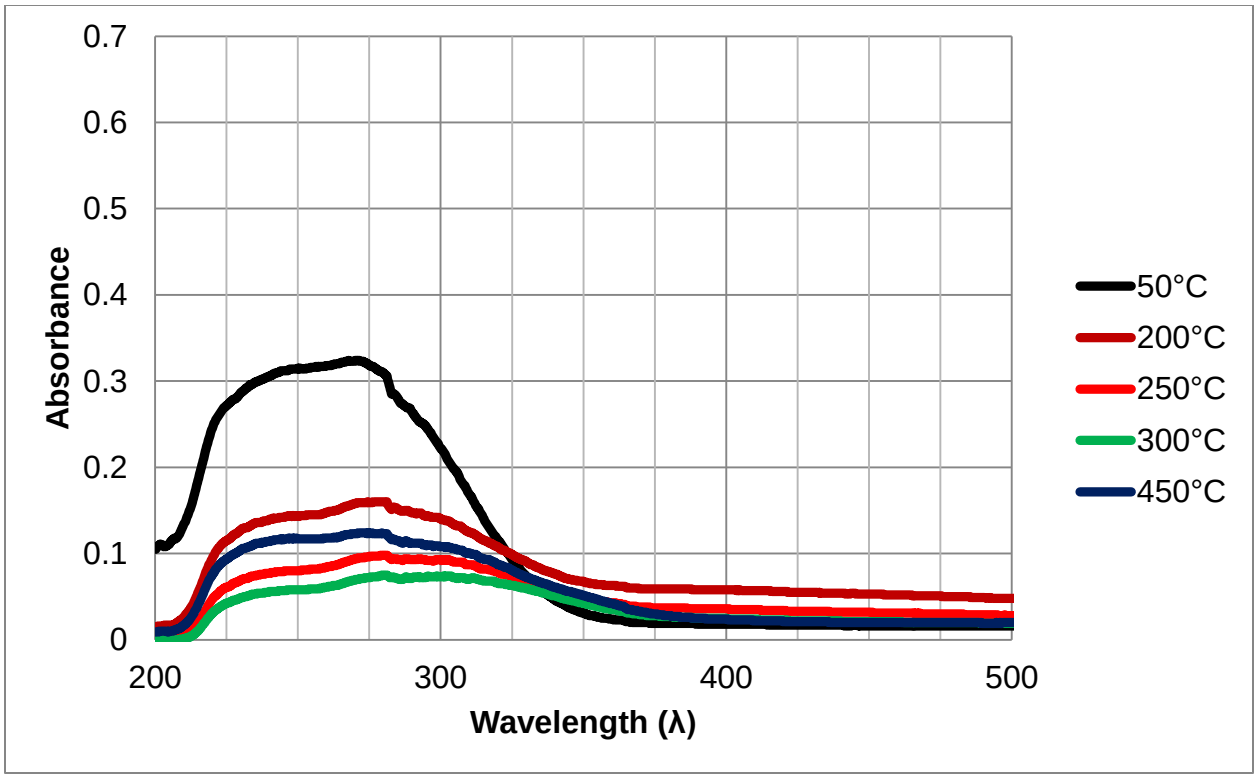

Figure 23: UV-Vis Diffuse Reflectance Spectra of 0.5% V-Ti aerogel

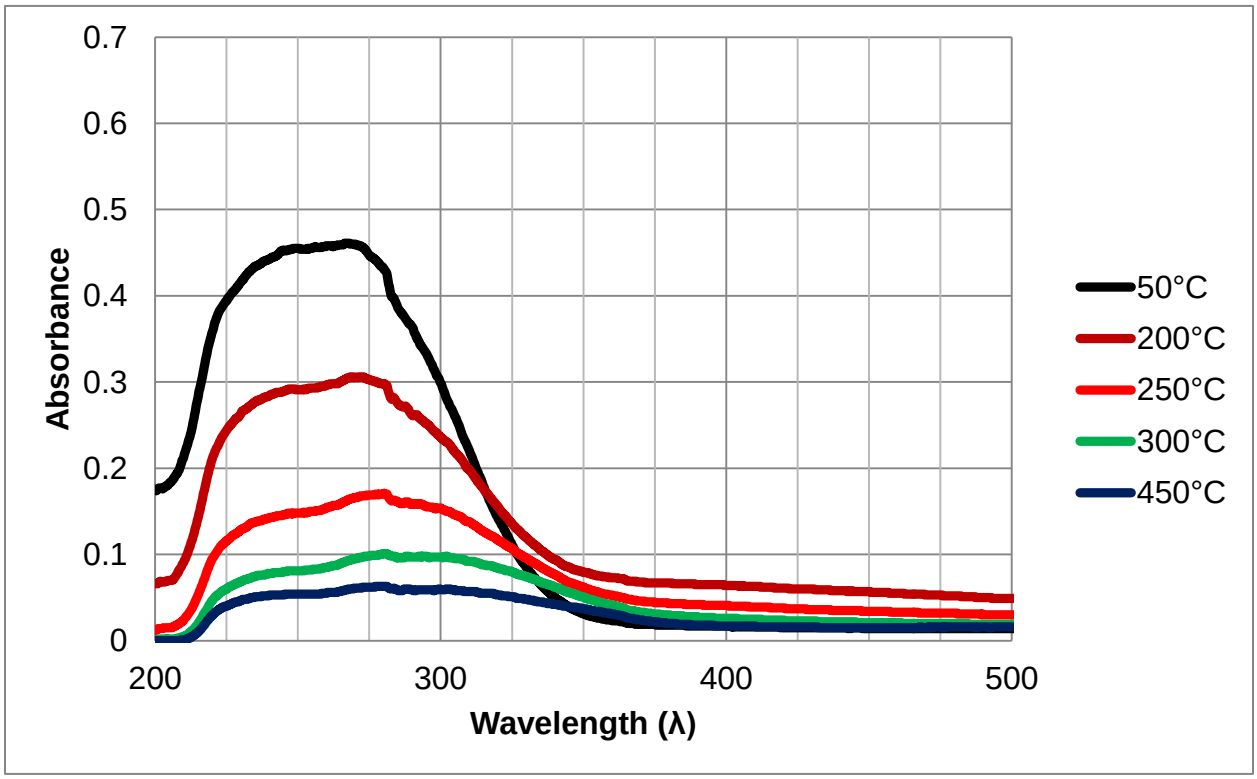

Figure 24: UV-Vis Diffuse Reflectance Spectra of 1.0% V-Ti aerogel

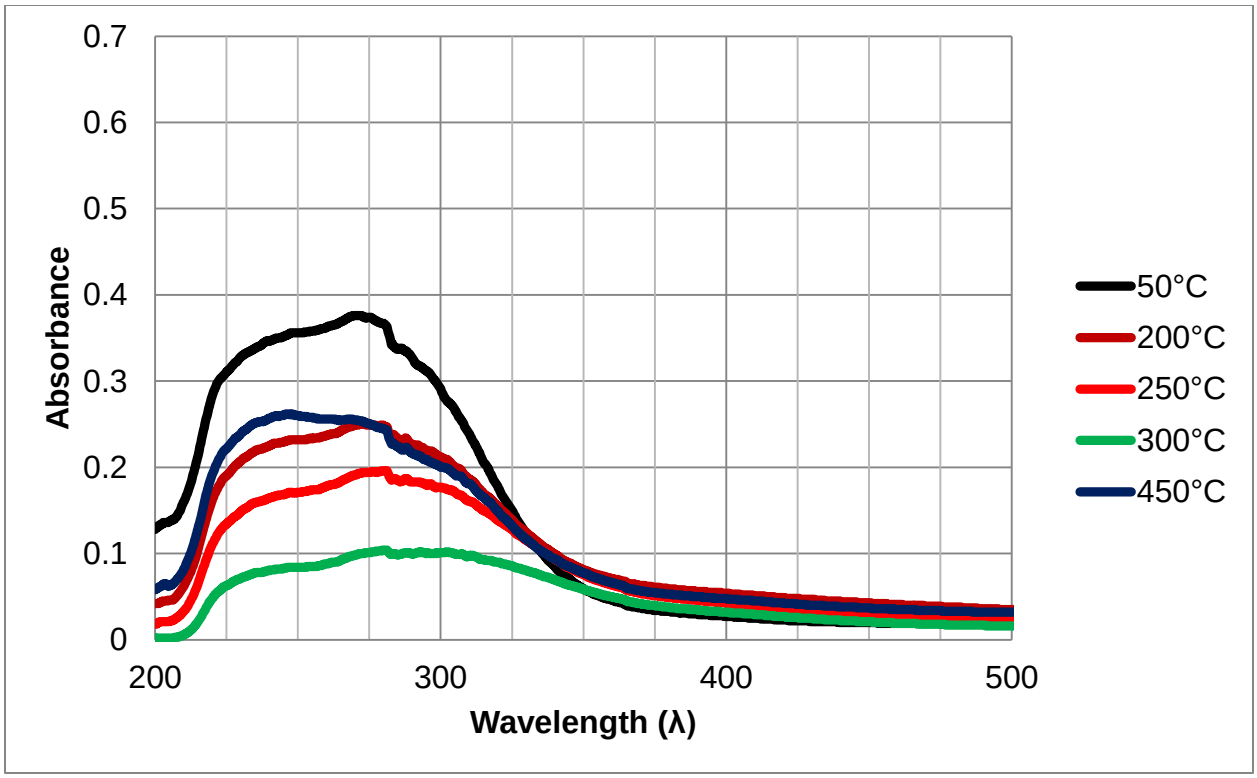

Figure 25: UV-Vis Diffuse Reflectance Spectra of 4.8% V-Ti aerogel

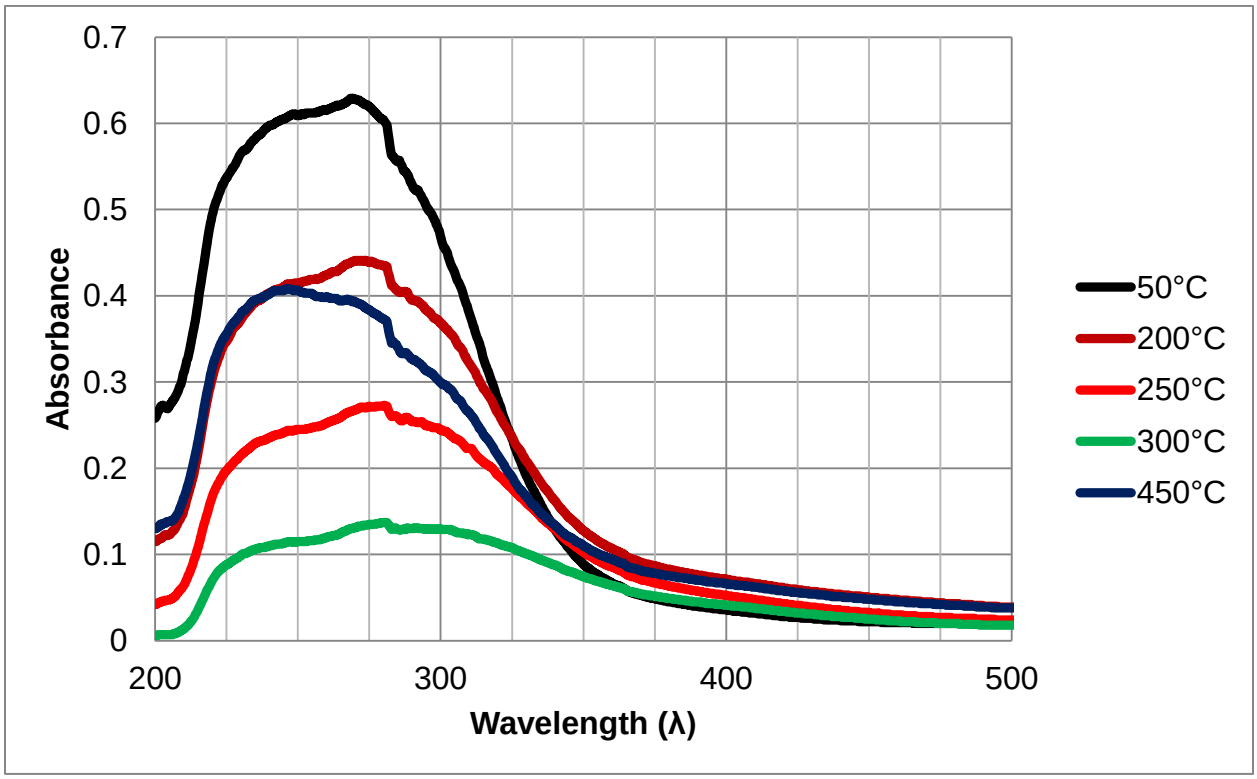

Figure 26: UV-Vis Diffuse Reflectance Spectra of 9.1% V-Ti aerogel

3.3 Gas-phase Photodegradation of Propionaldehyde

The best photocatalyst candidates were chosen based on surface area, pore volume, degree of crystallinity, and ability to absorb ultraviolet light. Because no single material and heat treatment is optimal for these criteria, a medium level of crystallinity, surface area and pore volume was chosen in the 300°C treated standard titania aerogel. Qualitative observation of the material's color seen in figure 27 suggests that most of the carbon residing on the surface was oxidized to CO_2 during heat treatment, increasing the active surface area. The 1.0% V-Ti aerogel

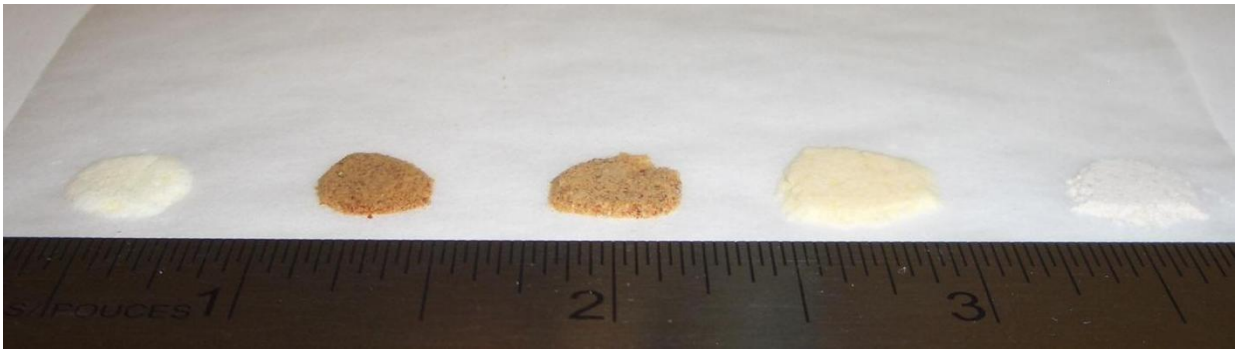

Figure 27: Titania aerogel color change with heat treatment
From L to R: 50°C, 225°C, 250°C, 275°C, 450°C

heat treated at 300°C was also selected as a medium concentration doped titania to determine if vanadium potentially present on the surface has beneficial or detrimental effects in the degradation of propionaldehyde.

Photocatalytic degradation of propionaldehyde was carried out using simulated atmospheric conditions with constant humidity, flow rate, catalyst loading of $15 mg cm^{-2}$ and UVA light intensity.[13] Pseudo-steady state conditions are assumed when approximately 10% degradation is achieved using a small area of catalyst exposed to radiation. The propionaldehyde concentration across the titania coated slides is assumed constant under these degradation conditions and allows for the use of an oxidation rate expression.[13, 41]

(1) $$r = 2.45(X_{in}-X_{out})Q/A$$

Equation one gives the oxidation rate in μ-molcm^{-2}h^{-1} from X_{in} and X_{out} in parts per million volume, volumetric flow rate Q (L/min), and area in cm^2.

Propionaldehyde Photodegradation using Degussa P25 and Titania Aerogels

P25	Humidity	UVA	Propionaldehyde Average Peak Area	Oxidation rate (μ-molcm^{-2}h^{-1})
Trial 1	No	Off	1700	1.84
	No	On	1458	
Trial 2	Yes	Off	1700	2.17
	Yes	On	1415	
Trial 3	Yes	Off	1700	1.58
	Yes	On	1492	
300°C	Humidity	UVA	Propionaldehyde Average Peak Area	Oxidation rate (μ-molcm^{-2}h^{-1})
Trial 1	Yes	Off	1700	1.09
	Yes	On	1557	
Trial 2	Yes	Off	1700	0.99
	Yes	On	1569	
1.0% V-Ti 300°C	Humidity	UVA	Propionaldehyde Average Peak Area	Oxidation rate (μ-molcm^{-2}h^{-1})
Trial 1	Yes	Off	1700	1.06
	Yes	On	1560	

Validation of the quartz plate flow-through reactor was performed using Degussa P25 TiO_2 to relate oxidation rates of propionaldehyde to reported results. A UVA intensity of 2.7 mWcm^{-2} was used with 1700 ppmv inlet concentration propionaldehyde. An average oxidation rate of 1.86 μ-molcm^{-2}h^{-1} was calculated for P25 compared to 1 μ-molcm^{-2}h^{-1} at 100 ppmv inlet concentration and 0.7 mWcm^{-2} UVA intensity.[11] UVA intensity to the 0.6 power impacts oxidation rate linearly[42], and normalizing the experimental rate based on $I^{0.6}$ gives a comparable 0.83 mWcm^{-2} to the reported value of 1 mWcm^{-2}. The values are comparable qualifying the experimental setup after accounting for the independence of oxidation rate from water vapor concentration at high VOC concentrations[13], As a preliminary test for photoactivity, titania aerogel and 1.0% V-Ti aerogel materials both showed respectable oxidation rates of 1.04 μ-

molcm^{-2}h^{-1} and 1.06 μ-molcm^{-2}h^{-1}, respectively. Vanadium doping did not affect the photoactivity of titania aerogel in degradation of propionaldehyde. Confirmation of the 300°C titania aerogel as an active photocatalyst opens up avenues for detailed studies of other titania aerogels for VOC photodegradation.

Chapter 4 Conclusions

The modification of accepted titania sol-gel methods resulted in high quality sol-gels displaying clarity, prominent bounce, and highly tunable gelation times. Supercritical drying successfully produced titania aerogels possessing surface areas over 400 m^2g^{-1} and pore volumes over 1.0 cm^3g^{-1}. The use of 1-butanol as the sol-gel solvent allows for greater flexibility in synthesis conditions and is the most probable source for observing pore volumes above 3.0 cm^3g^{-1} in titania aerogel after heat treatment at 200°C. In general, heat treatment of titania aerogels tailors pore volume and surface area. Doping titania sol-gels with different vanadium precursors successfully produced the same colored materials regardless of vanadium source or oxidation state. The sol-gel method was proven to be versatile and accommodating towards vanadium doping by precursor inclusion at different points in the sol-gel process as well as from solid or metal organic precursors. This method shows promise for extension to the doping of numerous transition metals and nonmetals into titania to produce homogeneous doped and mixed metal oxide materials.

The formation of anatase crystallites averaging 5 nm was shown to occur in two steps based on TGA/DSC and XRD data (figures 18, 9-14). Anatase began forming at 210°C and continues to grow along the (101) plane until 400°C where complete crystallinity is observed in titania aerogel. TEM images confirmed the average crystallite size in titania and V-Ti aerogels as well as showing the incorporation of vanadium into the titania framework, showing no distinct second phase or significant change in d-spacing (figures 16, 17). EDXS confirmed the elemental composition of V-Ti aerogels was similar to the theoretical values expected from the sol-gel. FE-SEM images showed the distribution of macropores characteristic of aerogels and confirmed the aggregation expected after heat treatment of aerogels.

UV/Vis absorption spectra of samples heat treated under various temperatures revealed the decreasing absorbance of titania and V-Ti aerogels in the presence of ultraviolet light (figures 21-26). Titania aerogel treated at 200°C broke this trend by displaying ultraviolet absorbance close to that of Degussa P25 TiO_2 (figure 21). Furthermore, the standard titania and all doped V-Ti aerogels heat treated at 200°C showed higher absorbance than P25 above 350 nm. Optimal heat treatment of titania aerogel was determined to be dependent on the desired level of crystallinity, pore volume, surface area, and ultraviolet absorption, with 300°C being a median heat treatment following these two criteria as well as the removal of residual organics and carbon from the material (figure 27).

The quartz plate photoreactor setup was validated by comparison of oxidation rates to previous work using P25 as a model photocatalyst for propionaldehyde degradation. Titania aerogel heat treated at 300°C demonstrated respectable photoactivity given its partial crystallinity and somewhat diminished ultraviolet absorption. Based on propionaldehyde removal rate, vanadium doping did not increase photodegradation of propionaldehyde given the same heat treatment and photoreactor conditions used for the titania aerogel. The higher surface area of titania aerogels compared to P25 suggests improved resistance towards catalyst deactivation by siloxanes in indoor air quality applications.[8]

Sol-gel synthesis and supercritical drying of titania and vanadium-doped titania aerogels for the degradation of propionaldehyde was successful. The synthesis, processing, and application of these materials lays the foundation for future studies in photoactive, high surface area titania-based aerogel materials.

Chapter 5 Future Work

Future studies will include the use of titania aerogels as catalysts, catalyst supports, and as high surface area matrices. The synthesis of titania aerogels with uncommon solvents during sol-gel preparation could provide a strong basis for producing aerogel materials with desirable properties. Determination of the sol-gel limits using various solvents, acids, and ratios between precursor:solvent:water:acid would be an ideal starting point. Doping titania with other metals such as iron, zirconium, nickel, copper, niobium, and molybdenum to the extent that they become mixed metal oxides would be of value for photocatalysis and thermal VOC catalysis.

Metal oxide aerogels spray coated on glass slides as a support, could in turn be coated by either atomic layer deposition (ALD) or sputter coating. This provides a method for control of surface composition and allows determination of potential bifunctional catalytic effects. Metal coatings would be particularly useful with respect to bifunctional catalysis. Metal oxide coatings should be considered as well, specifically manganese oxide, iron oxide, tungsten oxide, and vanadium oxide. Testing these materials in photocatalysis may show promise due to differences in various VOC's affinity for the catalyst surface based on the oxide chosen. The ability to form nanometer thick coatings or partial monolayers may prove beneficial in improved deactivation resistance of titania towards particular organic compounds and siloxanes.

Titania aerogels are useful materials for the encapsulation of nanoparticles or other nanomaterials without significant reduction in molecular accessibility to the encapsulated material. In one specific example, seeding of titania aerogels (anatase) with rutile nanoparticles of varying sizes could mimic the crystal structure of P25, with the additional high surface area and pore volume benefits of aerogels. This may aid in elucidating the effect of rutile on the enhanced photocatalytic properties of P25 compared to pure anatase materials.

Chapter 6 References

1. George SM. Introduction: Heterogeneous catalysis. Chem Rev (Washington, D C) 1995;95(3):475-6.

2. Palmisano G, García-López E, Marcì G, Loddo V, Yurdakal S, Augugliaro V, Palmisano L. Advances in selective conversions by heterogeneous photocatalysis. Chemical Communications 2010;46(38):7074-89.

3. Demeestere K, Dewulf J, Van Langenhove H. Heterogeneous photocatalysis as an advanced oxidation process for the abatement of chlorinated, monocyclic aromatic and sulfurous volatile organic compounds in air: State of the art. Crit Rev Environ Sci Technol 2007;37(6):489-538.

4. Kwon S, Fan M, Cooper AT, Yang H. Photocatalytic applications of micro- and nano-TiO2 in environmental engineering. Crit Rev Environ Sci Technol 2008;38(3):197-226.

5. Hong I. VOCs degradation performance of TiO2 aerogel photocatalyst prepared in SCF drying. Journal of Industrial and Engineering Chemistry 2006;12(6):918-25.

6. Wang S, Ang HM, Tade MO. Volatile organic compounds in indoor environment and photocatalytic oxidation: State of the art. Environ Int 2007;33(5):694-705.

7. Hodgson AT, Destaillats H, Sullivan DP, Fisk WJ. Performance of ultraviolet photocatalytic oxidation for indoor air cleaning applications. Indoor Air 2007;17(4):305-16.

8. Hay SO, Obee TN, Thibaud-Erkey C. The deactivation of photocatalytic based air purifiers by ambient siloxanes. Applied Catalysis B: Environmental 2010 9/9;99(3–4):435-41.

9. Cao L, Gao Z, Suib SL, Obee TN, Hay SO, Freihaut JD. Photocatalytic oxidation of toluene on nanoscale TiO2 catalysts: Studies of deactivation and regeneration. Journal of Catalysis 2000 12/10;196(2):253-61.

10. Maira AJ, Yeung KL, Soria J, Coronado JM, Belver C, Lee CY, Augugliaro V. Gas-phase photo-oxidation of toluene using nanometer-size TiO2 catalysts. Applied Catalysis B: Environmental 2001 2/12;29(4):327-36.

11. Obee TN, Hay SO. The estimation of photocatalytic rate constants based on molecular structure: Extending to multi-component systems. J Adv Oxid Technol 1999;4(2):147-52.

12. Hoffmann MR, Martin ST, Choi W, Bahnemann DW. Environmental applications of semiconductor photocatalysis. Chem Rev 1995;95(1):69-96.

13. Obee TN, Hay SO. Effects of moisture and temperature on the photooxidation of ethylene on titania. Environmental Science and Technology 1997;31(7):2034-8.

14. Baiju KV, Shukla S, Sandhya KS, James J, Warrier KGK. Photocatalytic activity of sol-gel-derived nanocrystalline titania. Journal of Physical Chemistry C 2007;111(21):7612-22.

15. Ohno T, Sarukawa K, Tokieda K, Matsumura M. Morphology of a TiO2 photocatalyst (degussa, P-25) consisting of anatase and rutile crystalline phases. Journal of Catalysis 2001 10/1;203(1):82-6.

16. Grzybowska-Swierkosz B. Vanadia-titania catalysts for oxidation of o-xylene and other hydrocarbons. Applied Catalysis A: General 1997 9/11;157(1-2):263-310.

17. Strobel R, Baiker A, Pratsinis SE. Aerosol flame synthesis of catalysts. Advanced Powder Technology 2006;17(5):457-80.

18. Chen X, Mao SS. Titanium dioxide nanomaterials: Synthesis, properties, modifications and applications. Chem Rev 2007;107(7):2891-959.

19. Fuerte A, Hernández-Alonso MD, Maira AJ, Martínez-Arias A, Fernández-García M, Conesa JC, Soria J. Visible light-activated nanosized doped-TiO2 photocatalysts. Chemical Communications 2001(24):2718-9.

20. Akgun BA, Durucan C, Mellott NP. Effect of silver incorporation on crystallization and microstructural properties of sol-gel derived titania thin films on glass. J Sol Gel Sci Technol 2011;58(1):277-89.

21. Hu Y, Liu H, Chen W, Chen D, Yin J, Guo X. Preparation and visible light photocatalytic activity of N-doped titania. Journal of Nanoscience and Nanotechnology 2010;10(3):2232-7.

22. Novel nanostructured photocatalyst of vanadium-doped silica-titania aerogel. AIP conference proceedings; 2009. .

23. Wu JC-, Chen C-. A visible-light response vanadium-doped titania nanocatalyst by sol-gel method. J Photochem Photobiol A 2004;163(3):509-15.

24. Sanchez C, Nabavi M, Taulelle F. Synthesis and characterization of vanadium oxide gels from alkoxy-vanadate precursors. Mater Res Soc Symp Proc 1988;121:93-104.

25. Campbell LK, Na BK, Ko EI. Synthesis and characterization of titania aerogels. Chemistry of Materials 1992;4(6):1329-33.

26. Dagan G, Tomkiewicz M. TiO2 aerogels for photocatalytic decontamination of aquatic environments. J Phys Chem 1993;97(49):12651-5.

27. Harreld JH, Dong W, Dunn B. Ambient pressure synthesis of aerogel-like vanadium oxide and molybdenum oxide. Mater Res Bull 1998 4;33(4):561-7.

28. Rolison DR, Dunn B. Electrically conductive oxide aerogels: New materials in electrochemistry. Journal of Materials Chemistry 2001;11(4):963-80.

29. Brinker CJ, Scherer GW. Sol-gel science: The physics and chemistry of sol-gel processing. San Diego, CA: Academic Press, Inc; 1990. .

30. Cao S, Yeung KL, Yue P-. Preparation of freestanding and crack-free titania-silica aerogels and their performance for gas phase, photocatalytic oxidation of VOCs. Applied Catalysis B: Environmental 2006;68(3-4):99-108.

31. Rolison DR. Catalytic nanoarchitectures - the importance of nothing and the unimportance of periodicity. Science 2003;299(5613):1698-701.

32. Chaput F, Dunn B, Fuqua P, Salloux K. Synthesis and characterization of vanadium oxide aerogels. J Non Cryst Solids 1995 7/2;188(1-2):11-8.

33. Hoang-Van C, Zegaoui O, Pichat P. Vanadia-titania aerogel deNOx catalysts. J Non Cryst Solids 1998;225(1-3):157-62.

34. Chen L-, Gan L-, Xu Z-. Preparation and characterization of monolithic TiO2 aerogels. Kao Teng Hsueh Hsiao Hua Heush Hsueh Pao/ Chemical Journal of Chinese Universities 2001;22(11):1918.

35. Parts and Schematics [Internet]: Aerogel.org [cited April 26th, 2012 04/26]. Available from: http://www.aerogel.org/?p=667.

36. Rivallin M, Benmami M, Gaunand A, Kanaev A. Temperature dependence of the titanium oxide sols precipitation kinetics in the sol-gel process. Chemical Physics Letters 2004;398(1-3):157-62.

37. Simonsen ME, Søgaard EG. Sol-gel reactions of titanium alkoxides and water: Influence of pH and alkoxy group on cluster formation and properties of the resulting products. J Sol Gel Sci Technol 2010;53(3):485-97.

38. Zhao Z, Yamada Y, Teng Y, Ueda A, Nakagawa K, Kobayashi T. Selective oxidation of ethane to acetaldehyde and acrolein over silica-supported vanadium catalysts using oxygen as oxidant. Journal of Catalysis 2000 3/10;190(2):215-27.

39. Léaustic A, Babonneau F, Livage J. Structural investigation of the hydrolysis-condensation process of titanium alkoxides ti(OR)4 (OR = OPri, OEt) modified by acetylacetone. 1. study of the alkoxide modification. Chemistry of Materials 1989;1(2):240-7.

40. Shannon RD. Revised effective ionic radii and systematic studies of interatomic distances in halides and chalcogenides. Acta Crystallogr , Sect A 1976;A32(5):751-67.

41. Li Puma G, Salvadó-Estivill I, Obee TN, Hay SO. Kinetics rate model of the photocatalytic oxidation of trichloroethylene in air over TiO2 thin films. Separation and Purification Technology 2009;67(2):226-32.

42 Benfeld P, Hall RJ, Obee TN, Hay SO, Sangiovani JJ, United Technologies Research Center Internal Report, R97-1.300.9702, 1997.

Chapter 7 Appendix

Section 7.1:

UV-Vis Diffuse Reflectance Spectra of Ti:1-BuOH Aerogels without Heat Treatment

UV-Vis Diffuse Reflectance Spectra of 0.5% V-Ti Aerogels from VTIP and NH_4VO_3 Precursors without Heat Treatment

Diffraction Patterns of V-Ti Aerogels Heat Treated at 400°C

Section 7.2

Diffraction Patterns of Heat Treated Titania Aerogel and Degussa P25 TiO_2

Degussa P25 TiO_2 Anatase Crystallite Size: 18.3 nm

Degussa P25 TiO_2 Rutile Crystallite Size: 45.2 nm

Standard Titania Aerogel 450°C Crystalline Size: 4.8 nm

0.1% V-Ti Aerogel 450°C Crystalline Size: 5.3 nm

0.5% V-Ti Aerogel 450°C Crystalline Size: 5.1 nm

1.0% V-Ti Aerogel 450°C Crystalline Size: 4.2 nm

4.8% V-Ti Aerogel 450°C Crystalline Size: 5.5 nm

9.1% V-Ti Aerogel 450°C Crystalline Size: 8.5 nm

Section 7.3

Anatase Titania d-spacing Calculations

Raw Data from TEM Images

Titania Aerogel 275°C

Titania Aerogel 450°C

9.1% V-Ti Aerogel 450°C

Section 7.4

Percent Decrease in Propionaldehyde Peak Areas

7.1 Supplemental UV-Vis DRS and XRD for Titania and V-Ti Aerogels

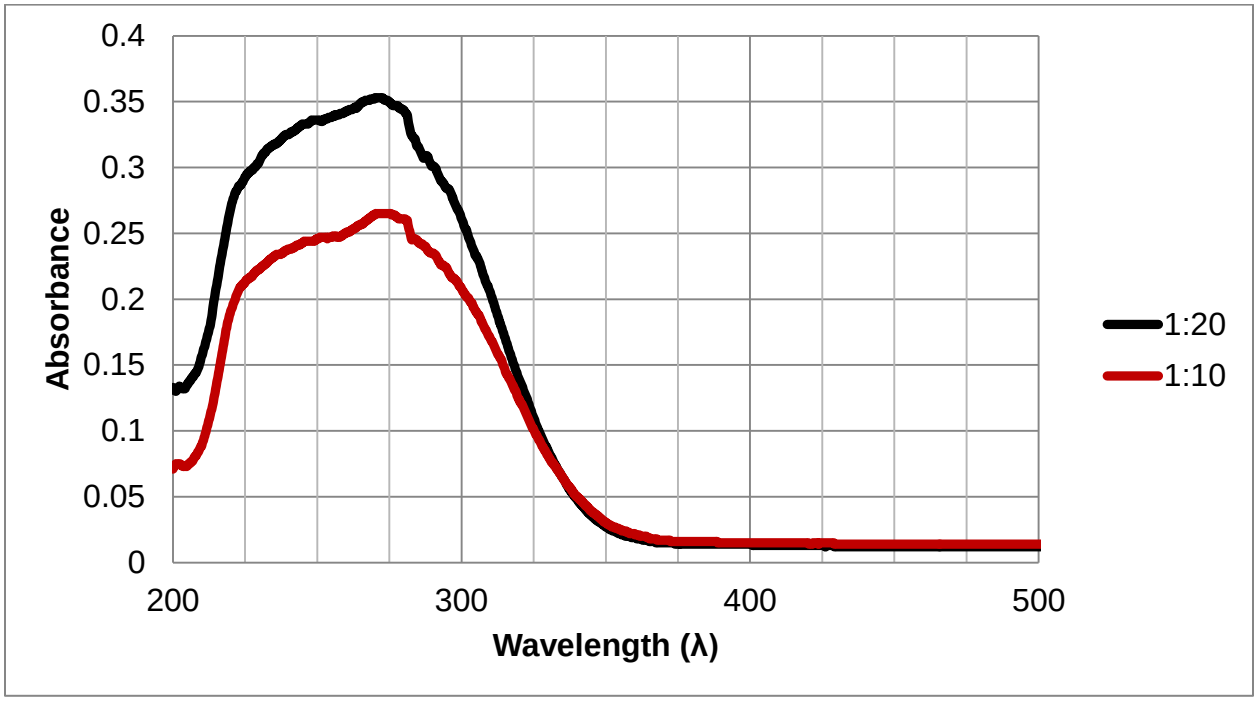

UV-Vis Diffuse Reflectance Spectra of Ti:1-BuOH Aerogels without Heat Treatment

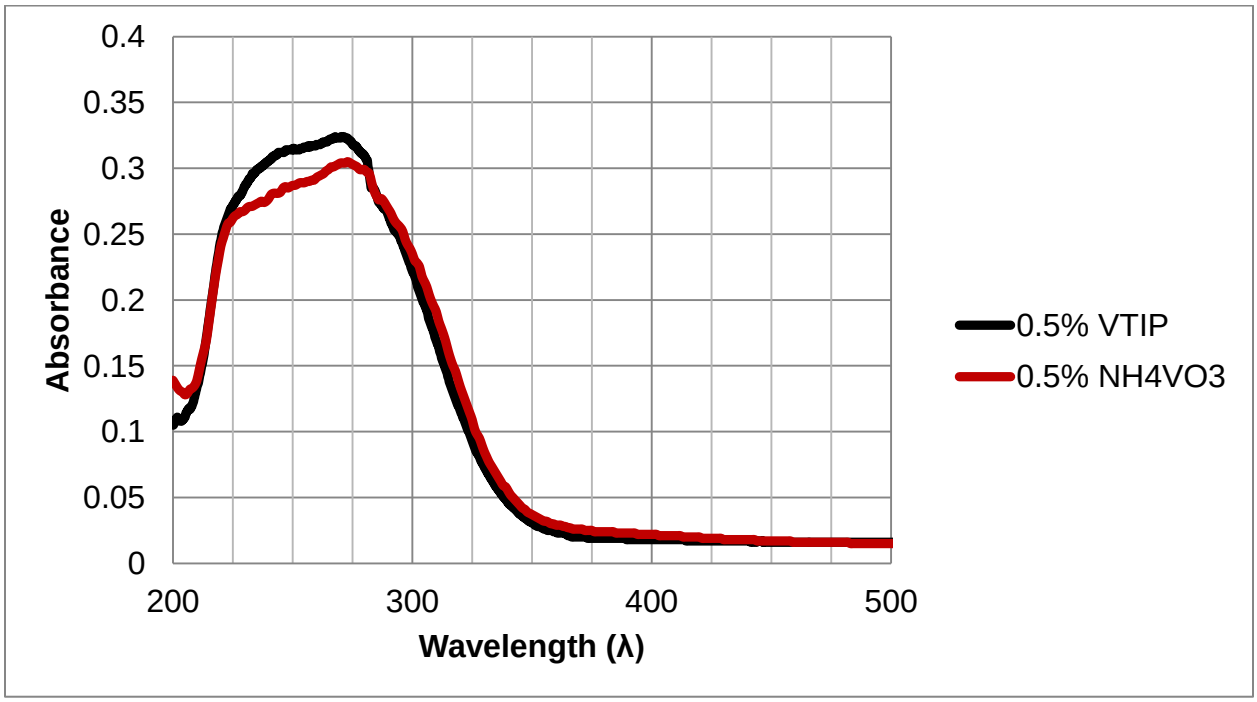

UV-Vis Diffuse Reflectance Spectra of 0.5% V-Ti Aerogels from VTIP and NH_4VO_3 Precursors without Heat Treatment

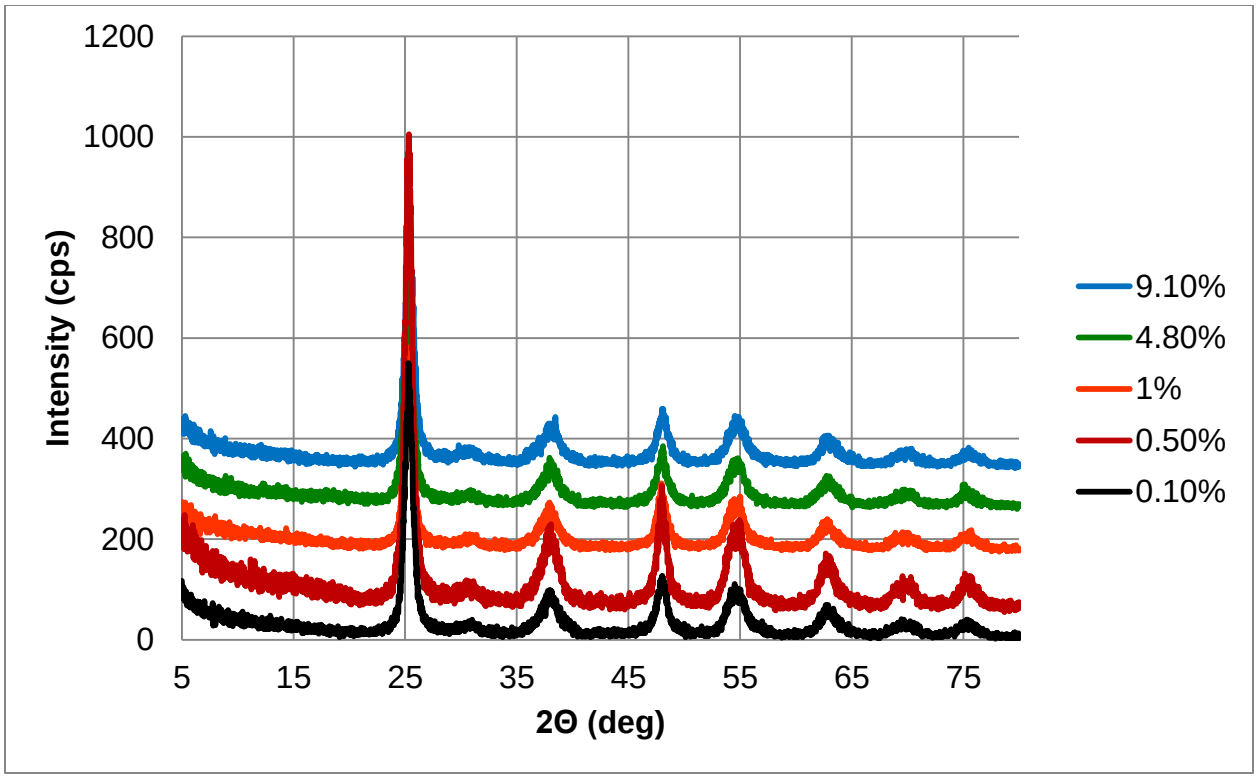

Diffraction Patterns of V-Ti Aerogels Heat Treated at 400°C

7.2 XRD Crystallite Size Determination

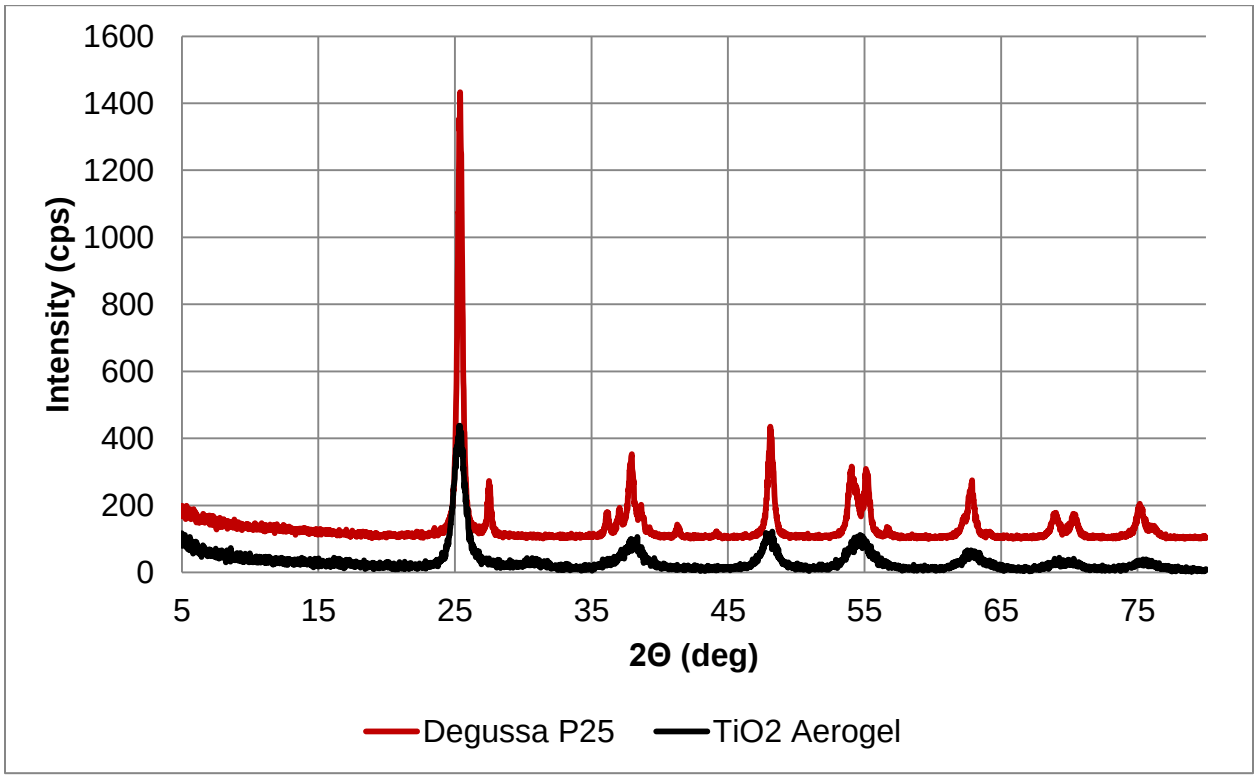

Diffraction Patterns of Heat Treated Titania Aerogel and Degussa P25 TiO_2

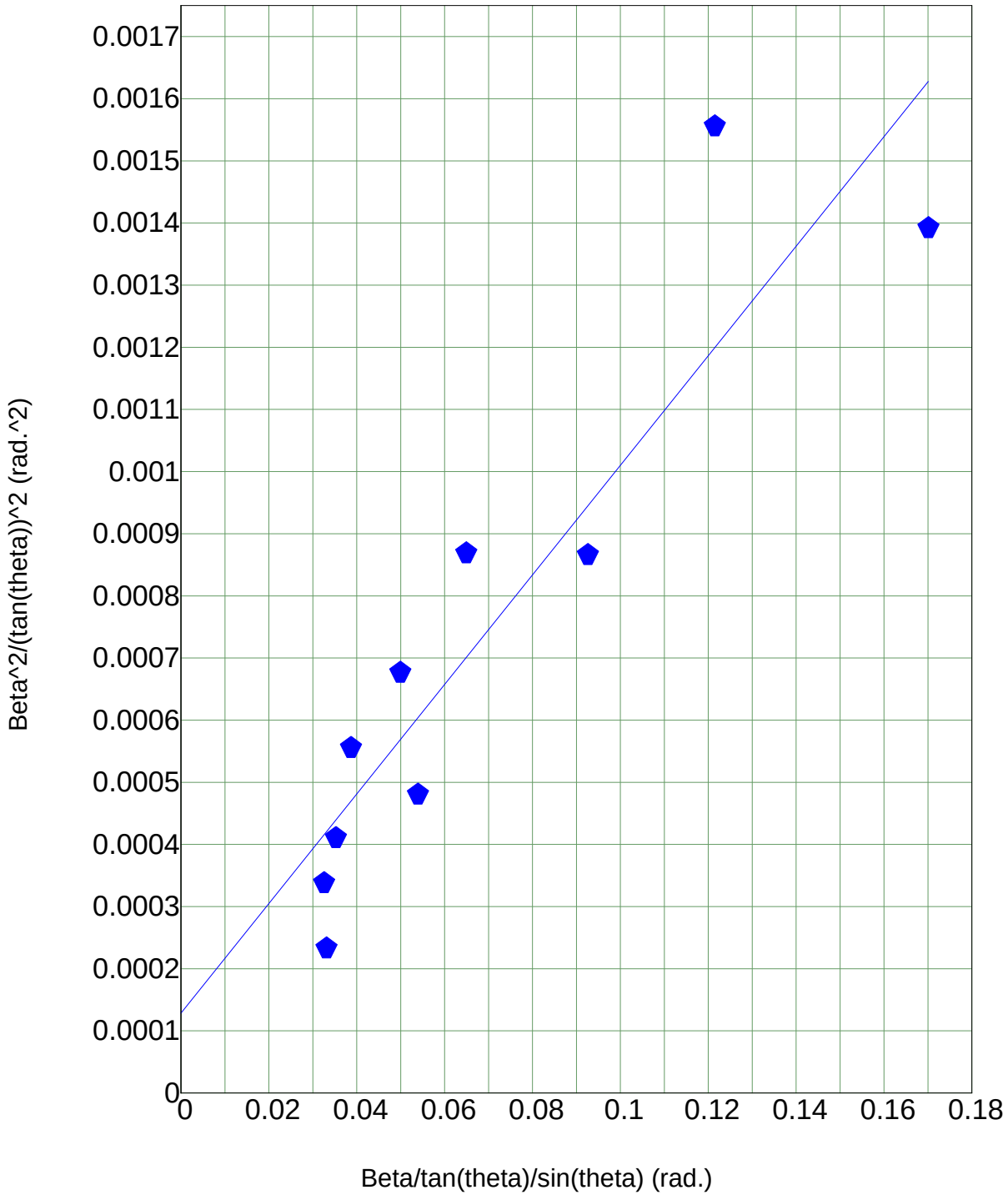

Degussa P25 TiO_2 Anatase Crystallite Size: 18.3 nm

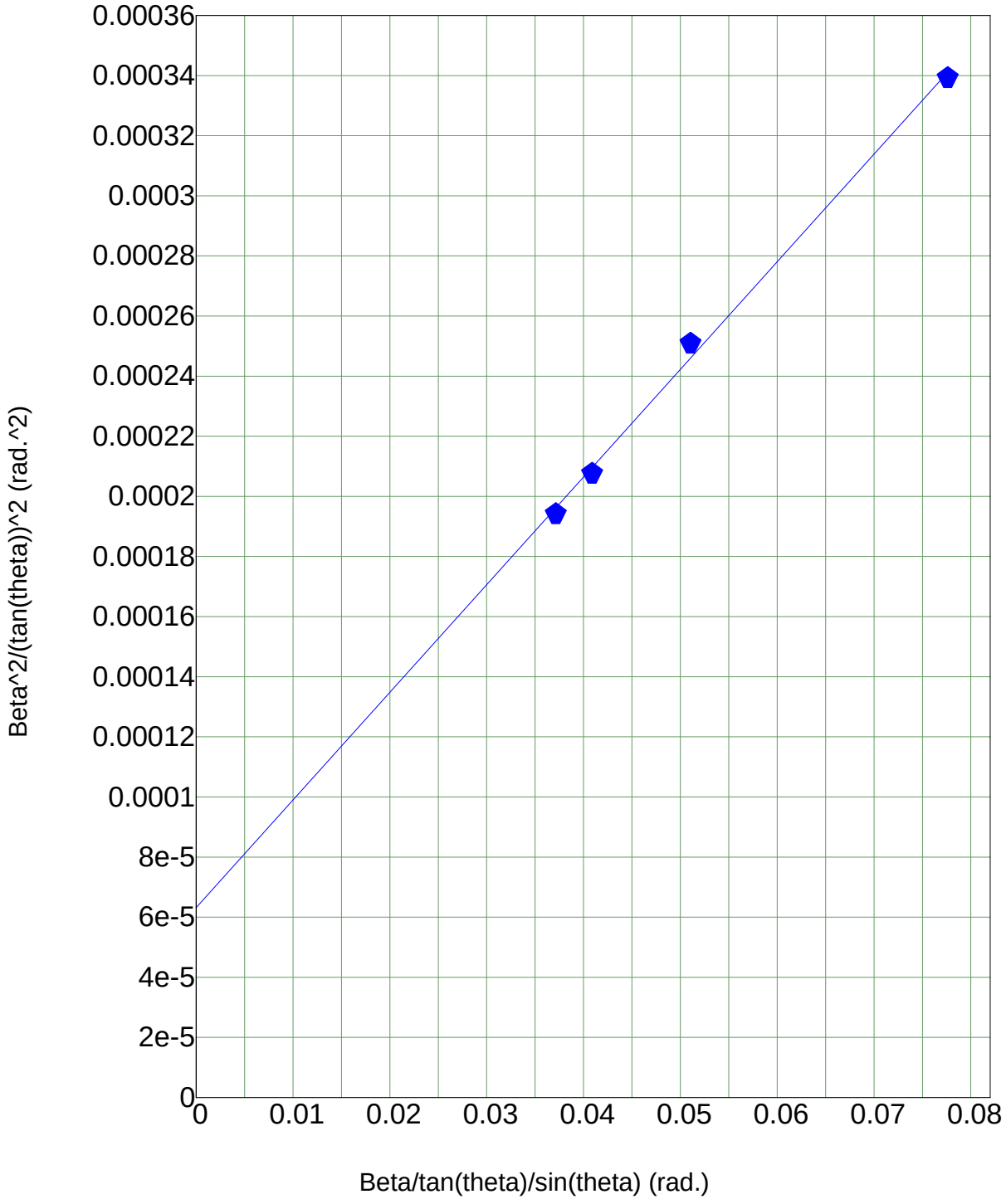

Degussa P25 TiO_2 Rutile Crystallite Size: 45.2 nm

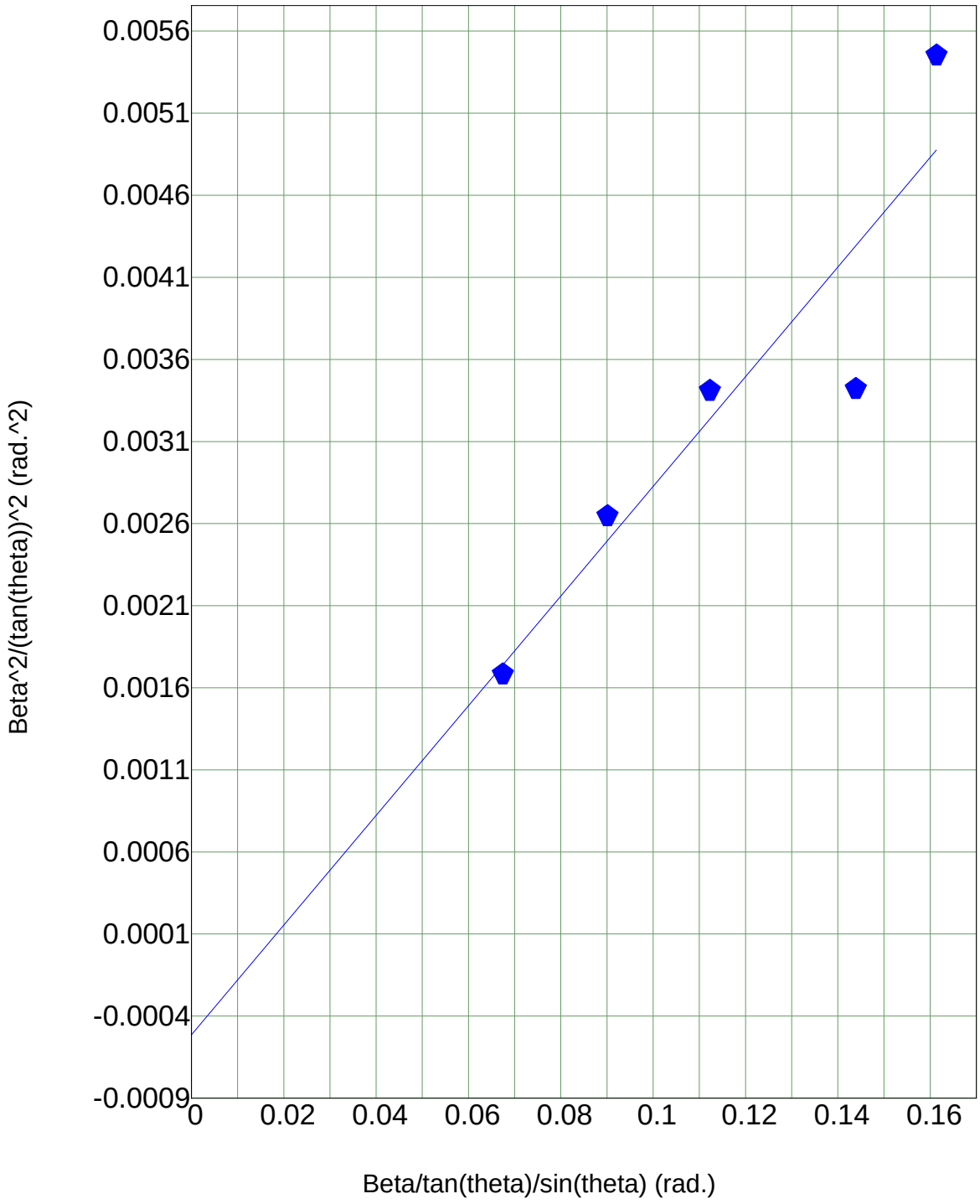

Standard Titania Aerogel 450°C Crystalline Size: 4.8 nm

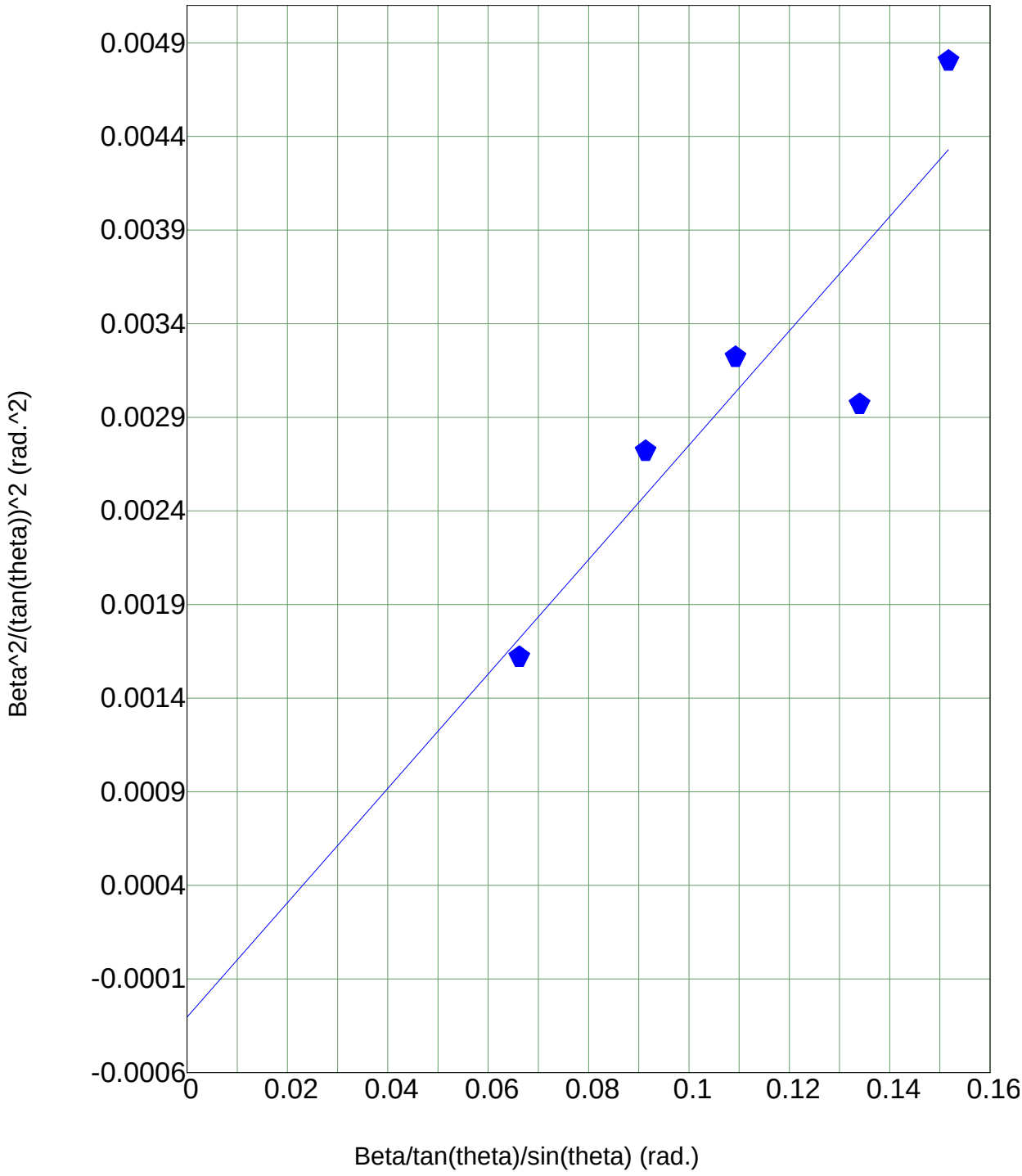

0.1% V-Ti Aerogel 450°C Crystalline Size: 5.3 nm

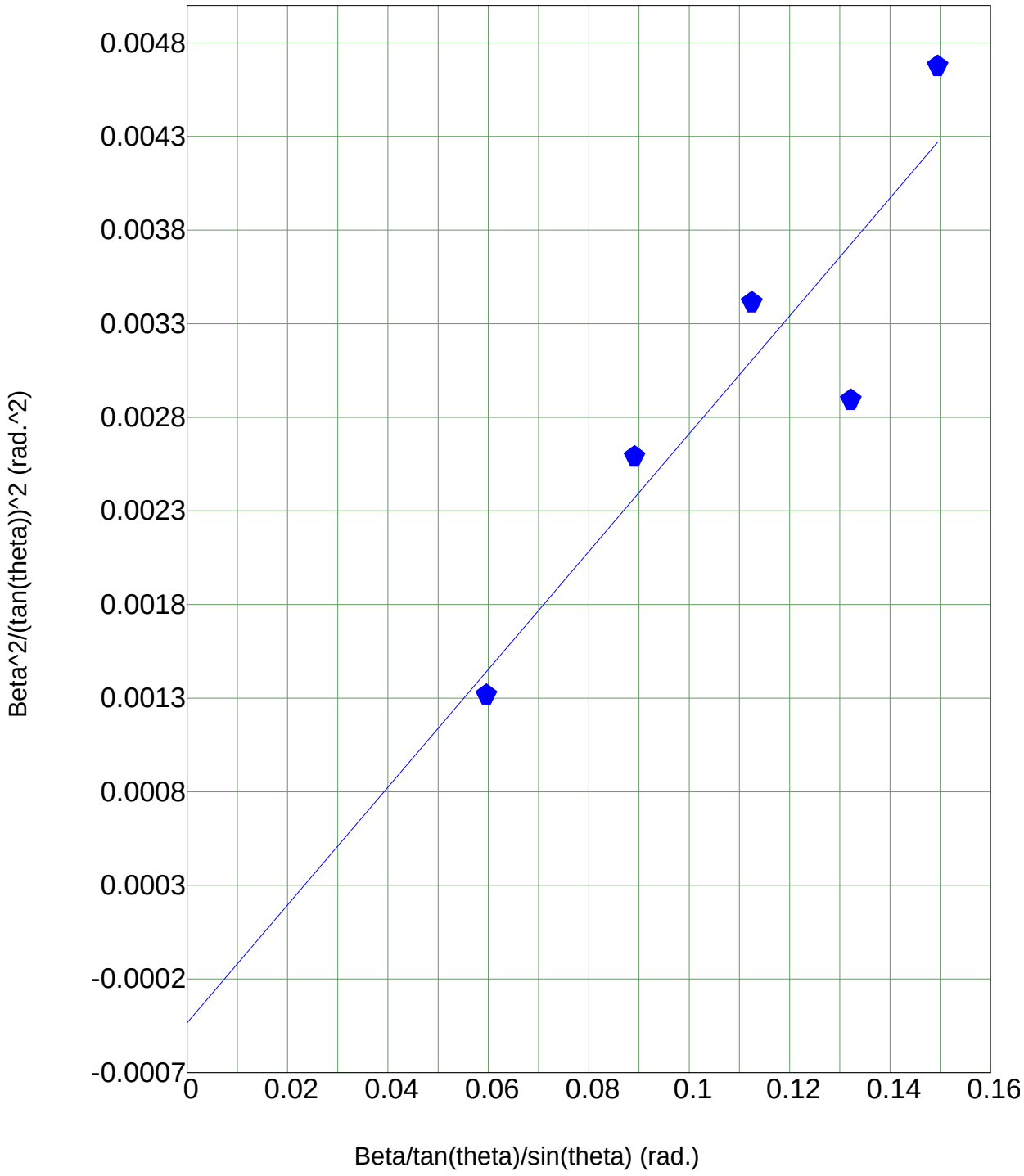

0.5% V-Ti Aerogel 450°C Crystalline Size: 5.1 nm

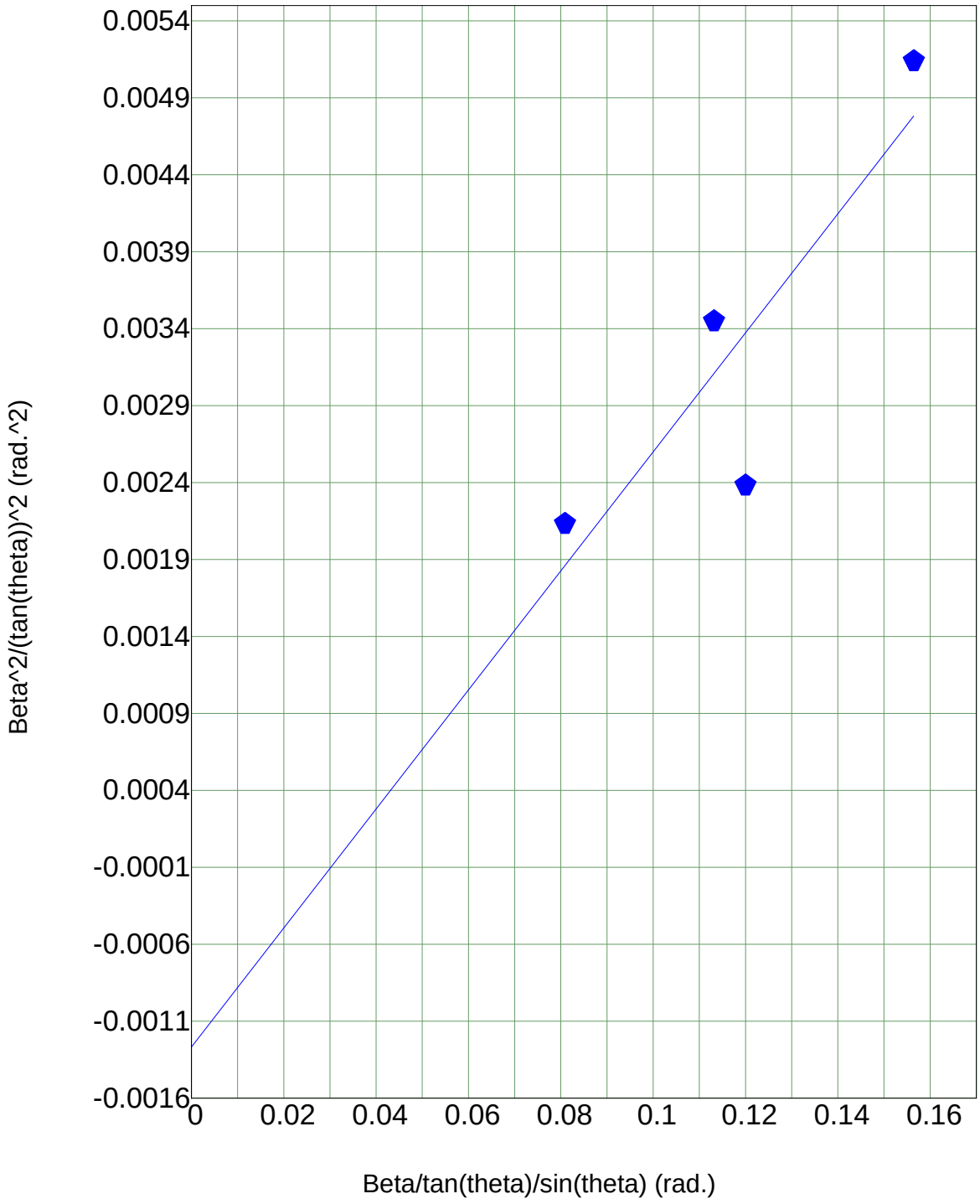

1.0% V-Ti Aerogel 450°C Crystalline Size: 4.2 nm

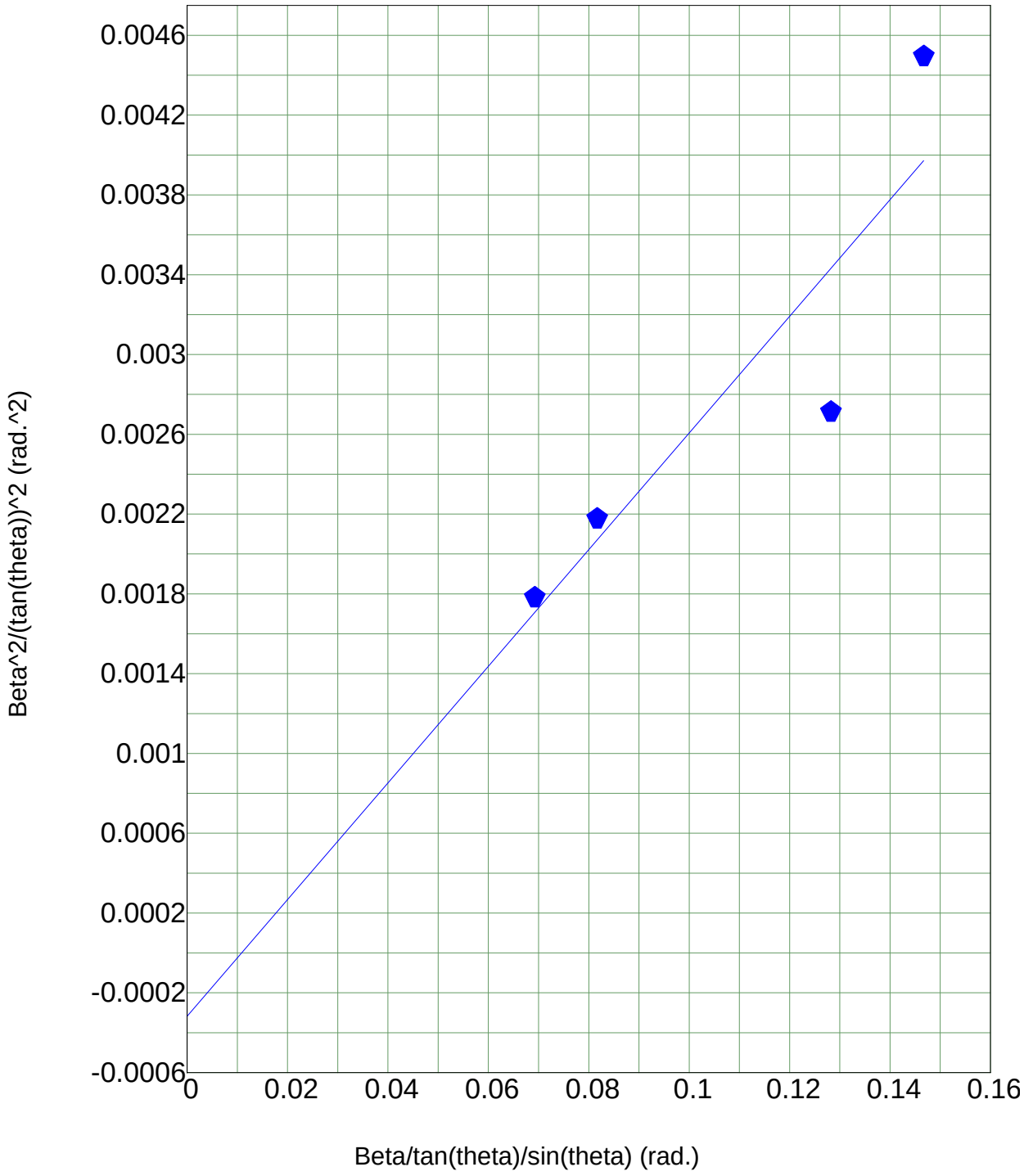

4.8% V-Ti Aerogel 450°C Crystalline Size: 5.5 nm

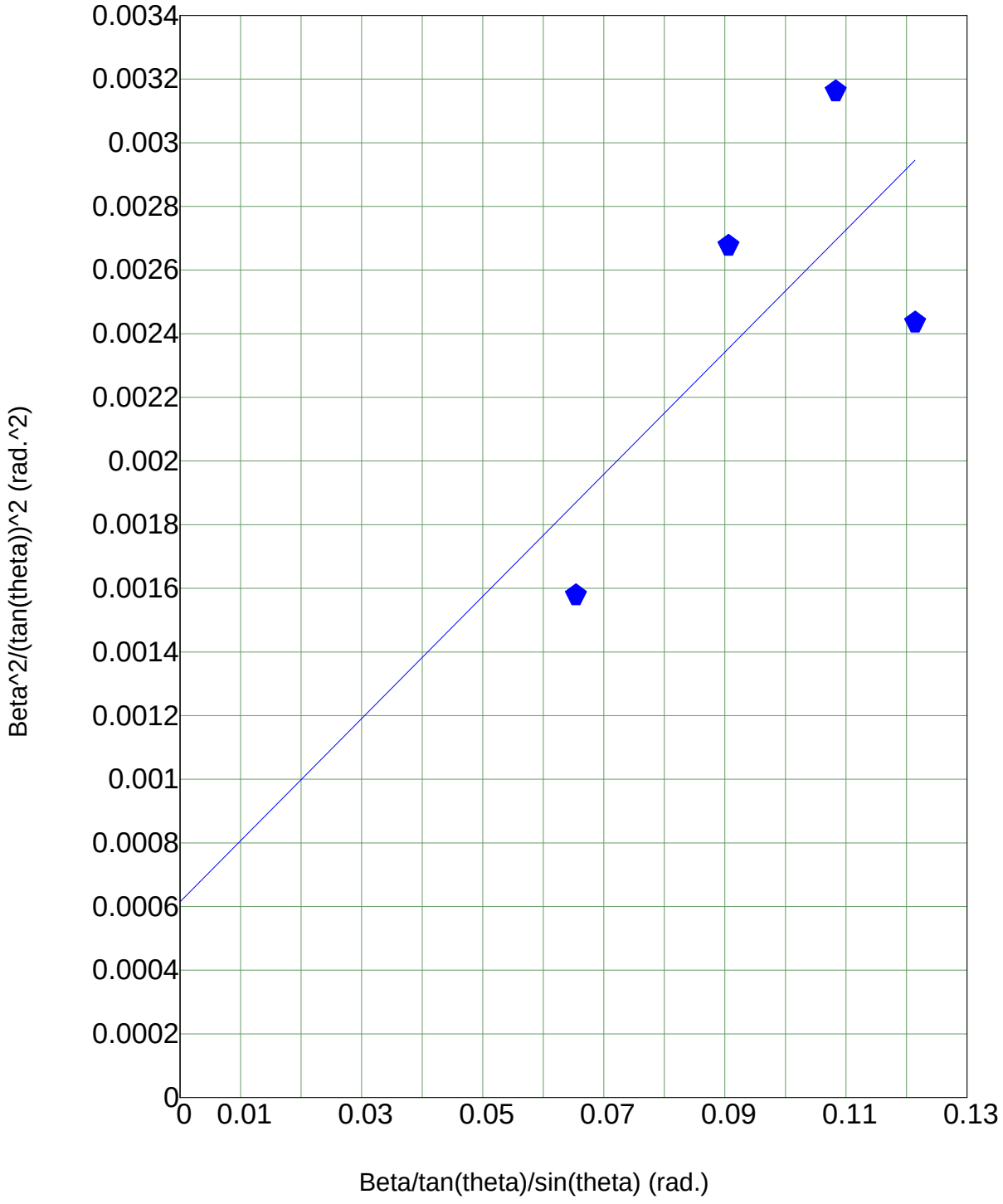

9.1% V-Ti Aerogel 450°C Crystalline Size: 8.5 nm

7.3 TEM Measurements

Anatase Titania Aerogel d-spacing Calculations

a	c	h	k	l	h^2+k^2	/a^2	l^2/c^2	sum	$(1/sum)^{1/2}$	Intensity	Order of Int.
3.7852	9.5139	1	0	1	1	0.0698	0.0110	0.0808	**3.517**	100	#1
3.7852	9.5139	1	0	3	1	0.0698	0.0994	0.1692	**2.431**	10	#6
3.7852	9.5139	0	0	4	0	0.0000	0.1768	0.1768	**2.378**	20	#3
3.7852	9.5139	1	1	2	2	0.1396	0.0442	0.1838	**2.333**	10	#7
3.7852	9.5139	2	0	0	4	0.2792	0.0000	0.2792	**1.893**	35	#2
3.7852	9.5139	1	0	5	1	0.0698	0.2762	0.3460	**1.700**	20	#4
3.7852	9.5139	2	1	1	5	0.3490	0.0110	0.3600	**1.667**	20	#5

The most visible lattice spacing in each specimen is the (101) plane due to the large 3.517 Å d-spacing.

Raw Data from TEM Images

Titania Aerogel 275°C			
Distance (nm)	# Fringes	nm	Å
8.075	23	0.3511	3.51087
4.556	13	0.3505	3.504615
4.906	14	0.3504	3.504286
8.034	23	0.3493	3.493043
5.459	16	0.3412	3.411875
5.956	17	0.3504	3.503529
5.566	16	0.3479	3.47875
6.283	18	0.3491	3.490556
5.903	17	0.3472	3.472353
7.555	32	0.2361	2.360938*
3.017	13	0.2321	2.320769*
		Average	**3.486**
		Stnd. Dev.	**0.030**
Titania Aerogel 450°C			
Distance (nm)	# Fringes	nm	Å
4.142	12	0.3452	3.451667
3.808	11	0.3462	3.461818
4.089	12	0.3408	3.4075
4.134	12	0.3445	3.445
5.282	15	0.3521	3.521333
6.534	19	0.3439	3.438947
3.710	11	0.3373	3.372727
4.072	12	0.3393	3.393333
		Average	**3.437**
		Stnd Dev.	**0.046**

9.1% V-Ti Aerogel 450°C			
Distance (nm)	# Fringes	nm	Å
6.211	18	0.3451	3.450556
3.766	11	0.3424	3.423636
2.736	8	0.3420	3.42
4.489	13	0.3453	3.453077
6.565	19	0.3455	3.455263
3.204	9	0.3560	3.56
2.051	6	0.3418	3.418333
4.934	14	0.3524	3.524286
4.933	14	0.3524	3.523571
3.461	10	0.3461	3.461
3.371	15	0.2247	2.247333*
2.871	14	0.2051	2.050714*
		Average	**3.469**
		Stnd Dev.	**0.050**

*Not included in average or standard deviation

<u>Titania Aerogel 275°C</u>

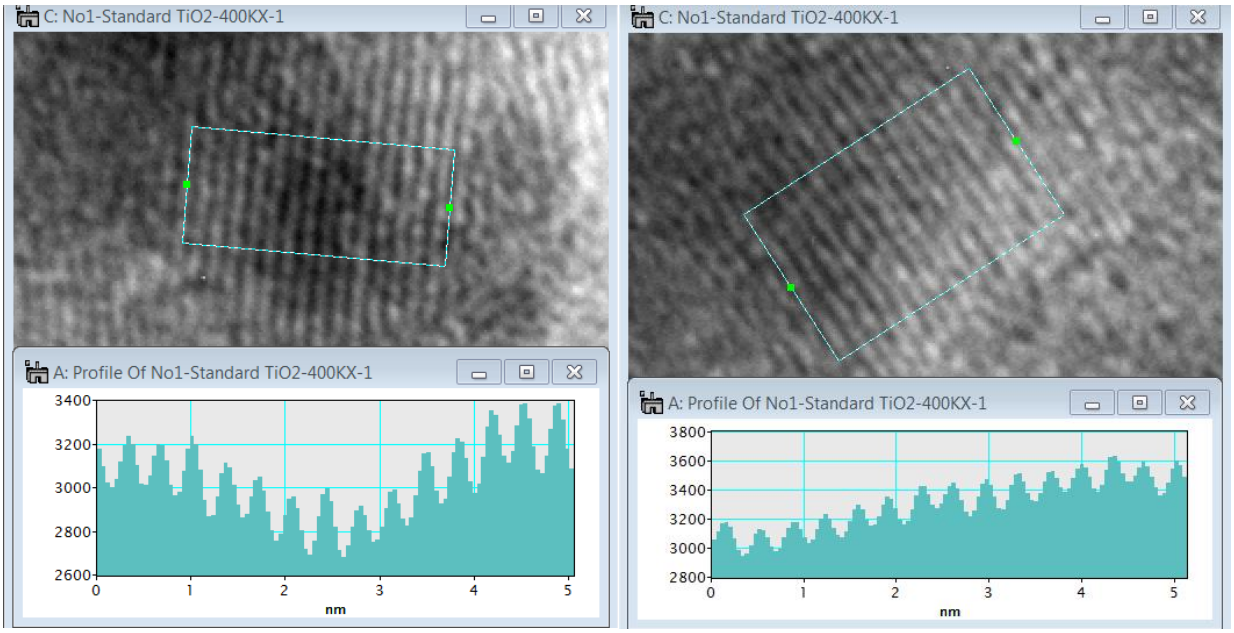

4.556 nm 13 spaces

4.906 nm 14 spaces

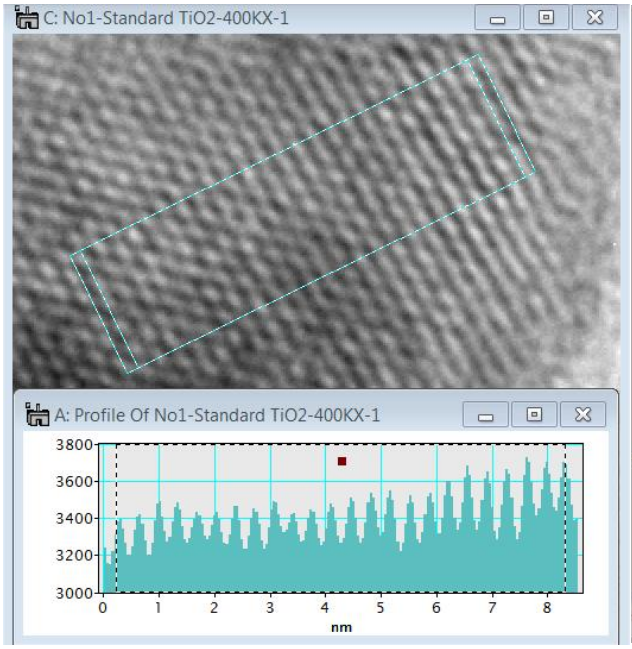

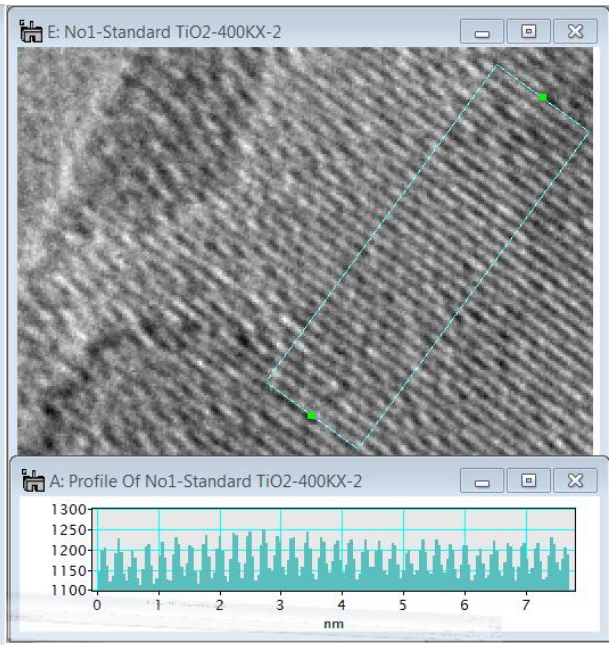

8.075 nm 23 spaces

7.555 nm 32 spaces

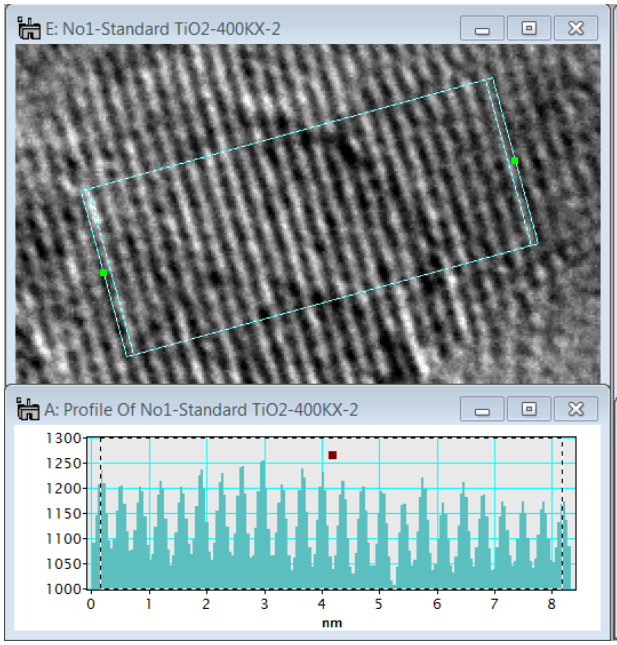

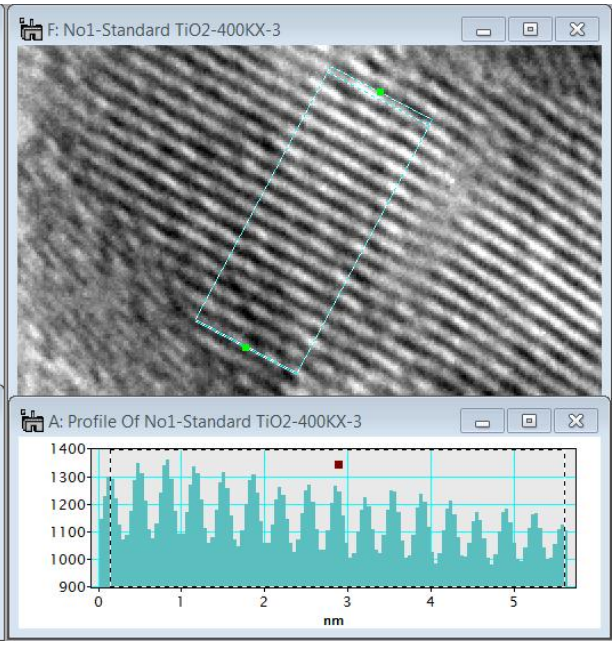

8.034 nm 23 spaces

5.459 nm 16 spaces

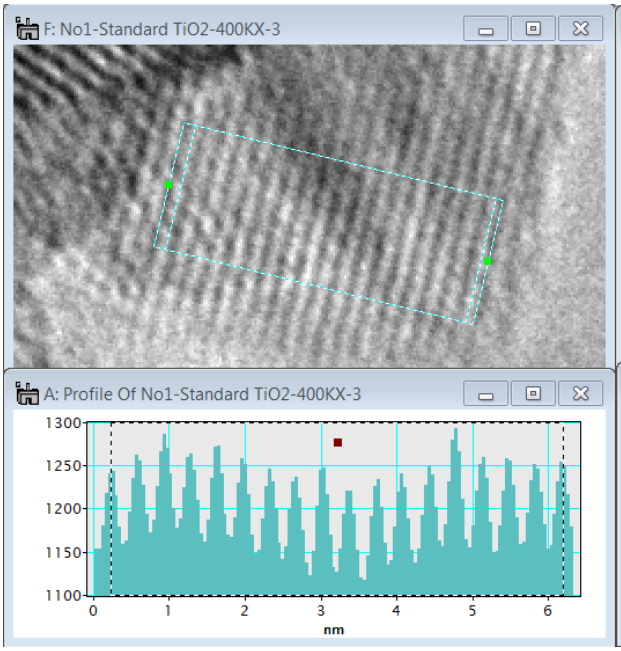

5.956 nm 17 spaces

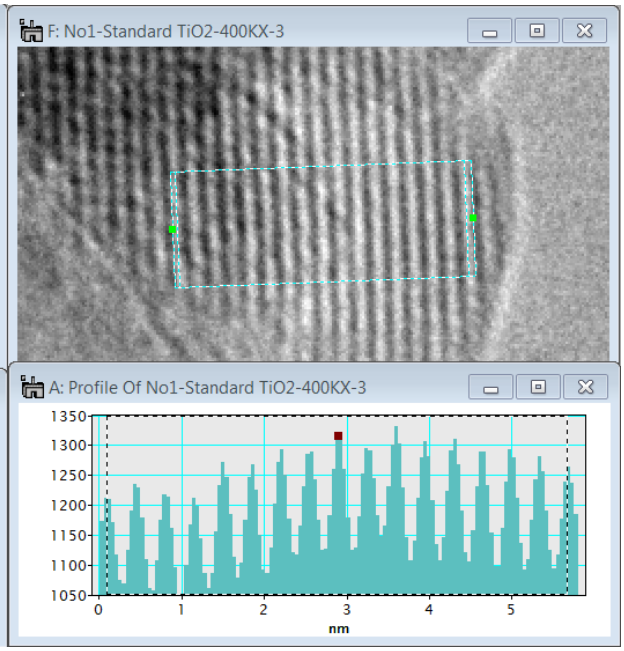

5.566 nm 16 spaces

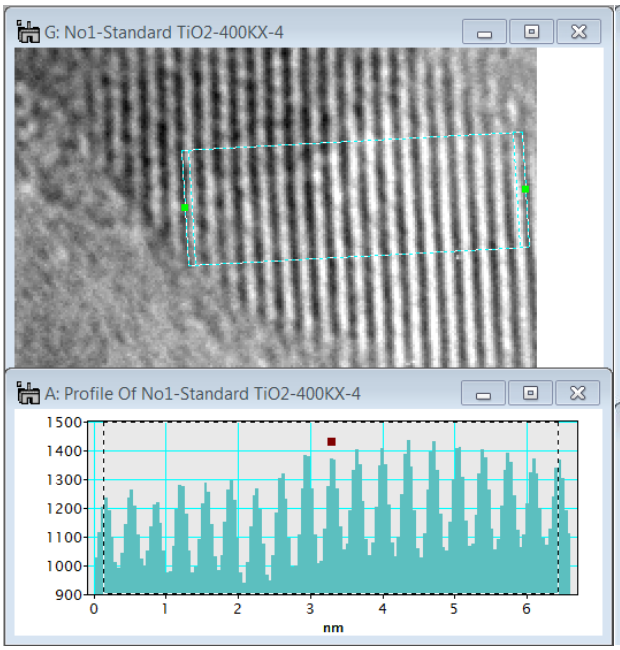

6.283nm 18 spaces

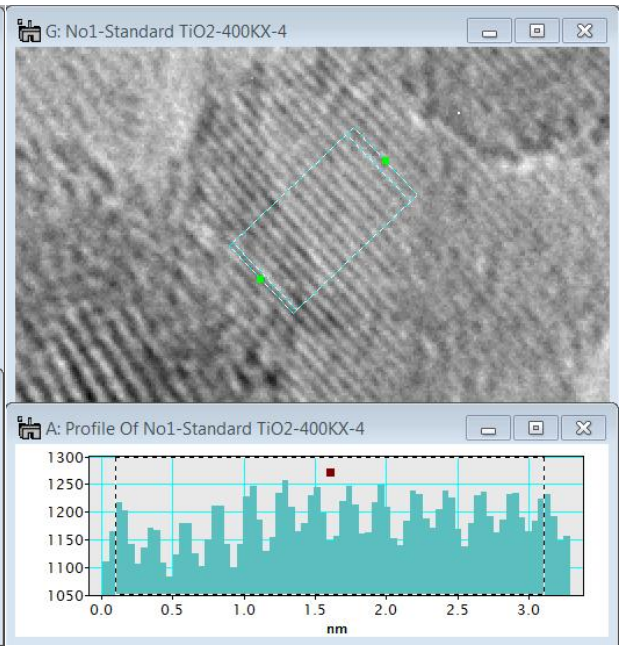

3.017 nm 13 spaces

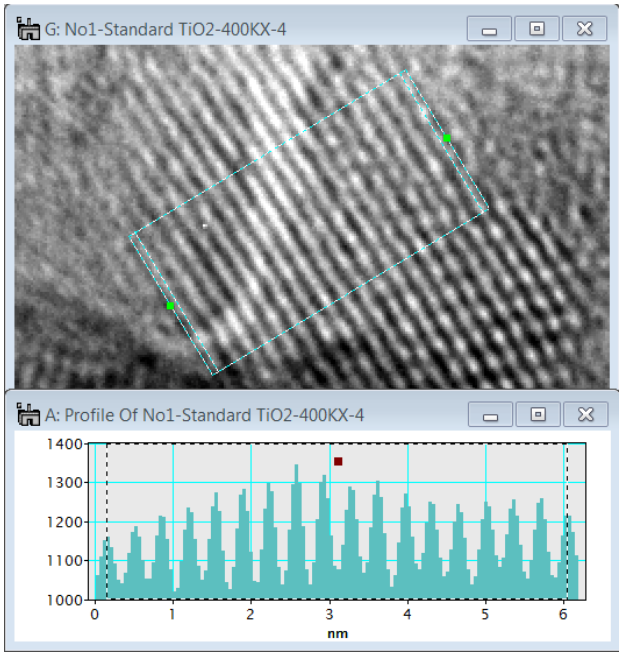

5.903 nm 17 spaces

Titania Aerogel 450°C

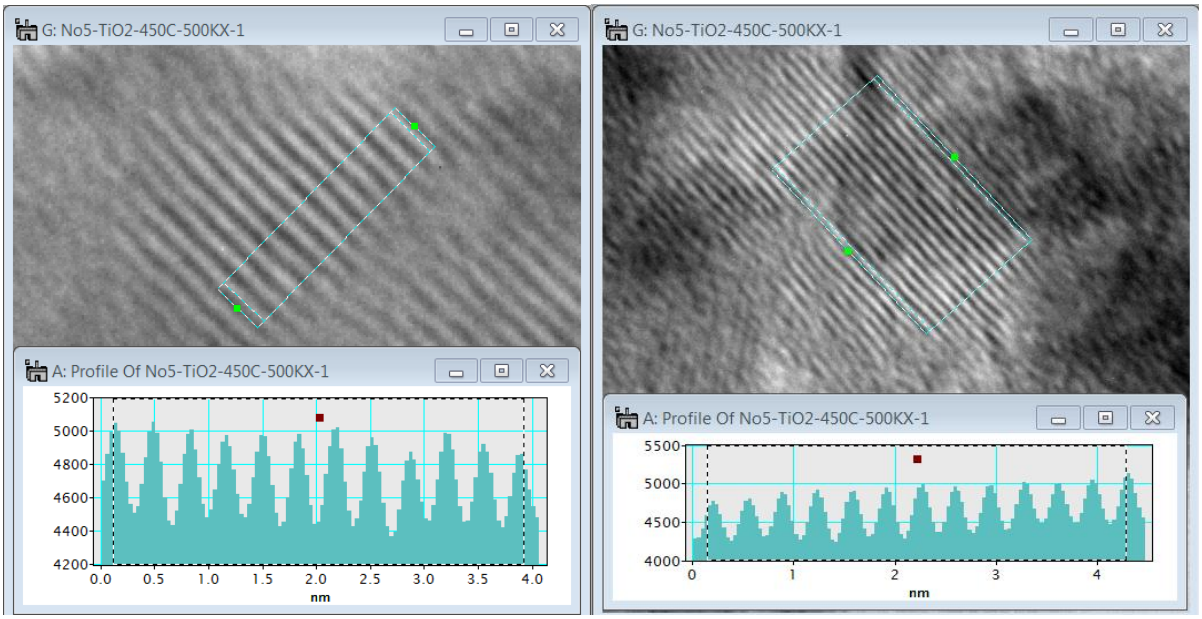

3.808 nm 11 spaces

4.142nm 12 spaces

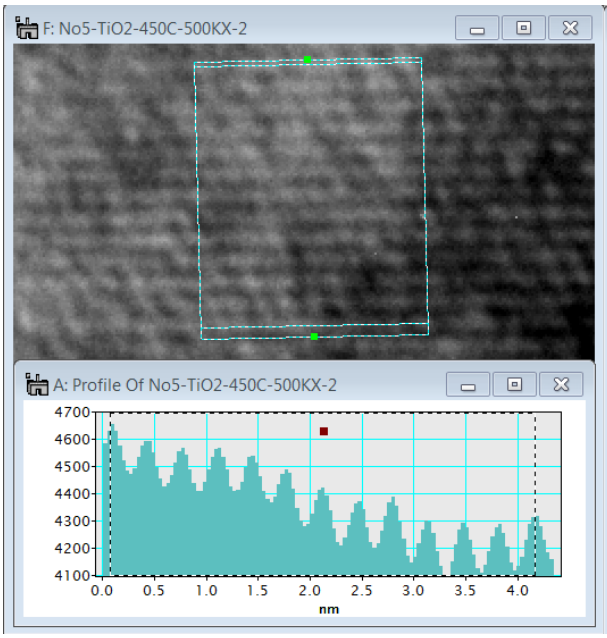

4.089 nm 12 spaces

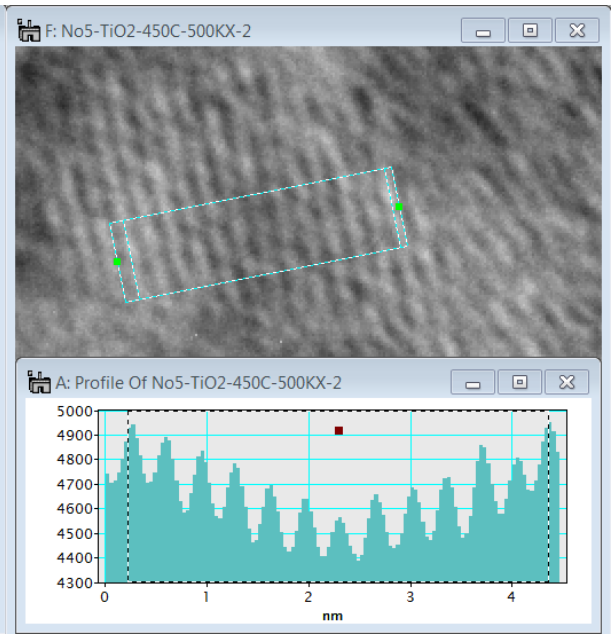

4.134 nm 12 spaces

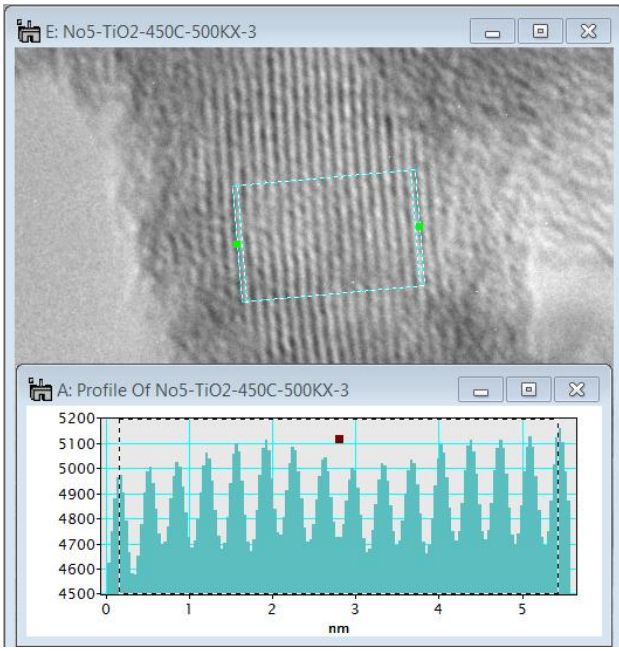

5.282 nm 15 spaces

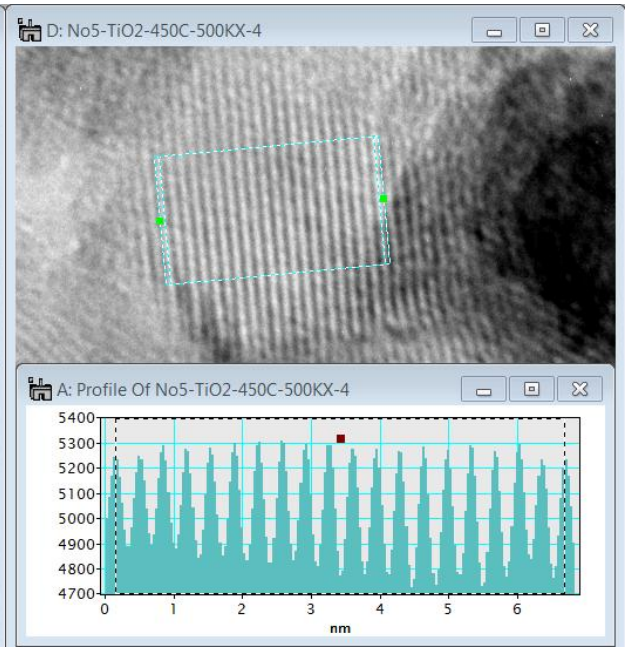

6.534 nm 19 spaces

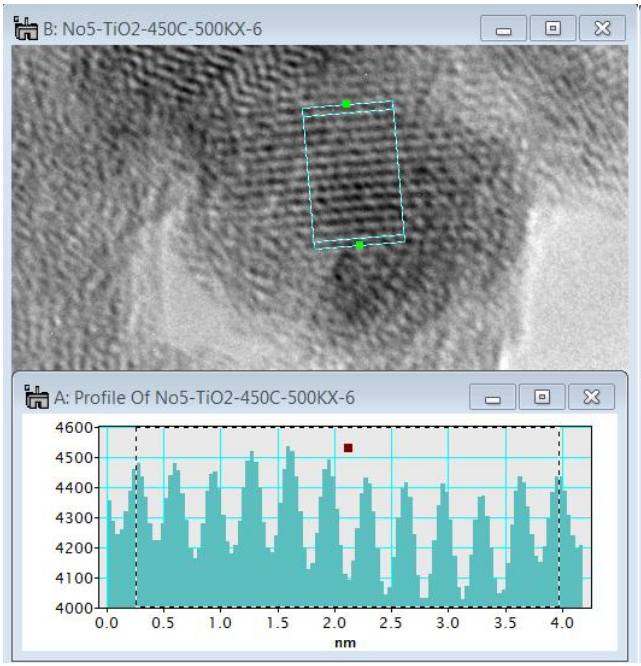

3.710 nm 11 spaces

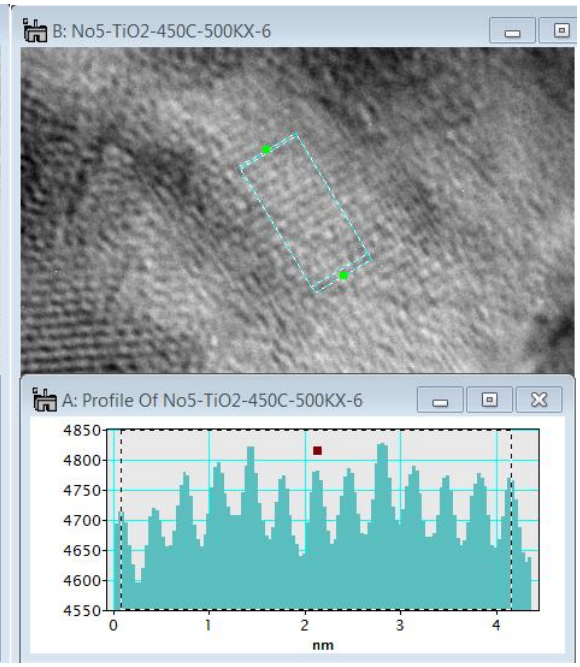

4.072 nm 12 spaces

9.1% V-Ti Aerogel 450°C

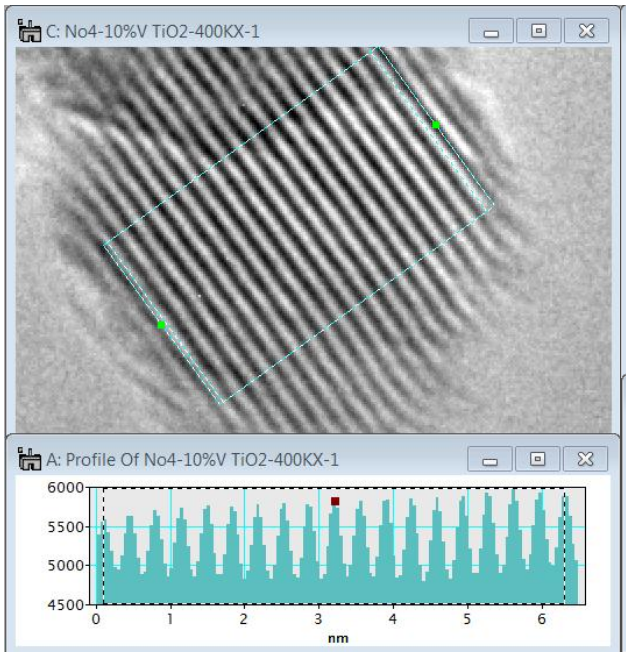

6.211 nm 18 spaces

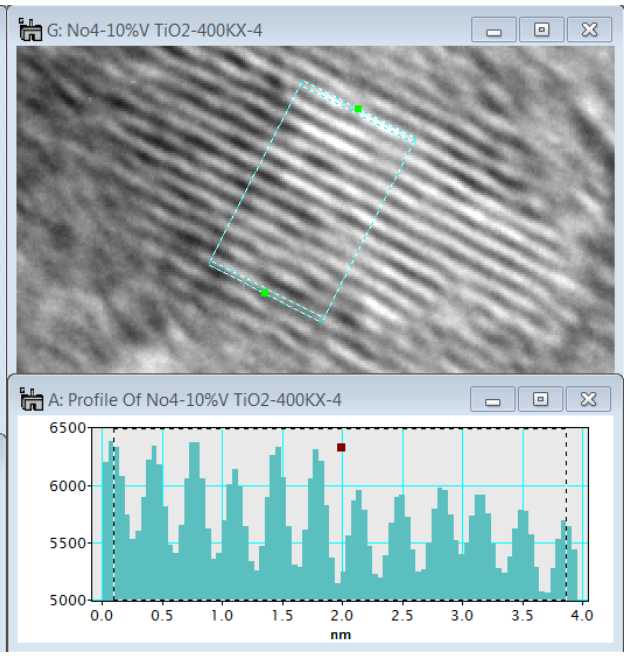

3.766 nm 11 spaces

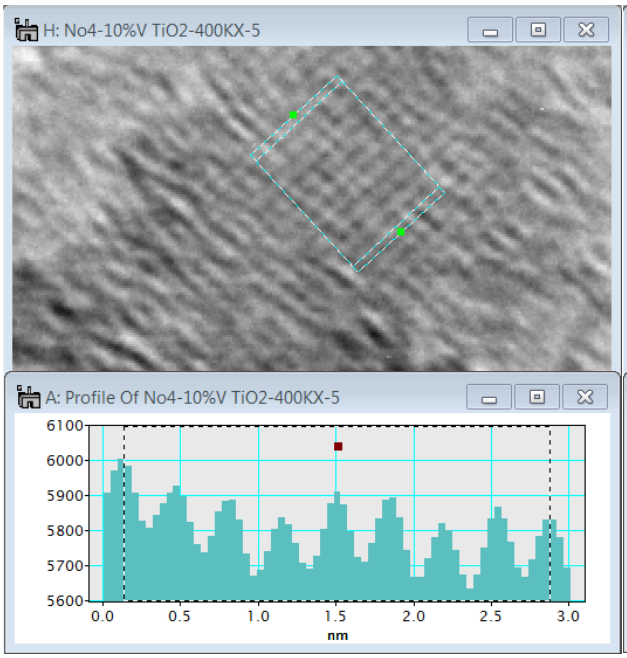

2.736 nm 8 spaces

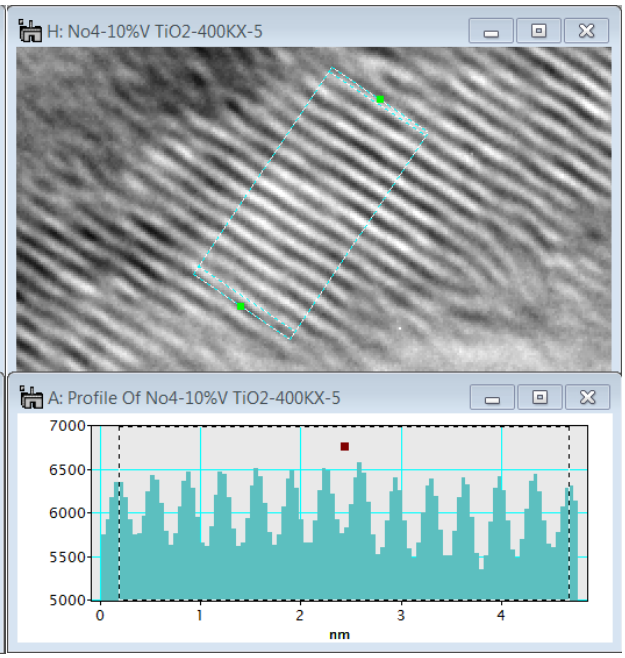

4.489 nm 13 spaces

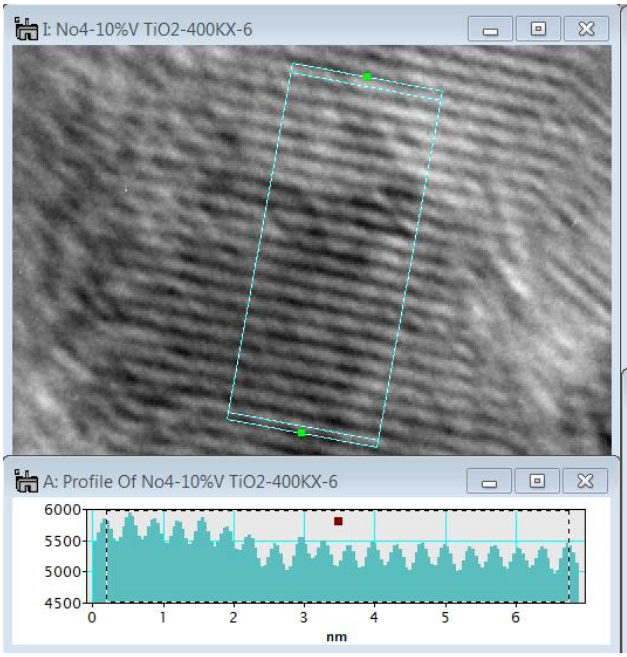

6.565 nm 19 spaces

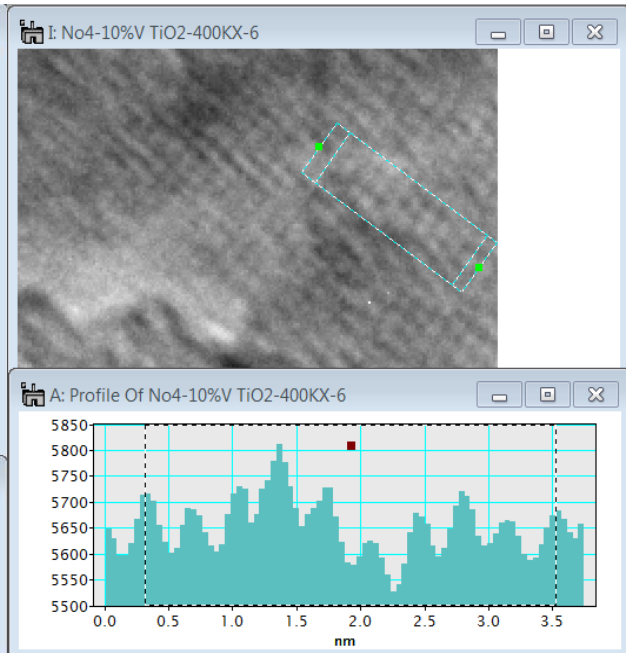

3.204 nm 9 spaces

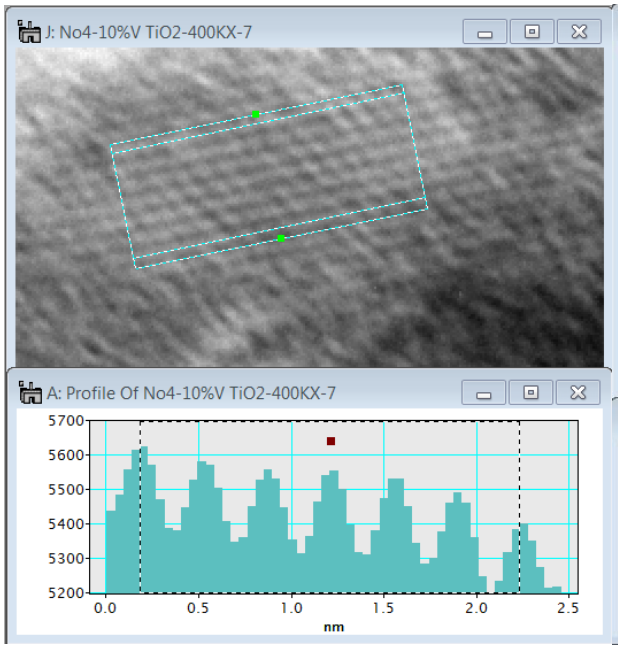

2.051 nm 6 spaces

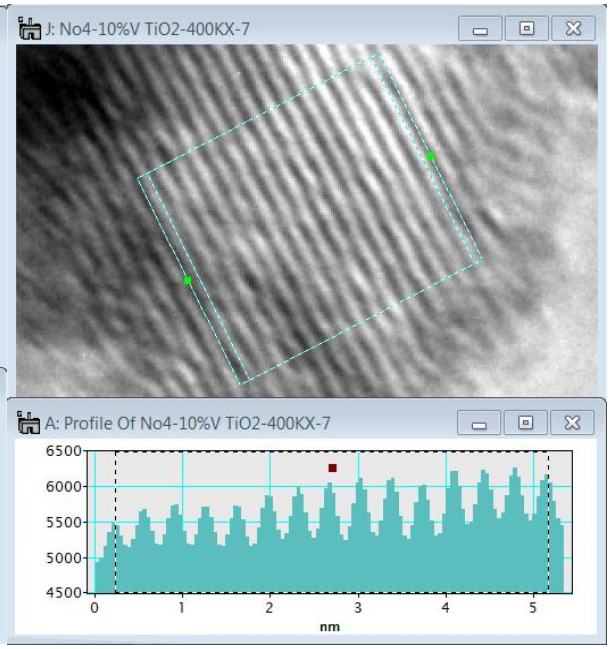

4.934 nm 14 spaces

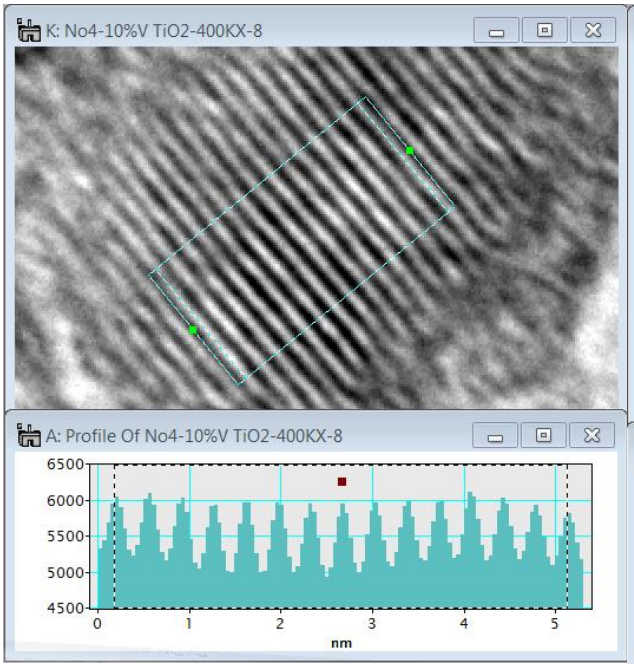

4.933 nm 14 spaces

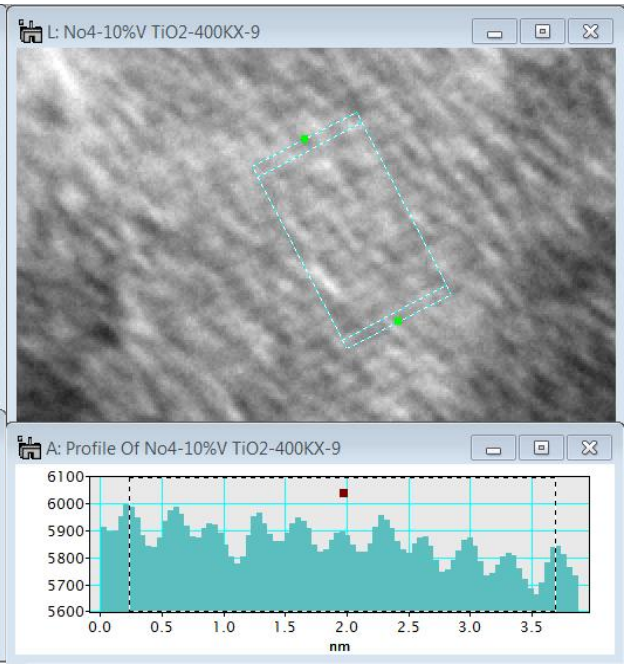

3.461 nm 10 spaces

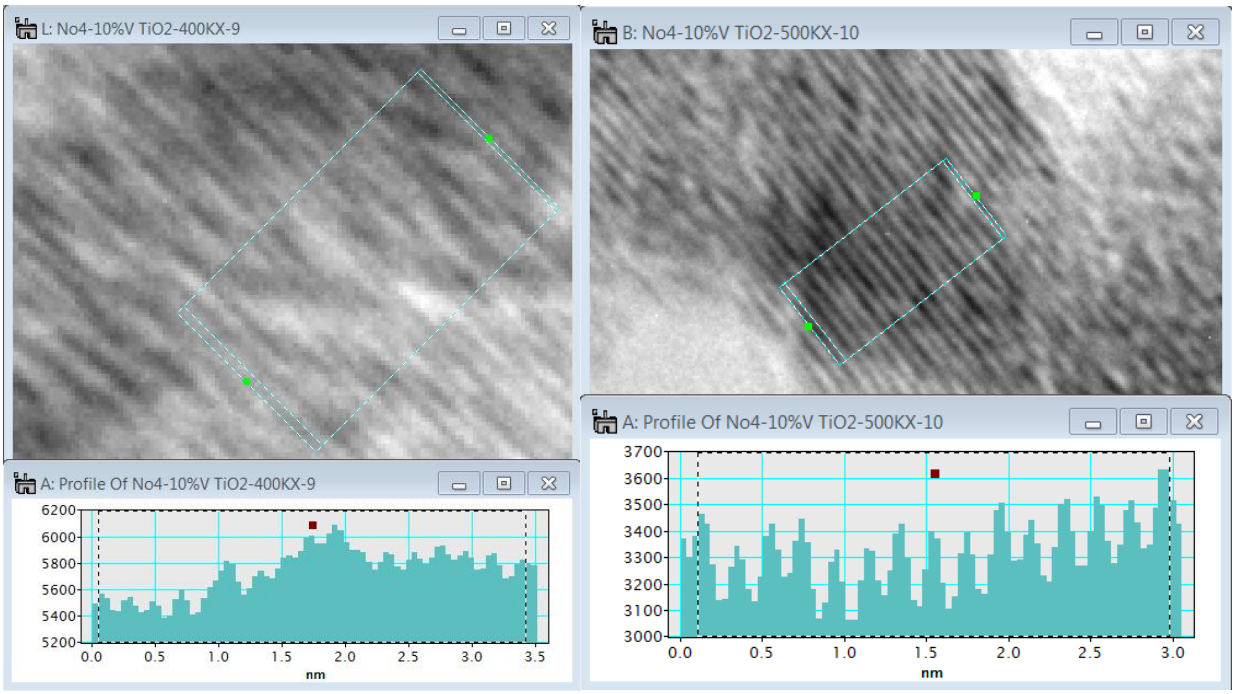

3.371 nm 15 spaces

2.871 nm 14 spaces

7.4 Percent Decrease in Propionaldehyde Peak Areas

Propionaldehyde Photodegradation Peak Areas and % Degradation

P25	Humidity	UVA	Propionaldehyde Average Peak Area	Standard Deviation	% Decrease in Propanal
Trial 1	No	Off	190771	1153	
Trial 1	No	On	163653	5733	14.2%
Trial 2	Yes	Off	238040	7559	
Trial 2	Yes	On	198083	5095	16.8%
Trial 3	Yes	Off	234762	2679	
Trial 3	Yes	On	206003	5216	12.3%
300°C	Humidity	UVA	Propionaldehyde Average Peak Area	Standard Deviation	% Decrease in Propanal
Trial 1	Yes	Off	226620	1205	
Trial 1	Yes	On	207559	7273	8.4%
Trial 2	Yes	Off	205597	4292	
Trial 2	Yes	On	189776	6718	7.7%